molecules

MDPI

Supplementary material

The targeted pesticides as Acetylcholinesterase inhibitors: comprehensive cross-organism molecular modelling studies performed to anticipate the pharmacology of harmfulness to humans *in vitro*

Milan Mladenović[1,*], Biljana B. Arsić[2,3], Nevena Stanković[1], Nezrina Mihović[1], Rino Ragno[4,5], Andrew Regan[6], Jelena S. Milićević[7], Tatjana M. Trtić-Petrović[7], Ružica Micić[8]

[1] Kragujevac Center for Computational Biochemistry, Faculty of Science, University of Kragujevac, Radoja Domanovića 12, 34000 Kragujevac, P.O. Box 60, Republic of Serbia
[2] Department of Mathematics, Faculty of Sciences and Mathematics, University of Niš, Višegradska 33, 18000 Niš, Republic of Serbia
[3] Division of Pharmacy and Optometry, University of Manchester, Oxford Road, M13 9PT, Manchester, United Kingdom
[4] Rome Center for Molecular Design, Department of Drug Chemistry and Technologies, Faculty of Pharmacy and Medicine, Sapienza Rome University, P.le A. Moro 5, 00185, Rome, Italy
[5] Alchemical Dynamics srl 00125 Rome, Italy
[6] School of Chemistry, University of Manchester, Oxford road, M13 9PL, Manchester, United Kingdom
[7] Vinča Institute of Nuclear Sciences, University of Belgrade, PO Box 522, 11001 Belgrade, Republic of Serbia
[8] Faculty of Sciences and Mathematics, University of Priština, Lole Ribara 29, 38220 Kosovska Mitrovica, Republic of Serbia
* Correspondence: mmladenovic@kg.ac.rs; Tel.: +381-34-336-223, ext. 255

CONTENTS

Figure S7. RMSDs (**a**), RMSFs (**b**), and Interaction diagrams (**c**) of *m*AChE in complex with ACh. The green bars present hydrogen bonds, the the purple bars show hydrophobic interactions, the pink bars show ionic interaction, the the blue bars present water bridges.

Figure S8. RMSDs (**a**), RMSFs (**b**), and Interaction diagrams (**c**) of *h*AChE in complex with ACh. The green bars present hydrogen bonds, the purple bars show hydrophobic interactions, the pink bars show ionic interaction, the blue bars present water bridges.

Figure S9. RMSDs (**a**), RMSFs (**b**), and Interaction diagrams (**c**) of *m*AChE in complex with atrazine. The green bars present hydrogen bonds, the purple bars show hydrophobic interactions, the pink bars show ionic interaction, the blue bars present water bridges.

Figure S10. RMSDs (**a**), RMSFs (**b**), and Interaction diagrams (**c**) of *h*AChE in complex with atrazine. The green bars present hydrogen bonds, the purple bars show hydrophobic interactions, the pink bars show ionic interaction, the blue bars present water bridges.

Figure S11. RMSDs (**a**), RMSFs (**b**), and Interaction diagrams (**c**) of *m*AChE in complex with propazine. The green bars present hydrogen bonds, the purple bars show hydrophobic interactions, the pink bars show ionic interaction, the blue bars present water bridges.

Figure S12. RMSDs (**a**), RMSFs (**b**), and Interaction diagrams (**c**) of *h*AChE in complex with propazine. The green bars present hydrogen bonds, the purple bars show hydrophobic interactions, the pink bars show ionic interaction, the blue bars present water bridges.

Figure S13. RMSDs (**a**), RMSFs (**b**), and Interaction diagrams (**c**) of *m*AChE in complex with simazine. The green bars present hydrogen bonds, the purple bars show hydrophobic interactions, the pink bars show ionic interaction, the blue bars present water bridges.

Figure S14. RMSDs (**a**), RMSFs (**b**), and Interaction diagrams (**c**) of *h*AChE in complex with simazine. The green bars present hydrogen bonds, the purple bars show hydrophobic interactions, the pink bars show ionic interaction, the blue bars present water bridges.

Figure S15. RMSDs (**a**), RMSFs (**b**), and Interaction diagrams (**c**) of *m*AChE in complex with carbofuran. The green bars present hydrogen bonds, the purple bars show hydrophobic interactions, the pink bars show ionic interaction, the blue bars present water bridges.

Figure S16. RMSDs (**a**), RMSFs (**b**), and Interaction diagrams (**c**) of *h*AChE in complex with carbofuran. The green bars present hydrogen bonds, the purple bars show hydrophobic interactions, the pink bars show ionic interaction, the blue bars present water bridges.

Figure S17. RMSDs (**a**), RMSFs (**b**), and Interaction diagrams (**c**) of *m*AChE in complex with monocrotophos. The green bars present hydrogen bonds, the purple bars show hydrophobic interactions, the pink bars show ionic interaction, the blue bars present water bridges.

Figure S18. RMSDs (**a**), RMSFs (**b**), and Interaction diagrams (**c**) of *h*AChE in complex with monocrotophos. The green bars present hydrogen bonds, the purple bars show hydrophobic interactions, the pink bars show ionic interaction, the blue bars present water bridges.

Figure S19. RMSDs (**a**), RMSFs (**b**), and Interaction diagrams (**c**) of *m*AChE in complex with dimethoate. The green bars present hydrogen bonds, the purple bars show hydrophobic interactions, the pink bars show ionic interaction, the blue bars present water bridges.

Figure S20. RMSDs (**a**), RMSFs (**b**), and Interaction diagrams (**c**) of *h*AChE in complex with dimethoate. The green bars present hydrogen bonds, the purple bars show hydrophobic interactions, the pink bars show ionic interaction, the blue bars present water bridges.

Figure S21. RMSDs (**a**), RMSFs (**b**), and Interaction diagrams (**c**) of *m*AChE in complex with carbaryl. The green bars present hydrogen bonds, the purple bars show hydrophobic interactions, the pink bars show ionic interaction, the blue bars present water bridges.

Figure S22. RMSDs (**a**), RMSFs (**b**), and Interaction diagrams (**c**) of *h*AChE in complex with carbaryl. The green bars present hydrogen bonds, the purple bars show hydrophobic interactions, the pink bars show ionic interaction, the blue bars present water bridges.

Figure S23. RMSDs (**a**), RMSFs (**b**), and Interaction diagrams (**c**) of *m*AChE in complex with tebufenozide. The green bars present hydrogen bonds, the purple bars show hydrophobic interactions, the pink bars show ionic interaction, the blue bars present water bridges.

Figure S24. RMSDs (**a**), RMSFs (**b**), and Interaction diagrams (**c**) of *h*AChE in complex with tebufenozide. The green bars present hydrogen bonds, the purple bars show hydrophobic interactions, the pink bars show ionic interaction, the blue bars present water bridges.

Figure S25. RMSDs (**a**), RMSFs (**b**), and Interaction diagrams (**c**) of *m*AChE in complex with imidacloprid. The green bars present hydrogen bonds, the purple bars show hydrophobic interactions, the pink bars show ionic interaction, the blue bars present water bridges.

Figure S26. RMSDs (**a**), RMSFs (**b**), Interaction diagrams (**c**) of *h*AChE in complex with imidacloprid. The green bars present hydrogen bonds, the purple bars show hydrophobic interactions, the pink bars show ionic interaction, the blue bars present water bridges.

Figure S27. RMSDs (**a**), RMSFs (**b**), and Interaction diagrams (**c**) of *m*AChE in complex with acetamiprid. The green bars present hydrogen bonds, the purple bars show hydrophobic interactions, the pink bars show ionic interaction, the blue bars present water bridges.

Figure S28. RMSDs (**a**), RMSFs (**b**), and Interaction diagrams (**c**) of *h*AChE in complex with acetamiprid. The green bars present hydrogen bonds, the purple bars show hydrophobic interactions, the pink bars show ionic interaction, the blue bars present water bridges.

Figure S29. RMSDs (**a**), RMSFs (**b**), and Interaction diagrams (**c**) of *m*AChE in complex with diuron. The green bars present hydrogen bonds, the purple bars show hydrophobic interactions, the pink bars show ionic interaction, the blue bars present water bridges.

Figure S30. RMSDs (**a**), RMSFs (**b**), and Interaction diagrams (**c**) of *h*AChE in complex with diuron. The green bars present hydrogen bonds, the purple bars show hydrophobic interactions, the pink bars show ionic interaction, the blue bars present water bridges.

Figure S31. RMSDs (**a**), RMSFs (**b**), and Interaction diagrams (**c**) of *m*AChE in complex with monuron. The green bars present hydrogen bonds, the purple bars show hydrophobic interactions, the pink bars show ionic interaction, the blue bars present water bridges.

Figure S32. RMSDs (**a**), RMSFs (**b**), and Interaction diagrams (**c**) of *h*AChE in complex with monuron. The green bars present hydrogen bonds, the purple bars show hydrophobic interactions, the pink bars show ionic interaction, the blue bars present water bridges.

Figure S33. RMSDs (**a**), RMSFs (**b**), and Interaction diagrams (**c**) of *m*AChE in complex with linuron. The green bars present hydrogen bonds, the purple bars show hydrophobic interactions, the pink bars show ionic interaction, the blue bars present water bridges.

Figure S34. RMSDs (**a**), RMSFs (**b**), and Interaction diagrams (**c**) of *m*AChE in complex with linuron. The green bars present hydrogen bonds, the purple bars show hydrophobic interactions, the pink bars show ionic interaction, the blue bars present water bridges.

Figure S35. The SB alignment of azamethiphos (**a**), azinphos-methyl (**b**), chlorpyrifos (**c**), DDVP (**d**), diazinon (**e**), and fenitrothion (**f**) into the *m*AChE active site. The enzyme ribbons are presented in blue, active site amino acids are depicted in white. For the clarity purpose, hydrogen atoms are omitted from presentation.

Figure S36. The SB alignment of glyphosate (**a**), malathion (**b**), methyl parathion (**c**), naled (dibrom) (**d**), parathion (**e**), and phosmet (**f**) into the *m*AChE active site. The enzyme ribbons are presented in blue, active site amino acids are depicted in white. For the clarity purpose, hydrogen atoms are omitted from presentation.

Figure S37. The SB alignment of TCVP (**a**), terbufos (**b**), methiocarb (**c**), methomyl (**d**), oxamyl (**e**), and DDT (**f**) into the *m*AChE active site. The enzyme ribbons are presented in blue, active site amino acids are depicted in white. For the clarity purpose, hydrogen atoms are omitted from presentation.

Figure S38. The SB alignment of 2,4-D (**a**), dicamba (**b**), DEET (**c**), and sulfoxaflor (**d**) into the *m*AChE active site. The enzyme ribbons are presented in blue, active site amino acids are depicted in white. For the clarity purpose, hydrogen atoms are omitted from presentation.

Figure S39. The SB alignment of azamethiphos (**a**), azinphos-methyl (**b**), chlorpyrifos (**c**), DDVP (**d**), diazinon (**e**), and fenitrothion (**f**) into the *h*AChE active site. The enzyme ribbons are presented in orange, active site amino acids are depicted in white. For the clarity purpose, hydrogen atoms are omitted from presentation.

Figure S40. The SB alignment of glyphosate (**a**), malathion (**b**), methyl parathion (**c**), naled (dibrom) (**d**), parathion (**e**), and phosmet (**f**) into the *h*AChE active site. The enzyme ribbons are presented in orange, active site amino acids are depicted in white. For the clarity purpose, hydrogen atoms are omitted from presentation.

Figure S41. The SB alignment of TCVP (**a**), terbufos (**b**), methiocarb (**c**), methomyl (**d**), oxamyl (**e**), and DDT (**f**) into the *h*AChE active site. The enzyme ribbons are presented in blue, active site amino acids are depicted in white. For the clarity purpose, hydrogen atoms are omitted from presentation.

Figure S42. The SB alignment of 2,4-D (**a**), dicamba (**b**), DEET (**c**), and sulfoxaflor (**d**) into the *h*AChE active site. The enzyme ribbons are presented in orange, active site amino acids are depicted in white. For the clarity purpose, hydrogen atoms are omitted from presentation.

Figure S43. The quantum chemical mechanism of *Homo sapiens* acetylcholinesterase inhibition by propazine. The extracted geometry of IS1 (a); TS1 (b); IS2 (c); TS2 (d).

Figure S44. The quantum chemical mechanism of *Homo sapiens* acetylcholinesterase inhibition by simazine. The extracted geometry of IS1 (a); TS1 (b); IS2 (c); TS2 (d).

Figure S45. Free energy profile for *Homo sapiens* acetylcholinesterase inhibition by propazine (**a**), and simazine (**b**) by means of B3LYP (6-31G*) QM simulations.

Table S1. Training set pesticides chemical structures, conformational analysis, superposition of generated global minima using various force fields.

Table S2. Training set pesticides chemical structures, conformational analysis, superposition of generated global minima using various force fields.

Table S3. Training set pesticides chemical structures, conformational analysis, superposition of generated global minima using various force fields.

Table S4. Test set pesticides chemical structures and obtained global minima using MMFF as the best performing force field.

Table S5. Linear regression parameters for QSAR model 2 (acute toxicity against *Mus musculus*).

Table S6. External validation of QSAR model 2 (acute toxicity against *Mus musculus*).

Table S7. Linear regression parameters for QSAR model 4 (acute toxicity against *Homo sapiens*).

Table S8. External validation of QSAR model 4 (acute toxicity against *Homo sapiens*).

Table S9. Structure-based alignment assessment for wild type *Mus musculus* AChE inhibitors.

Table S10. Structure-based alignment assessment for wild type *Homo sapiens* AChE inhibitors.

Table S11. Binding free energies and individual energy terms of *Mus Musculus* (upper part) and *Homo sapiens* (lower part) AChE in complex with acetylcholine and various targeted pesticides inhibitors.

Supplementary material references (SRs)

Figure S1. The sequence alignment between the *Mus musculus* and *Homo sapiens* AChE.

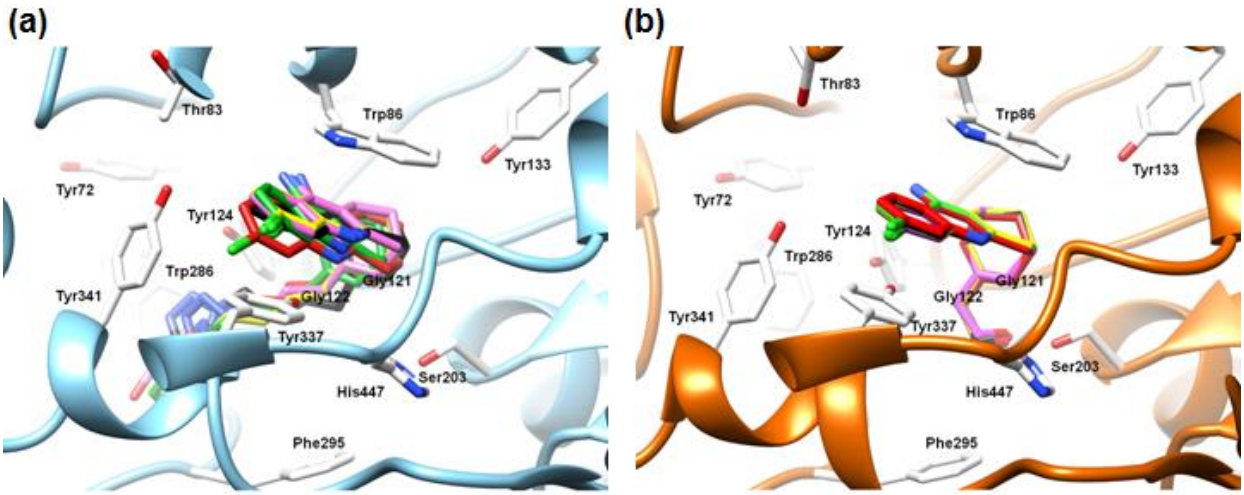

Figure S2. The Vina-based The SB alignment assessment of (**a**) co-crystallized *m*AChE inhibitor (PDB ID: 4A16), EC pink, ECRD yellow, RCRD green, ECCD black, RCCD red, and (**b**) co-crystallized *h*AChE inhibitor (PDB ID: 4BDT), EC pink, ECRD yellow, RCRD green, ECCD black, RCCD red.

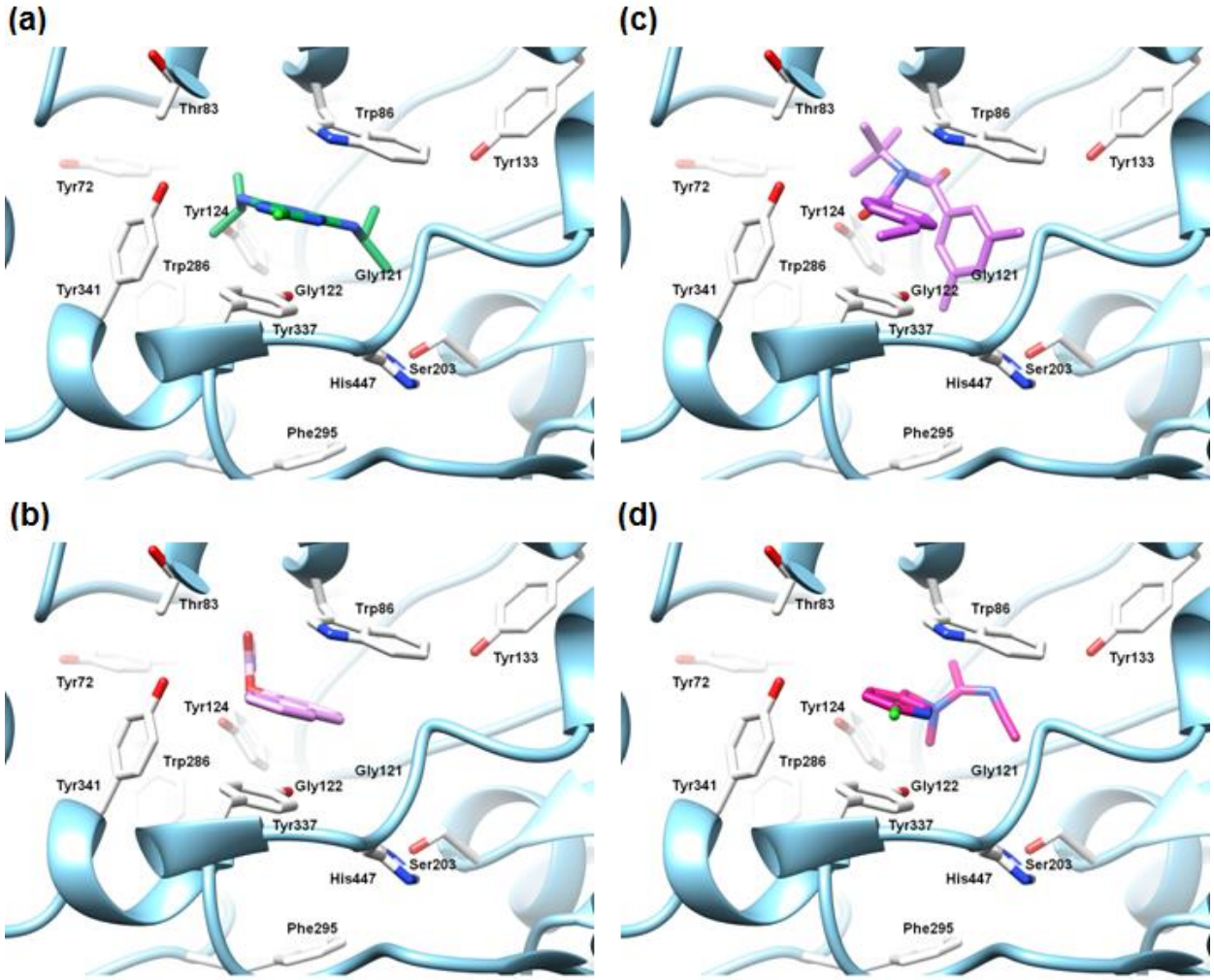

Figure S3. The The SB alignment of propazine (**a**), carbaryl (**b**), tebufenozide (**c**), and acetamiprid (**d**) into the *m*AChE active site. The The enzyme ribbons are presented in blue, active site amino acids are depicted in white. For the clarity purpose, hydrogen atoms are omitted from presentation.

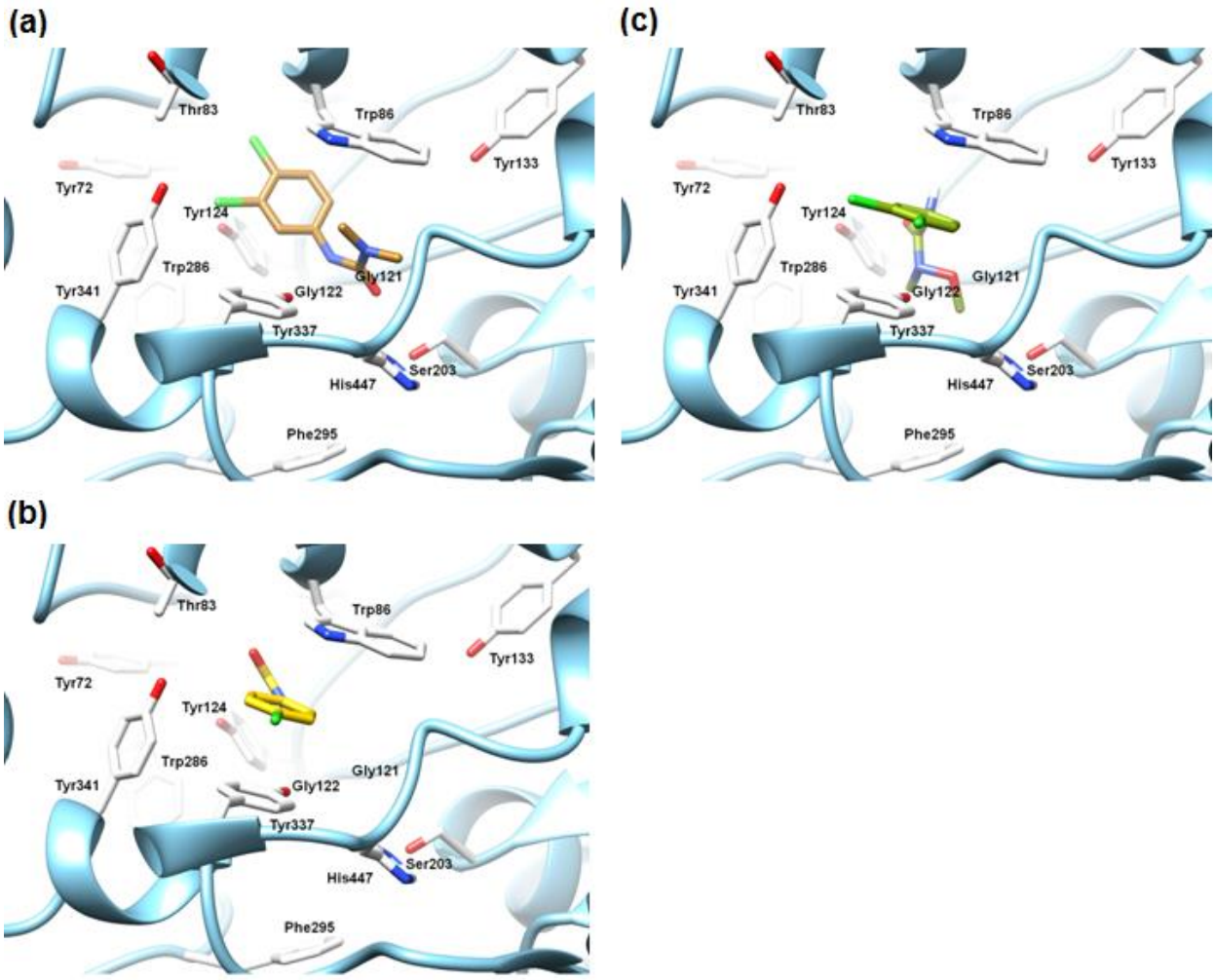

Figure S4. The The SB alignment of diuron (**a**), monuron (**b**), and linuron (**c**) into the *m*AChE active site. The The enzyme ribbons are presented in blue, active site amino acids are depicted in white. For the clarity purpose, hydrogen atoms are omitted from presentation.

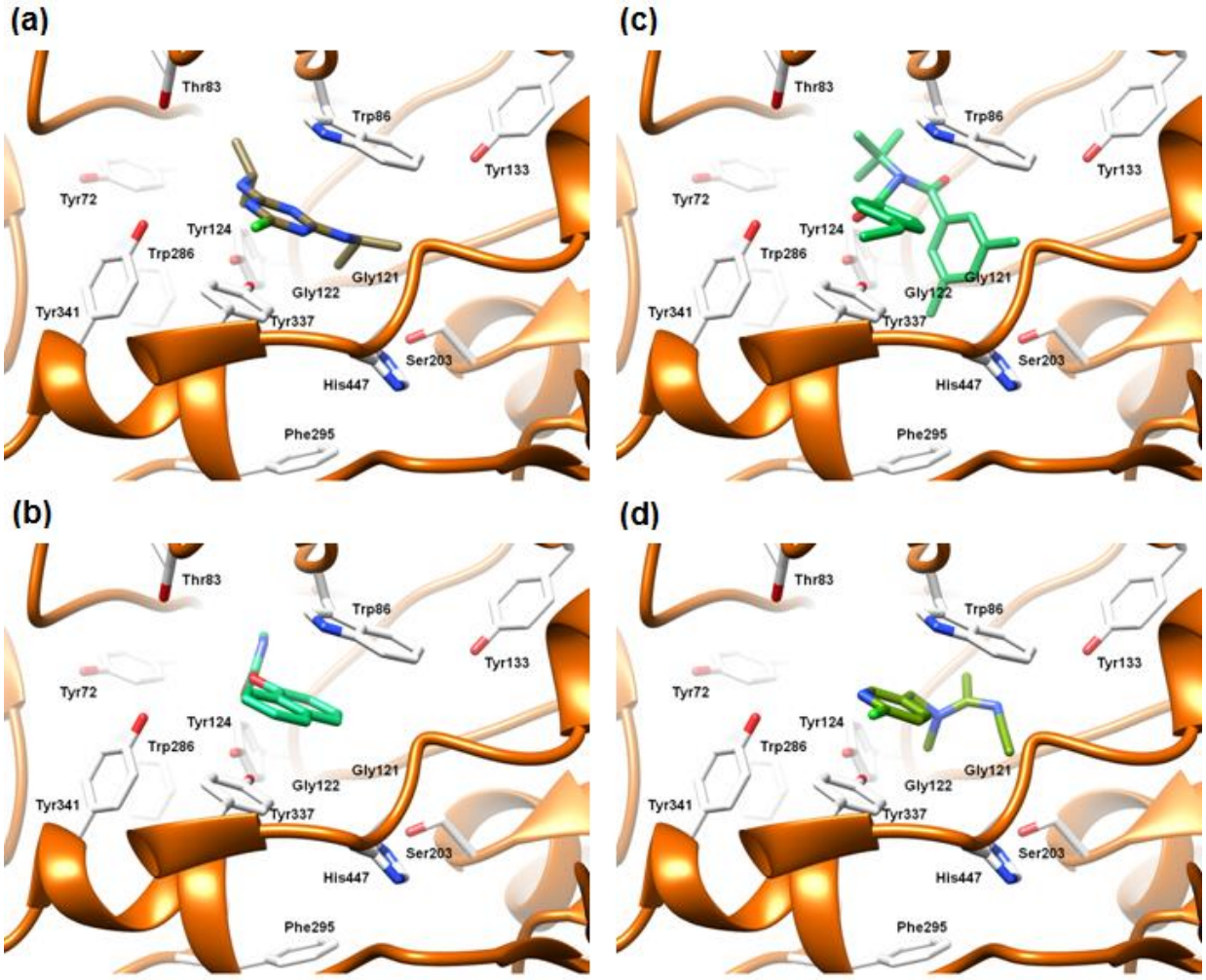

Figure S5. The The SB alignment of propazine (**a**), carbaryl (**b**), tebufenozide (**c**), and acetamiprid (**d**) into the *h*AChE active site. The The enzyme ribbons are presented in blue, active site amino acids are depicted in white. For the clarity purpose, hydrogen atoms are omitted from presentation.

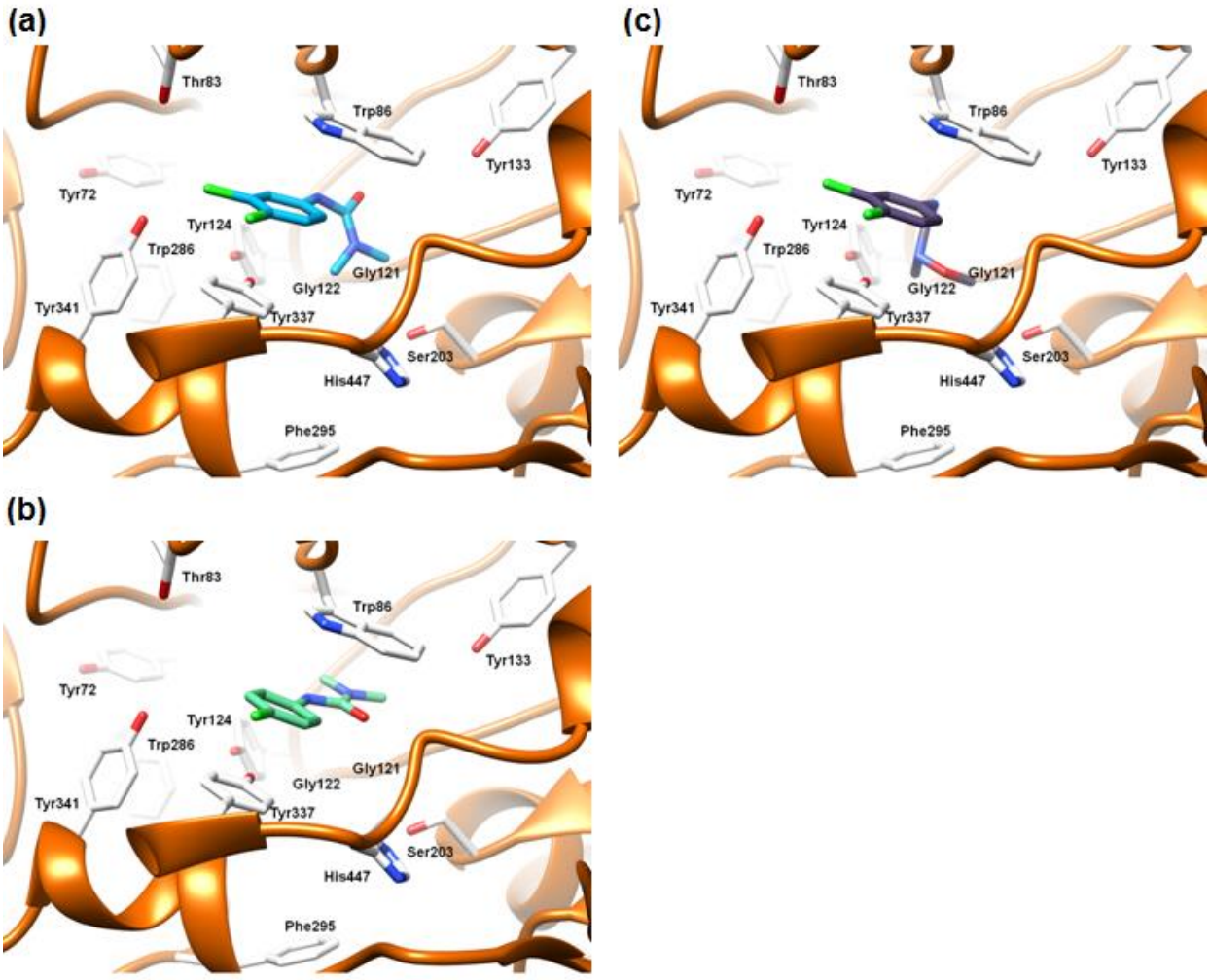

Figure S6. The The SB alignment of diuron (**a**), monuron (**b**), and linuron (**c**) into the *h*AChE active site. The The enzyme ribbons are presented in blue, active site amino acids are depicted in white. For the clarity purpose, hydrogen atoms are omitted from presentation.

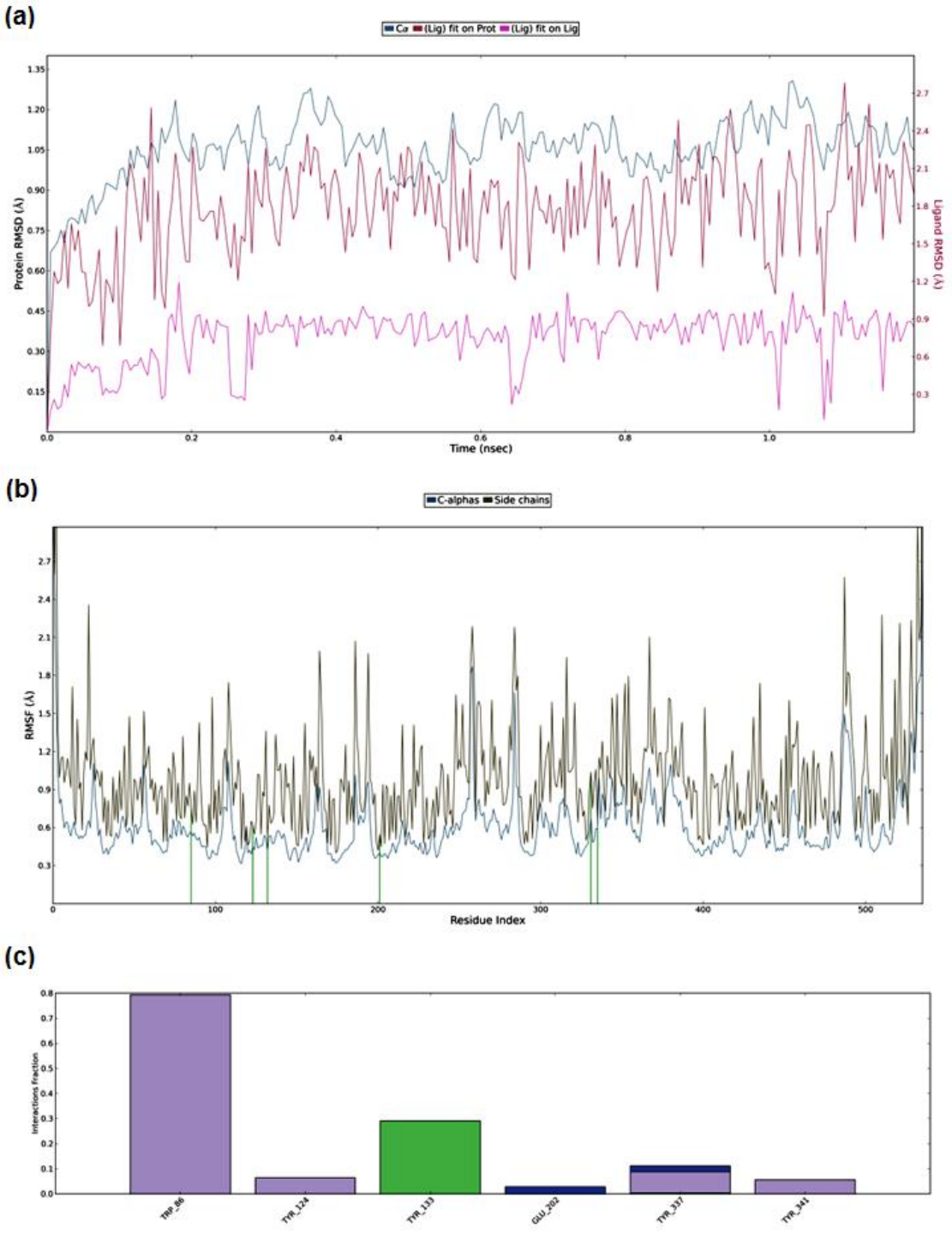

Figure S7. RMSDs (**a**), RMSFs (**b**), and Interaction diagrams (**c**) of *m*AChE in complex with ACh. The green bars present hydrogen bonds, the purple bars show hydrophobic interactions, the pink bars show ionic interaction, the blue bars present water bridges.

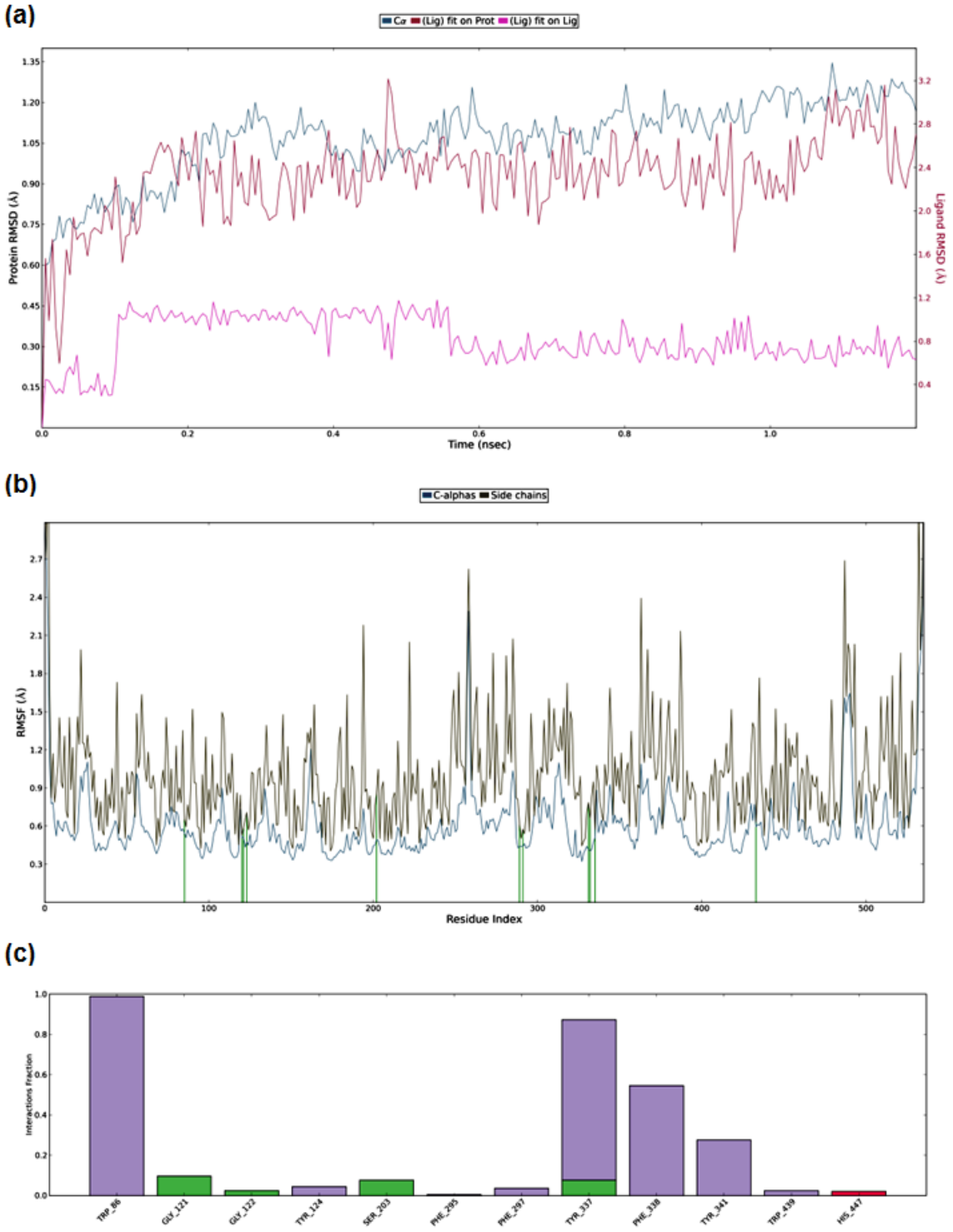

Figure S8. RMSDs (**a**), RMSFs (**b**), and Interaction diagrams (**c**) of *h*AChE in complex with ACh. The green bars present hydrogen bonds, the purple bars show hydrophobic interactions, the pink bars show ionic interaction, the blue bars present water bridges.

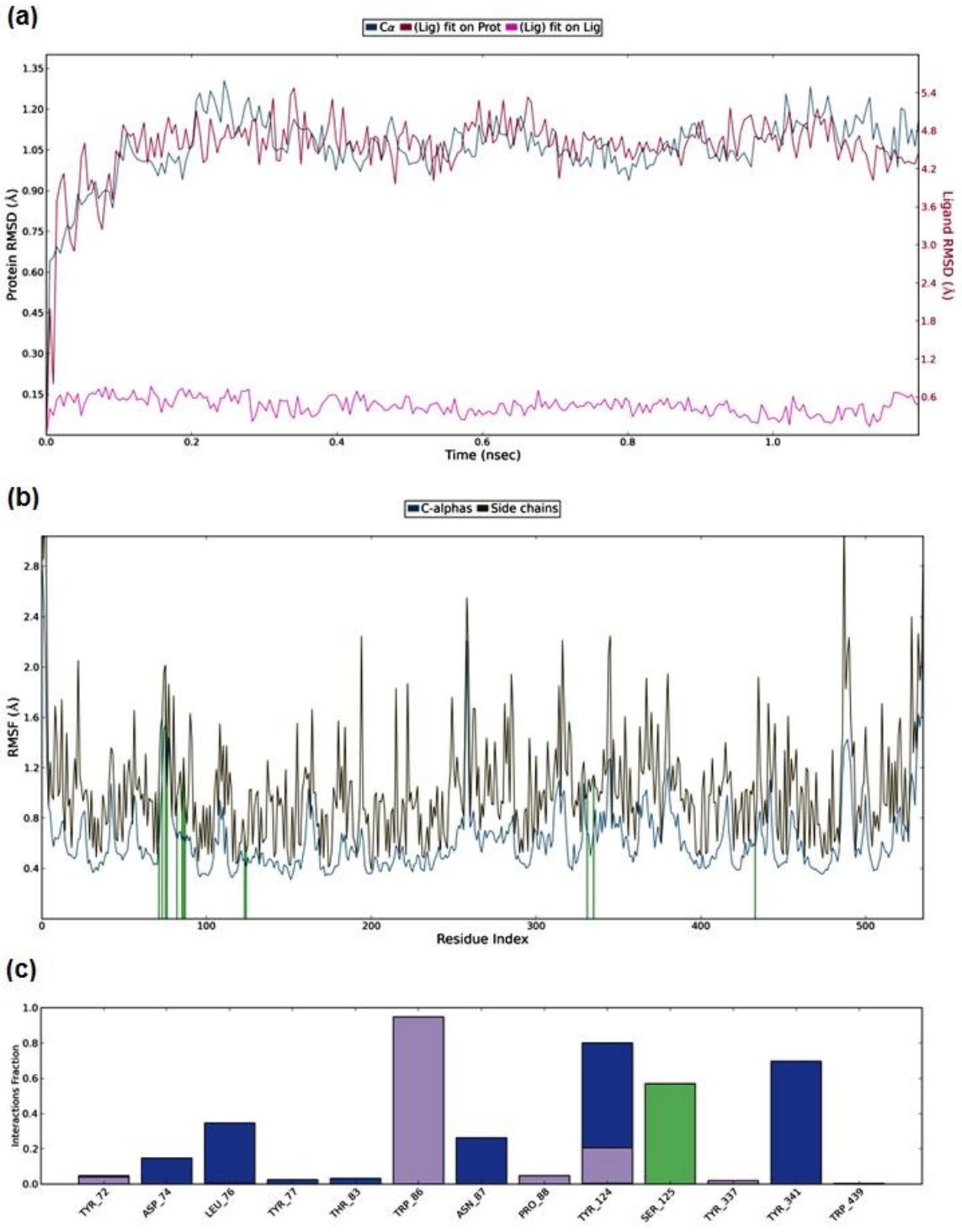

Figure S9. RMSDs (**a**), RMSFs (**b**), and Interaction diagrams (**c**) of *m*AChE in complex with atrazine. The green bars present hydrogen bonds, the purple bars show hydrophobic interactions, the pink bars show ionic interaction, the blue bars present water bridges.

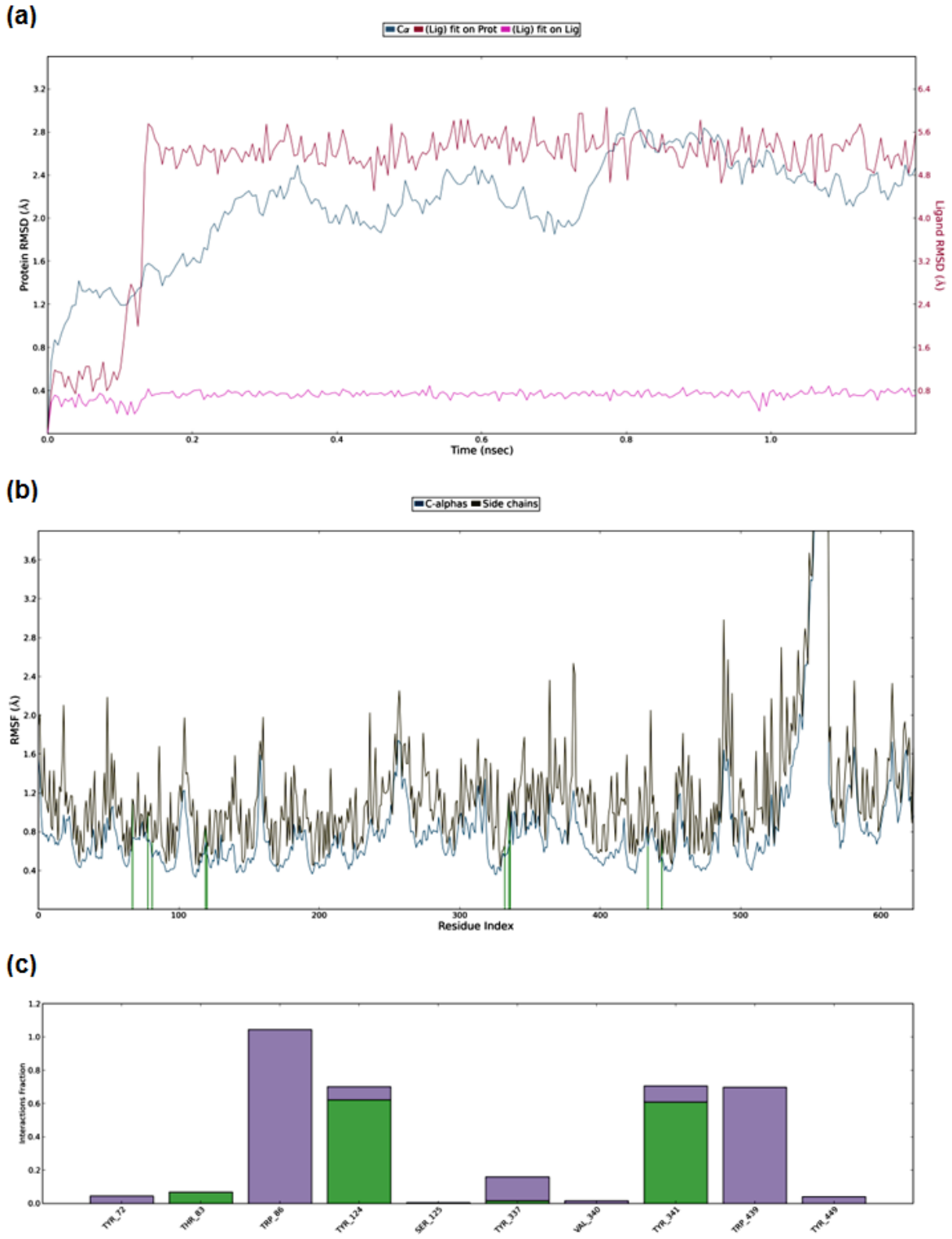

Figure S10. RMSDs (**a**), RMSFs (**b**), and Interaction diagrams (**c**) of *h*AChE in complex with atrazine. The green bars present hydrogen bonds, the purple bars show hydrophobic interactions, the pink bars show ionic interaction, the blue bars present water bridges.

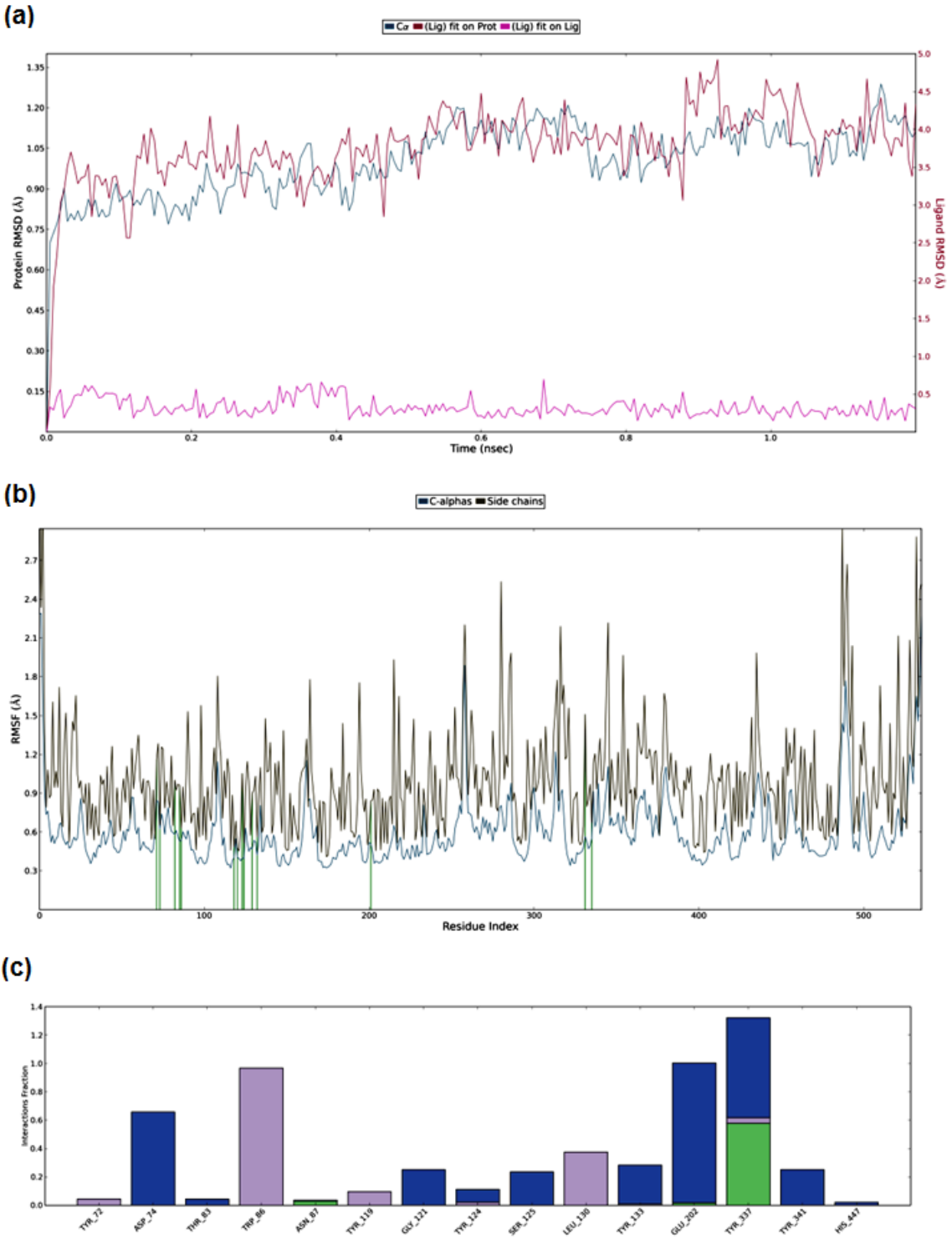

Figure S11. RMSDs (**a**), RMSFs (**b**), and Interaction diagrams (**c**) of *m*AChE in complex with propazine. The green bars present hydrogen bonds, the purple bars show hydrophobic interactions, the pink bars show ionic interaction, the blue bars present water bridges.

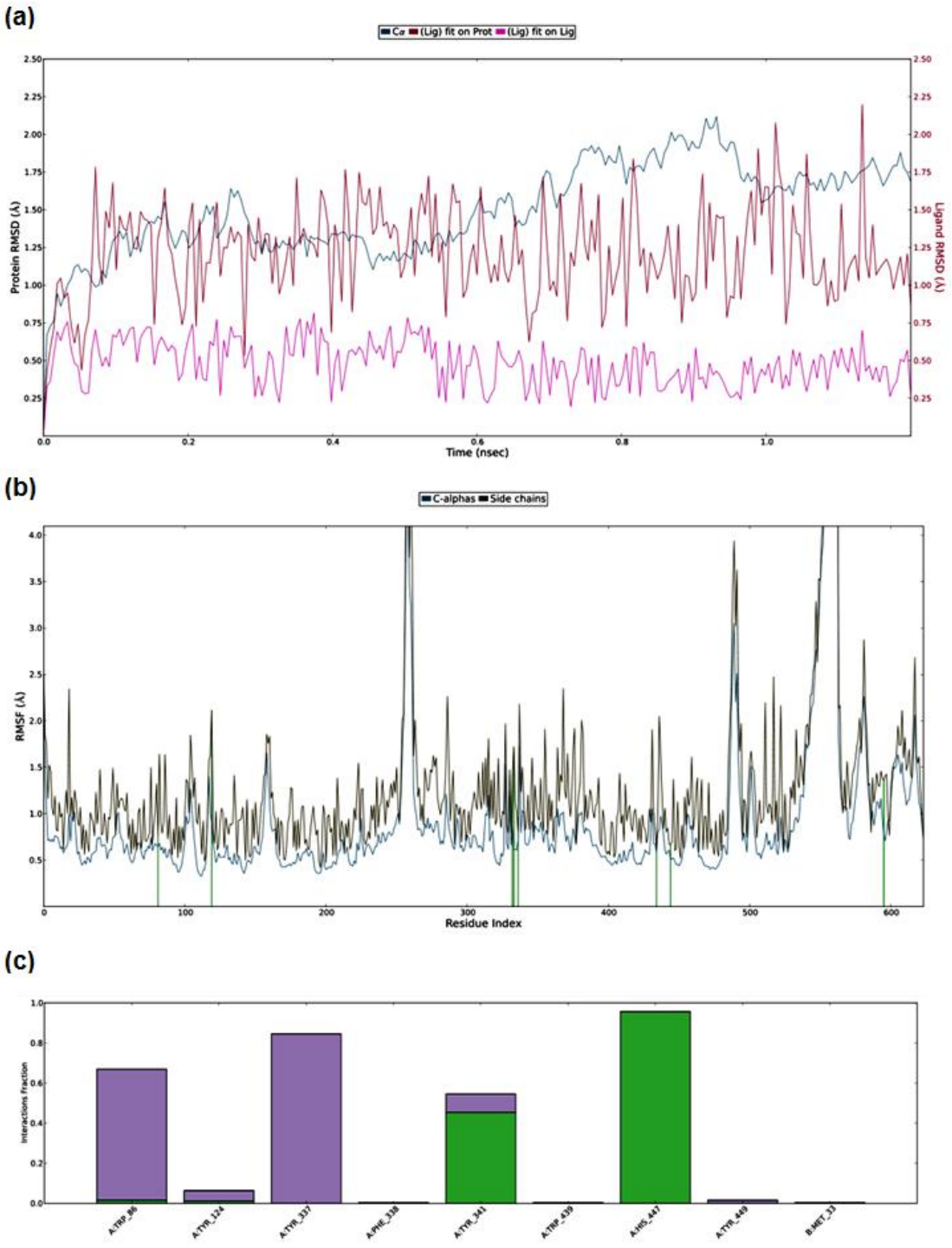

Figure S12. RMSDs (**a**), RMSFs (**b**), and Interaction diagrams (**c**) of *h*AChE in complex with propazine. The green bars present hydrogen bonds, the purple bars show hydrophobic interactions, the pink bars show ionic interaction, the blue bars present water bridges.

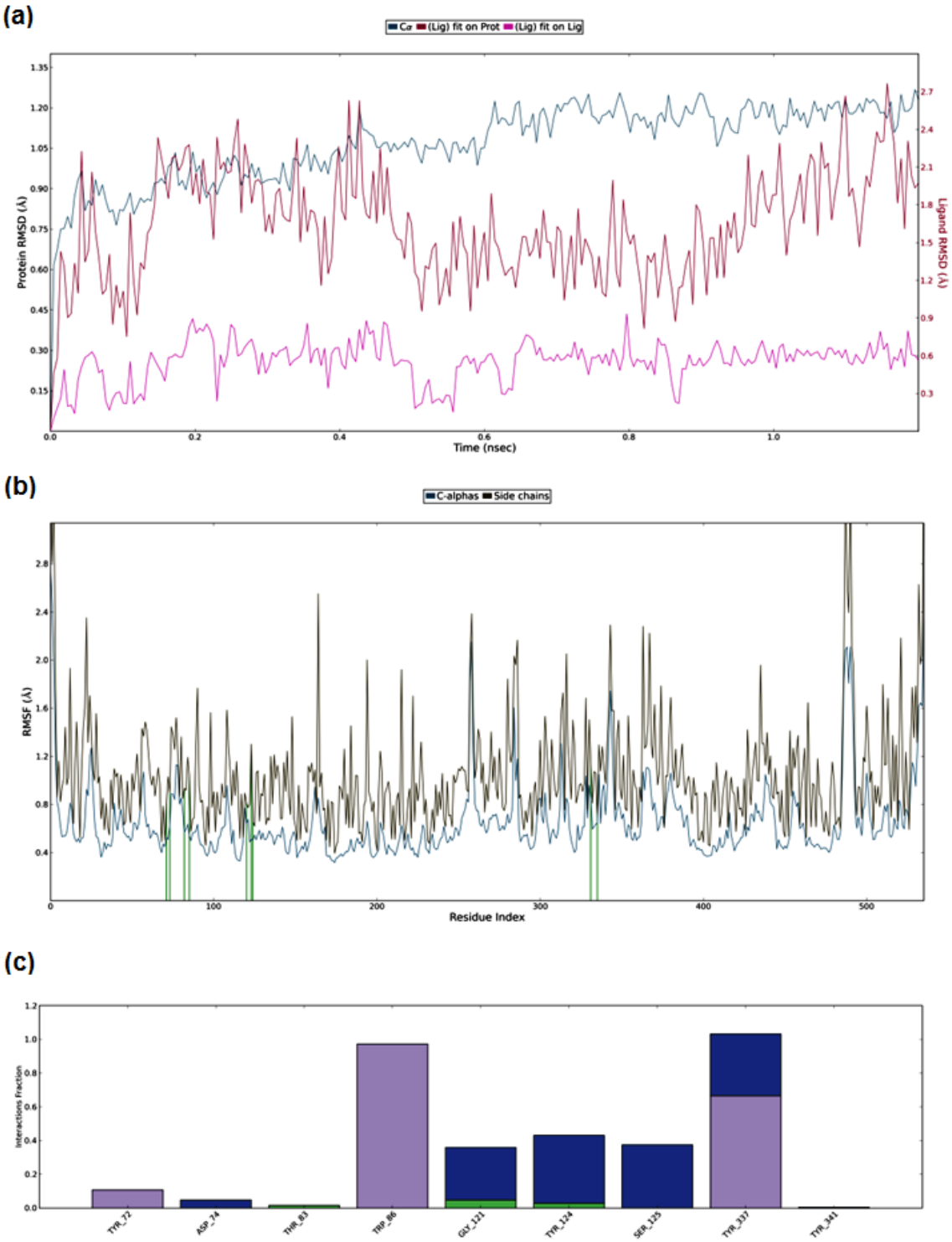

Figure S13. RMSDs (**a**), RMSFs (**b**), and Interaction diagrams (**c**) of *m*AChE in complex with simazine. The green bars present hydrogen bonds, the purple bars show hydrophobic interactions, the pink bars show ionic interaction, the blue bars present water bridges.

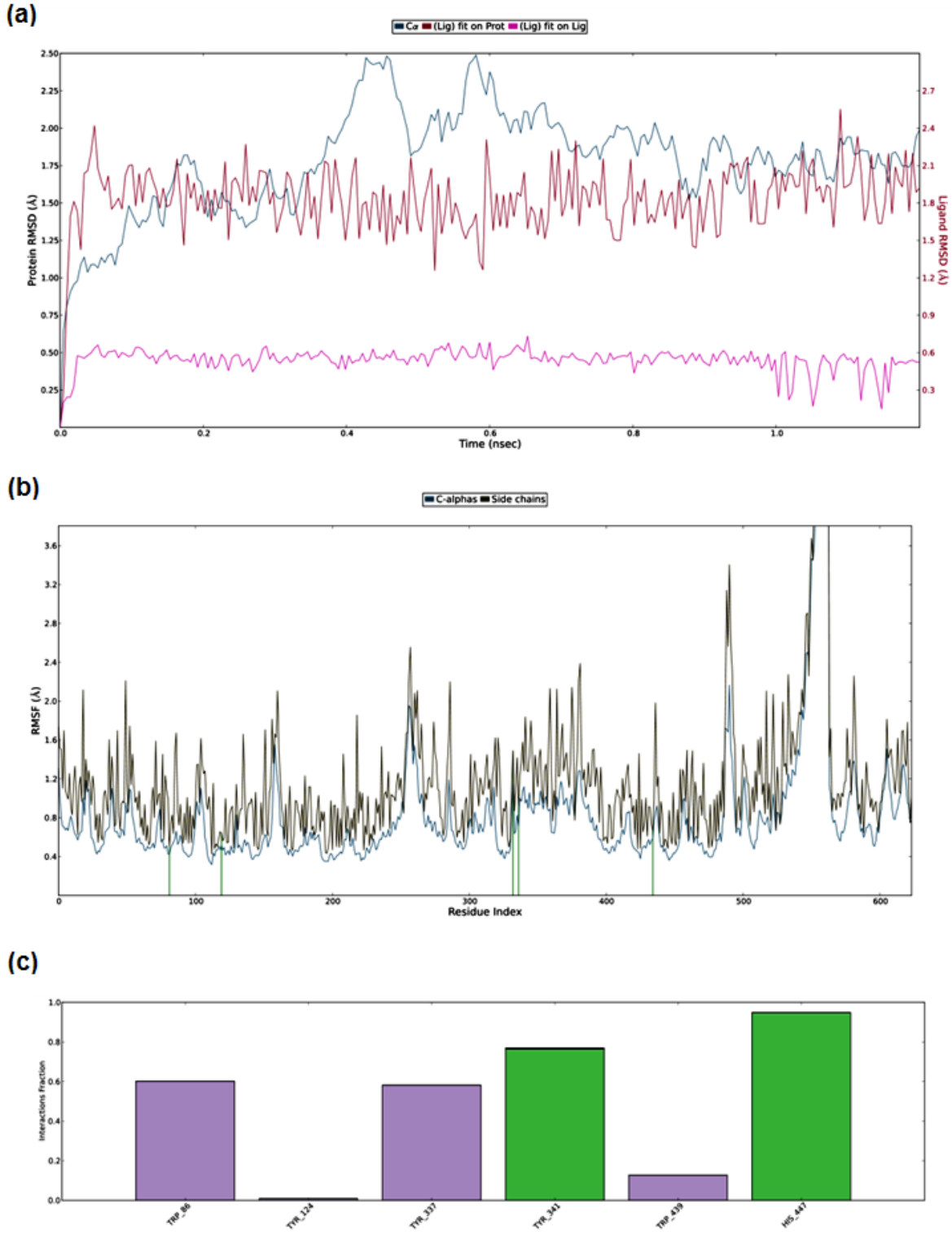

Figure S14. RMSDs (**a**), RMSFs (**b**), and Interaction diagrams (**c**) of *h*AChE in complex with simazine. The green bars present hydrogen bonds, the purple bars show hydrophobic interactions, the pink bars show ionic interaction, the blue bars present water bridges.

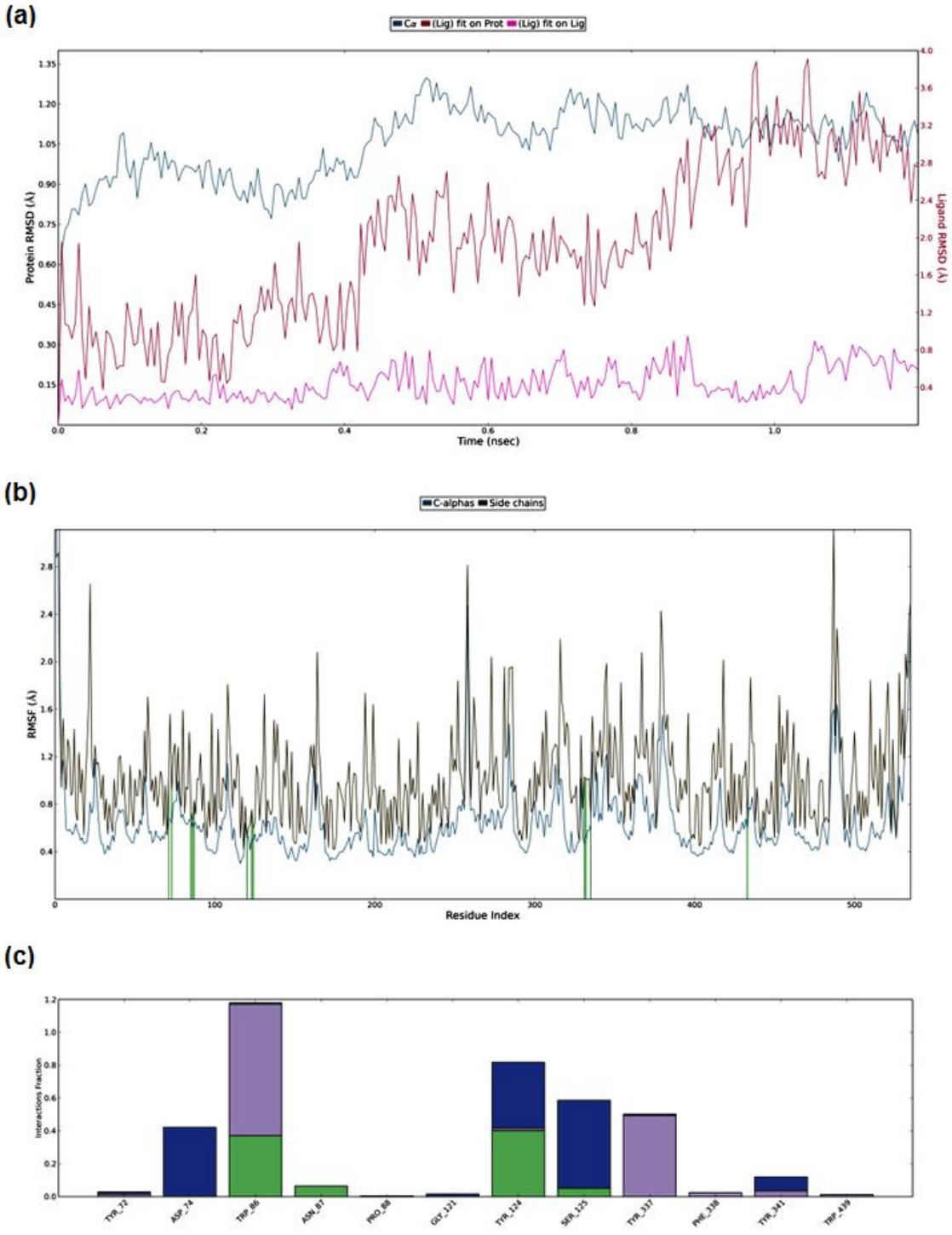

Figure S15. RMSDs (**a**), RMSFs (**b**), and Interaction diagrams (**c**) of *m*AChE in complex with carbofuran. The green bars present hydrogen bonds, the purple bars show hydrophobic interactions, the pink bars show ionic interaction, the blue bars present water bridges.

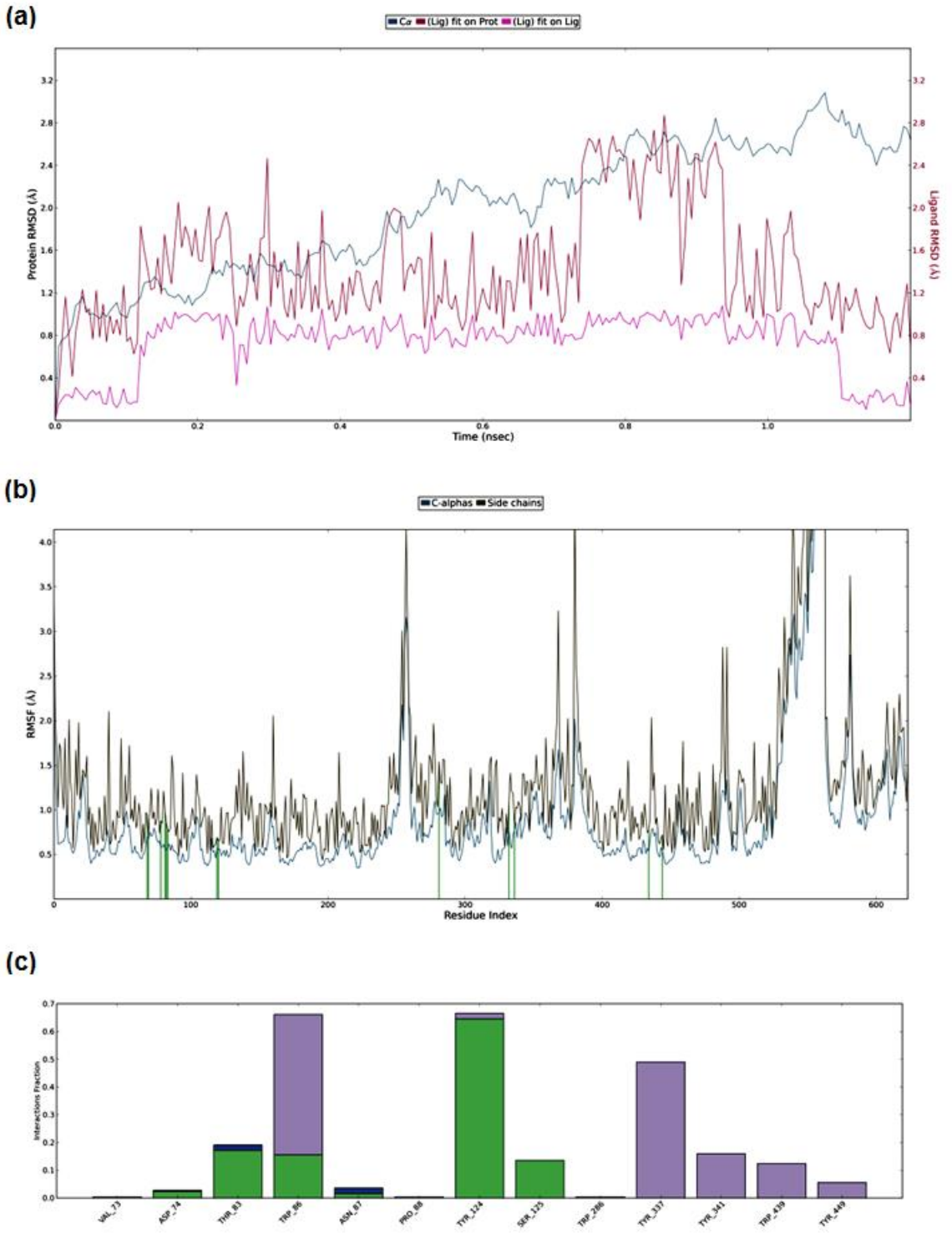

Figure S16. RMSDs (**a**), RMSFs (**b**), and Interaction diagrams (**c**) of *h*AChE in complex with carbofuran. The green bars present hydrogen bonds, the purple bars show hydrophobic interactions, the pink bars show ionic interaction, the blue bars present water bridges.

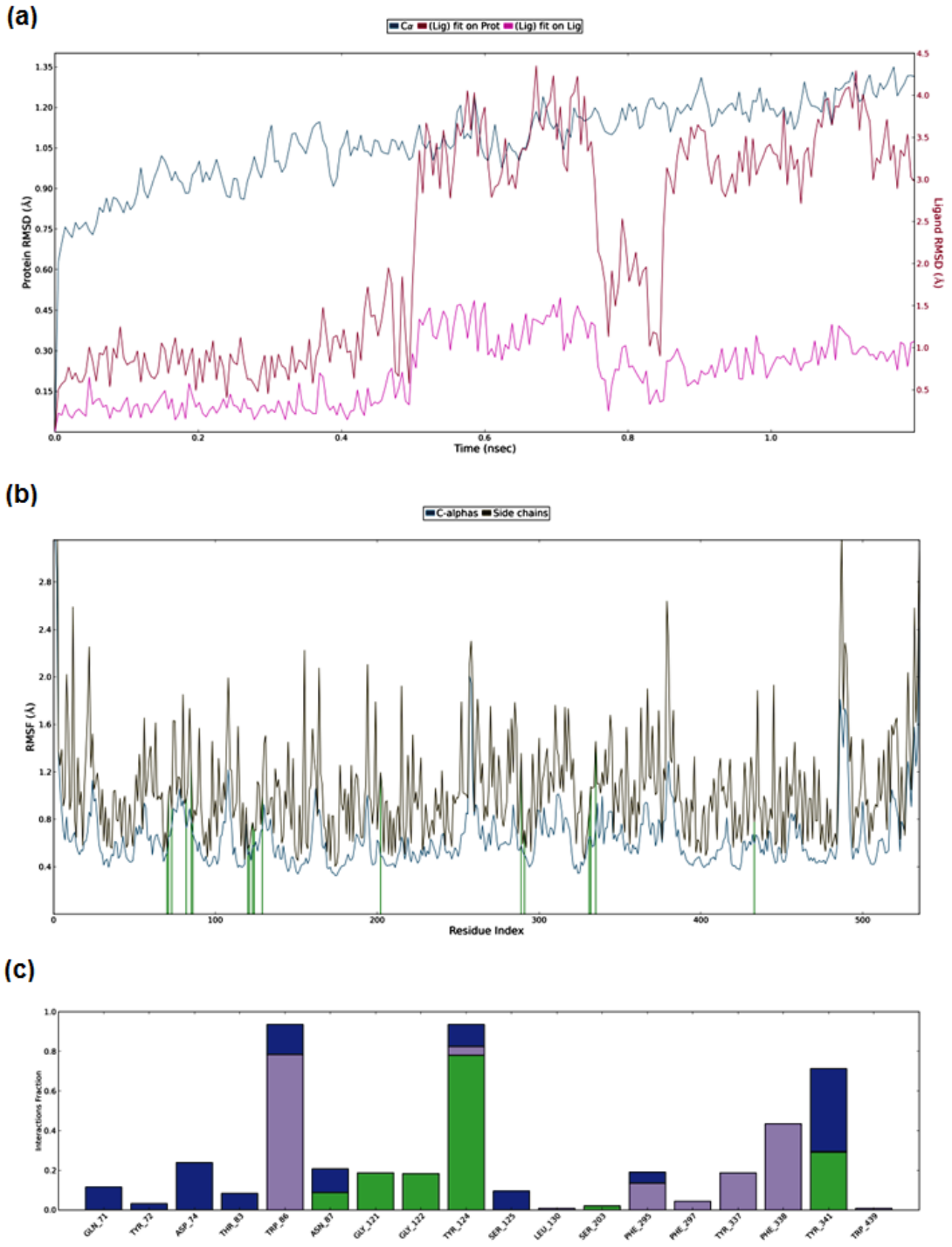

Figure S17. RMSDs (**a**), RMSFs (**b**), and Interaction diagrams (**c**) of *m*AChE in complex with monocrotophos. The green bars present hydrogen bonds, the purple bars show hydrophobic interactions, the pink bars show ionic interaction, the blue bars present water bridges.

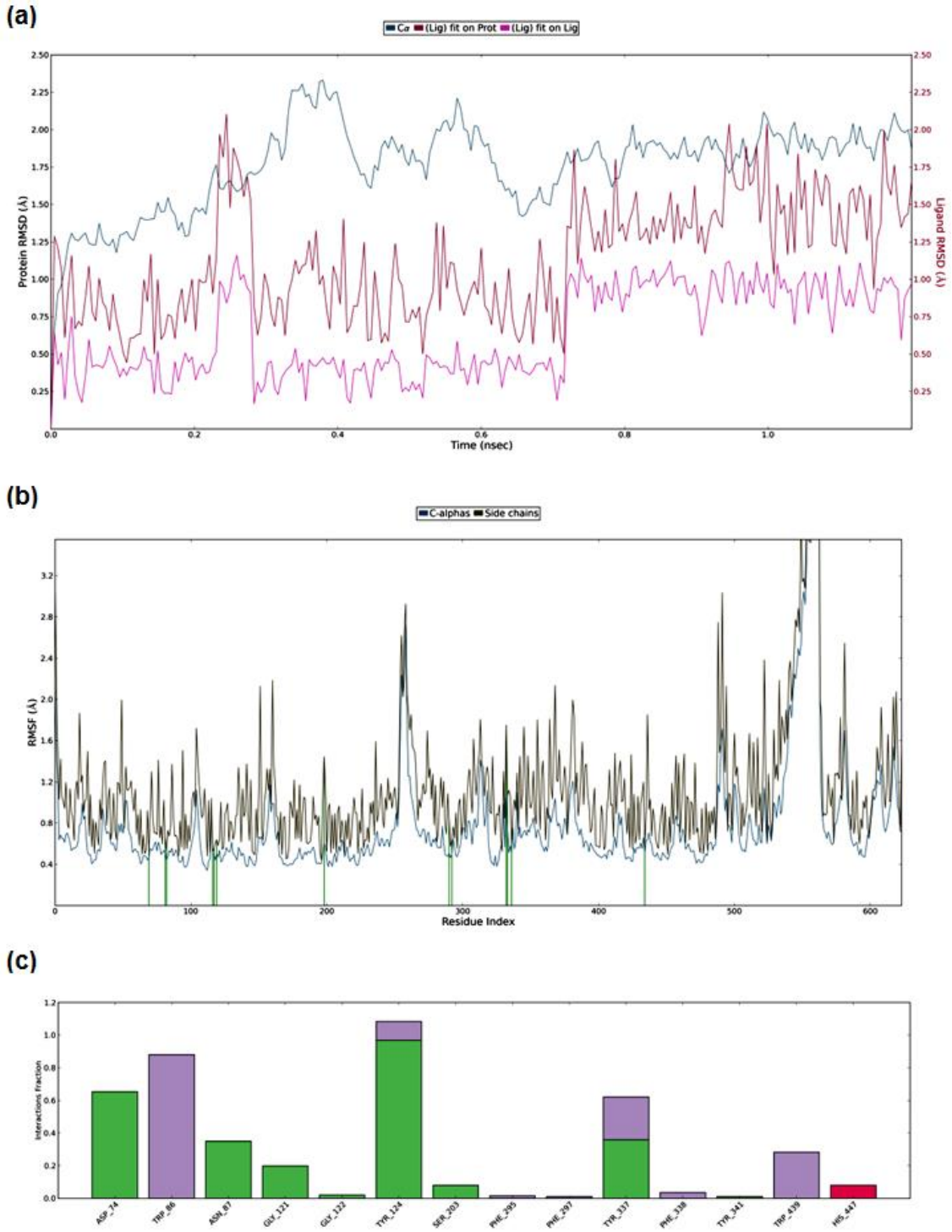

Figure S18. RMSDs (**a**), RMSFs (**b**), and Interaction diagrams (**c**) of *h*AChE in complex with monocrotophos. The green bars present hydrogen bonds, the purple bars show hydrophobic interactions, the pink bars show ionic interaction, the blue bars present water bridges.

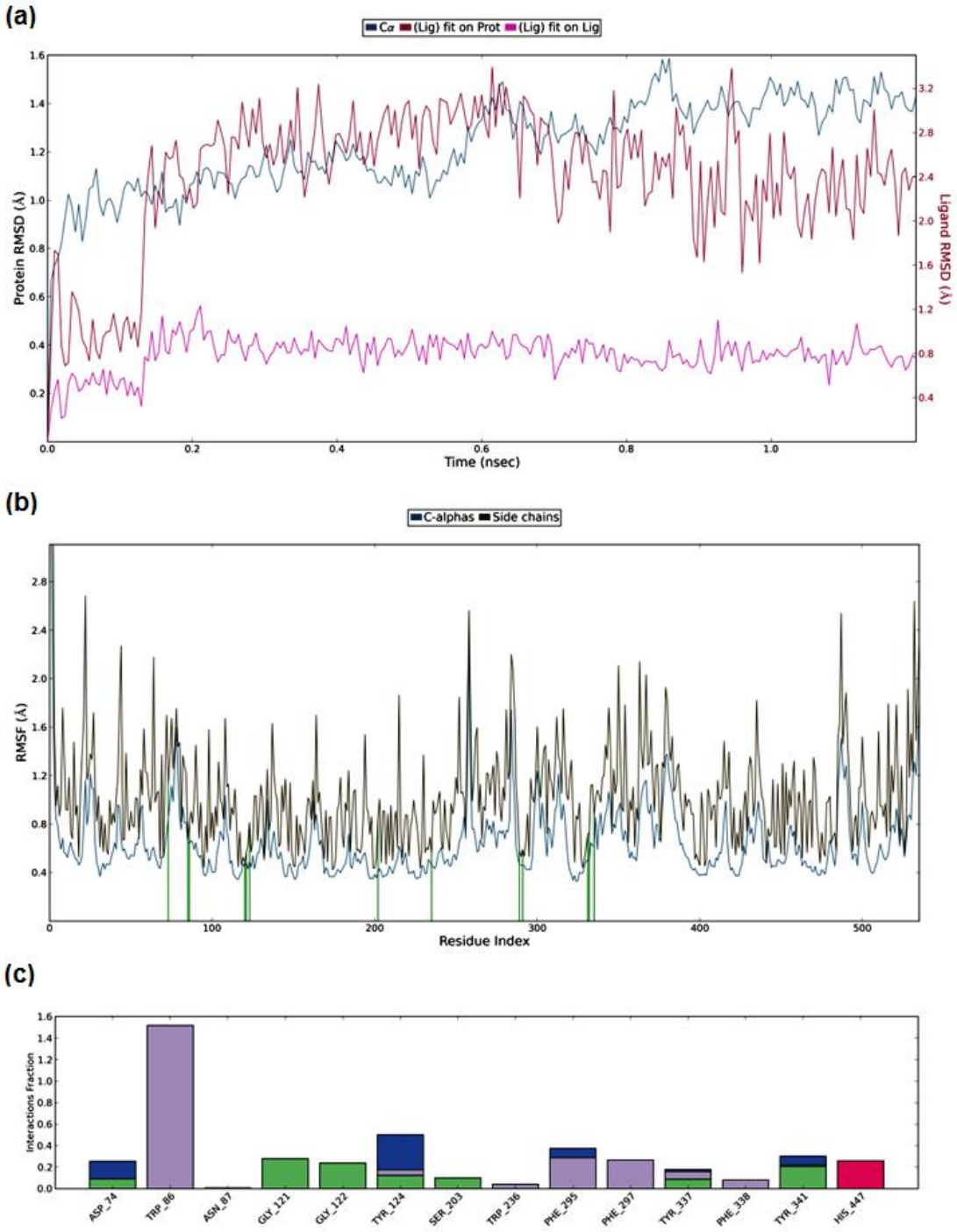

Figure S19. RMSDs (**a**), RMSFs (**b**), and Interaction diagrams (**c**) of *m*AChE in complex with dimethoate. The green bars present hydrogen bonds, the purple bars show hydrophobic interactions, the pink bars show ionic interaction, the blue bars present water bridges.

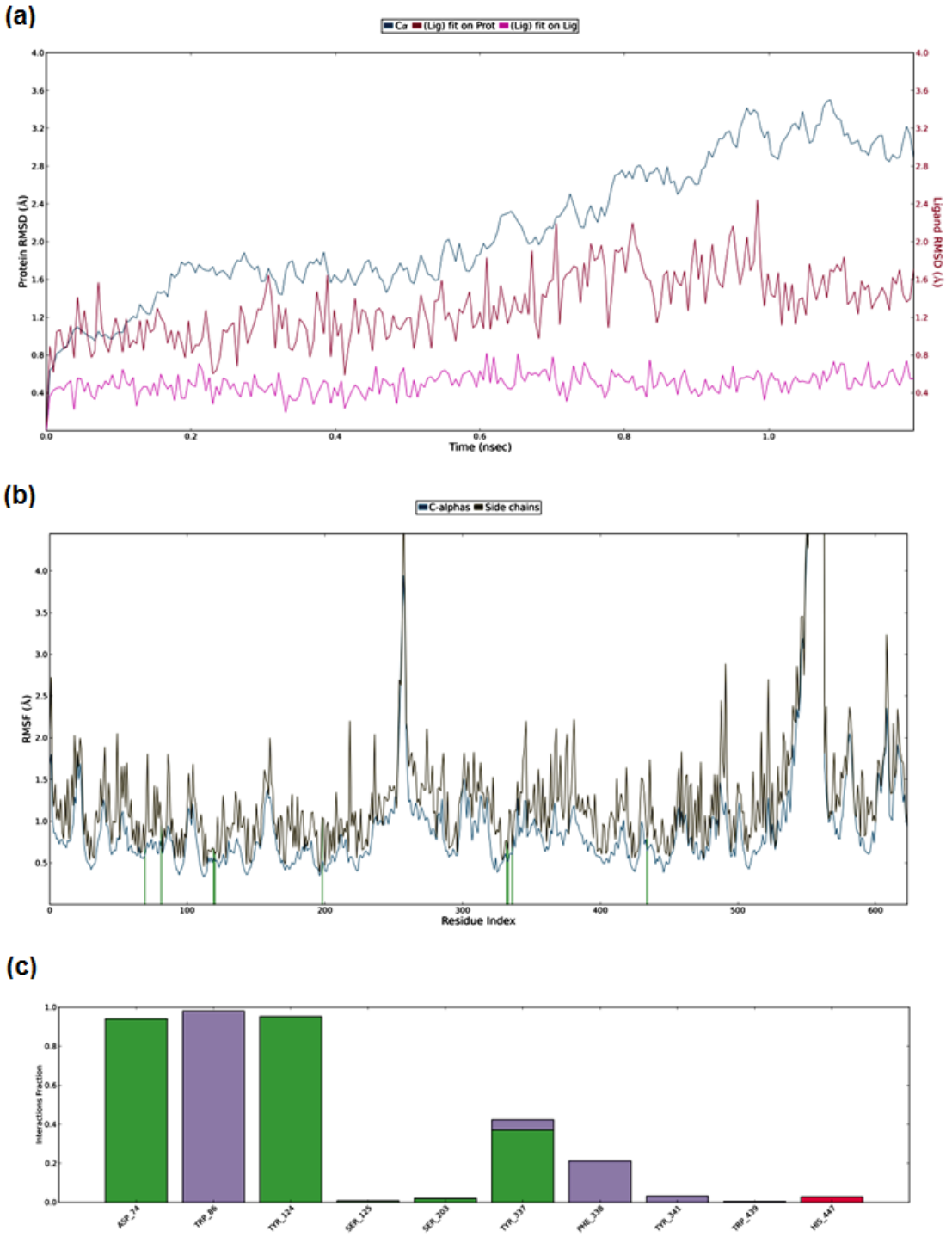

Figure S20. RMSDs (**a**), RMSFs (**b**), and Interaction diagrams (**c**) of *h*AChE in complex with dimethoate. The green bars present hydrogen bonds, the purple bars show hydrophobic interactions, the pink bars show ionic interaction, the blue bars present water bridges.

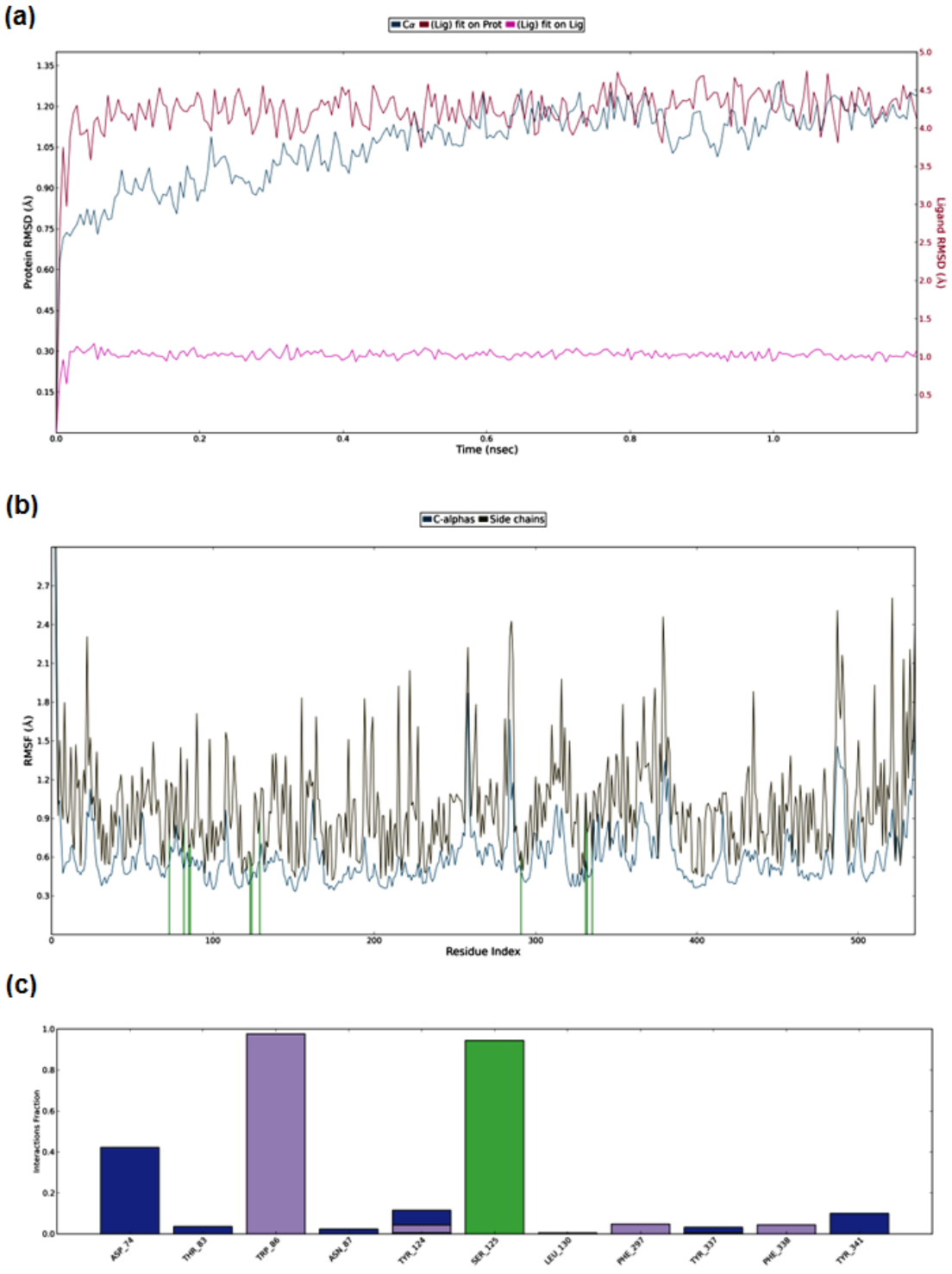

Figure S21. RMSDs (**a**), RMSFs (**b**), and Interaction diagrams (**c**) of *m*AChE in complex with carbaryl. The green bars present hydrogen bonds, the purple bars show hydrophobic interactions, the pink bars show ionic interaction, the blue bars present water bridges.

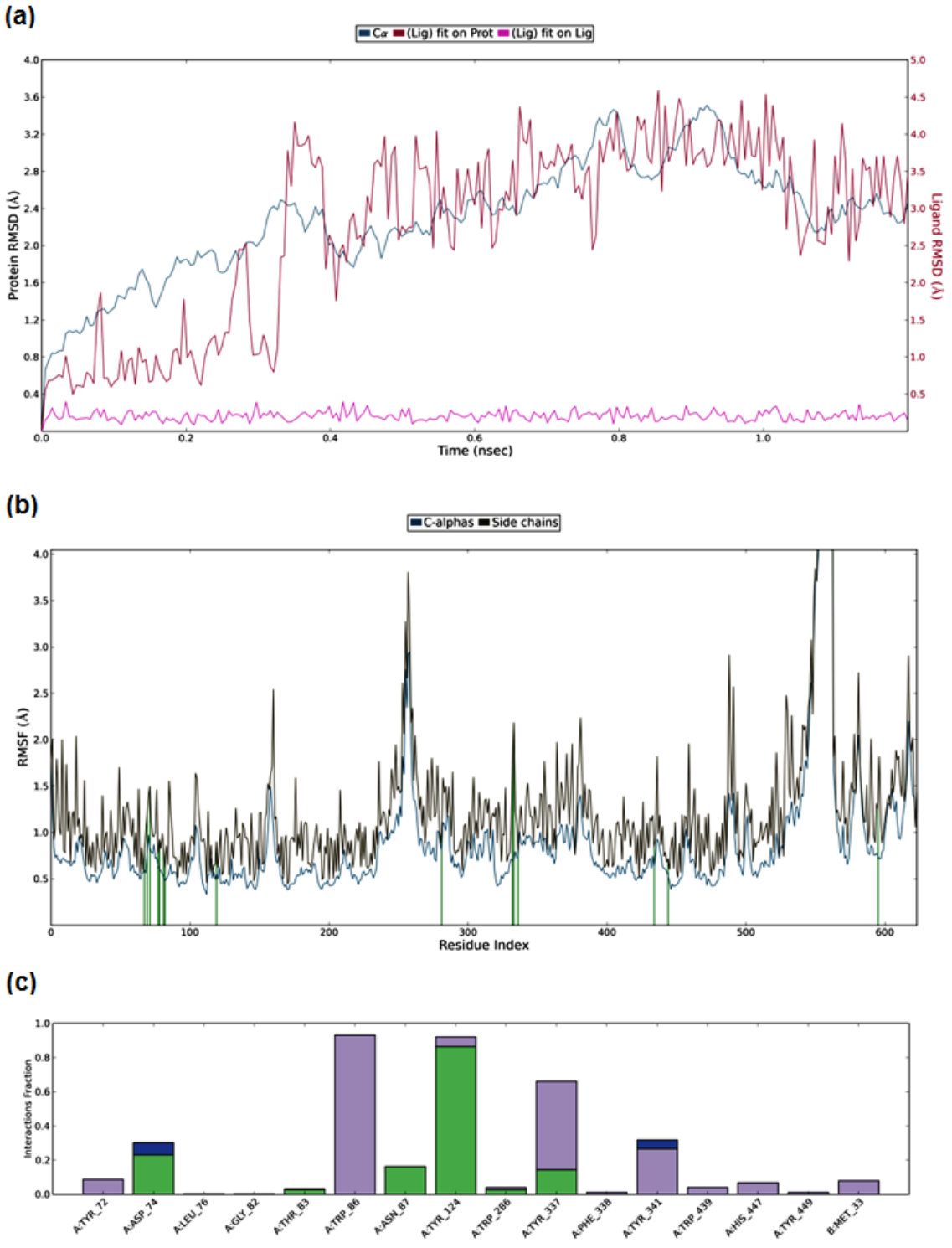

Figure S22. RMSDs (**a**), RMSFs (**b**), and Interaction diagrams (**c**) of *h*AChE in complex with carbaryl. The green bars present hydrogen bonds, the purple bars show hydrophobic interactions, the pink bars show ionic interaction, the blue bars present water bridges.

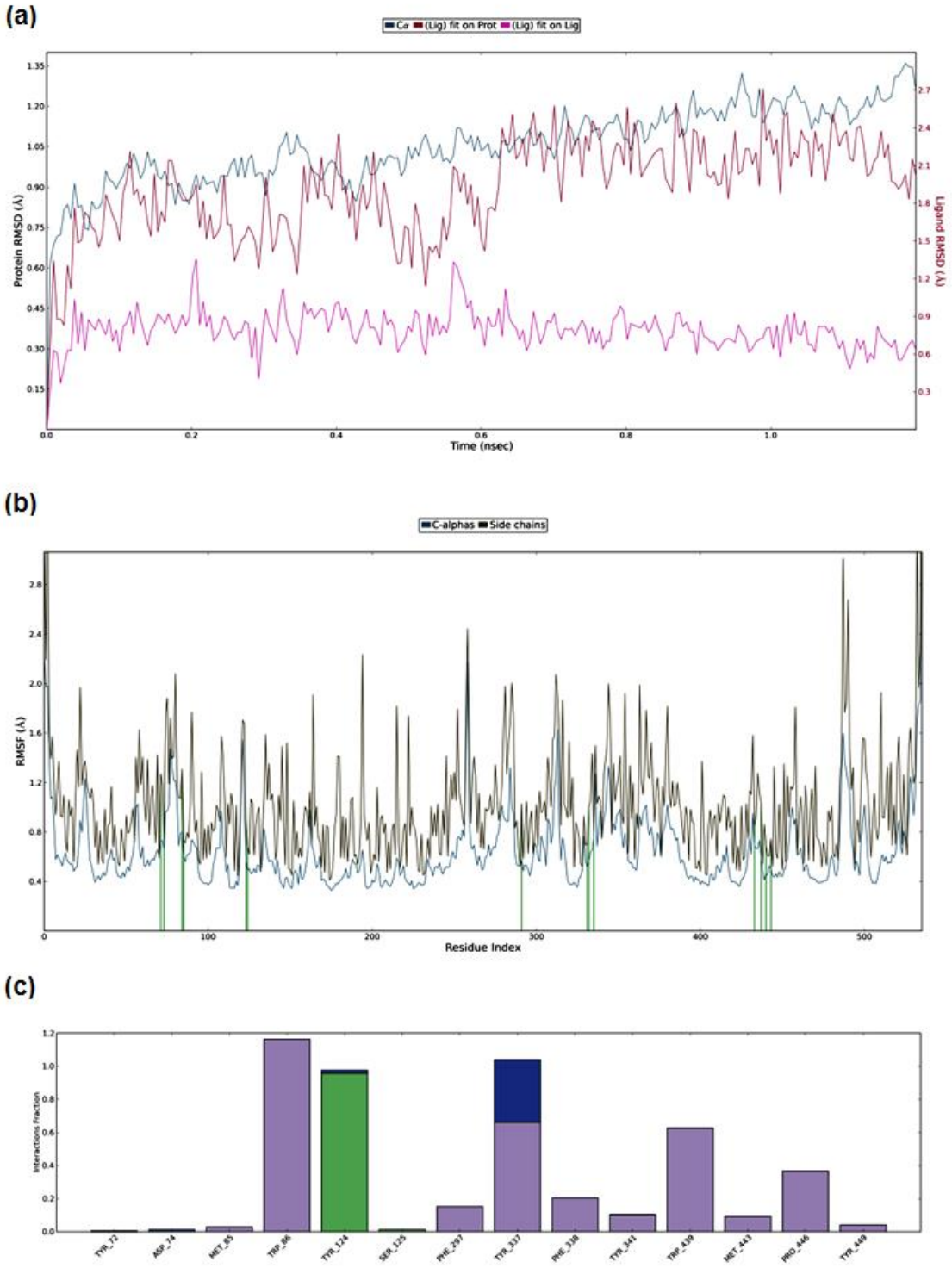

Figure S23. RMSDs (**a**), RMSFs (**b**), and Interaction diagrams (**c**) of *m*AChE in complex with tebufenozide. The green bars present hydrogen bonds, the purple bars show hydrophobic interactions, the pink bars show ionic interaction, the blue bars present water bridges.

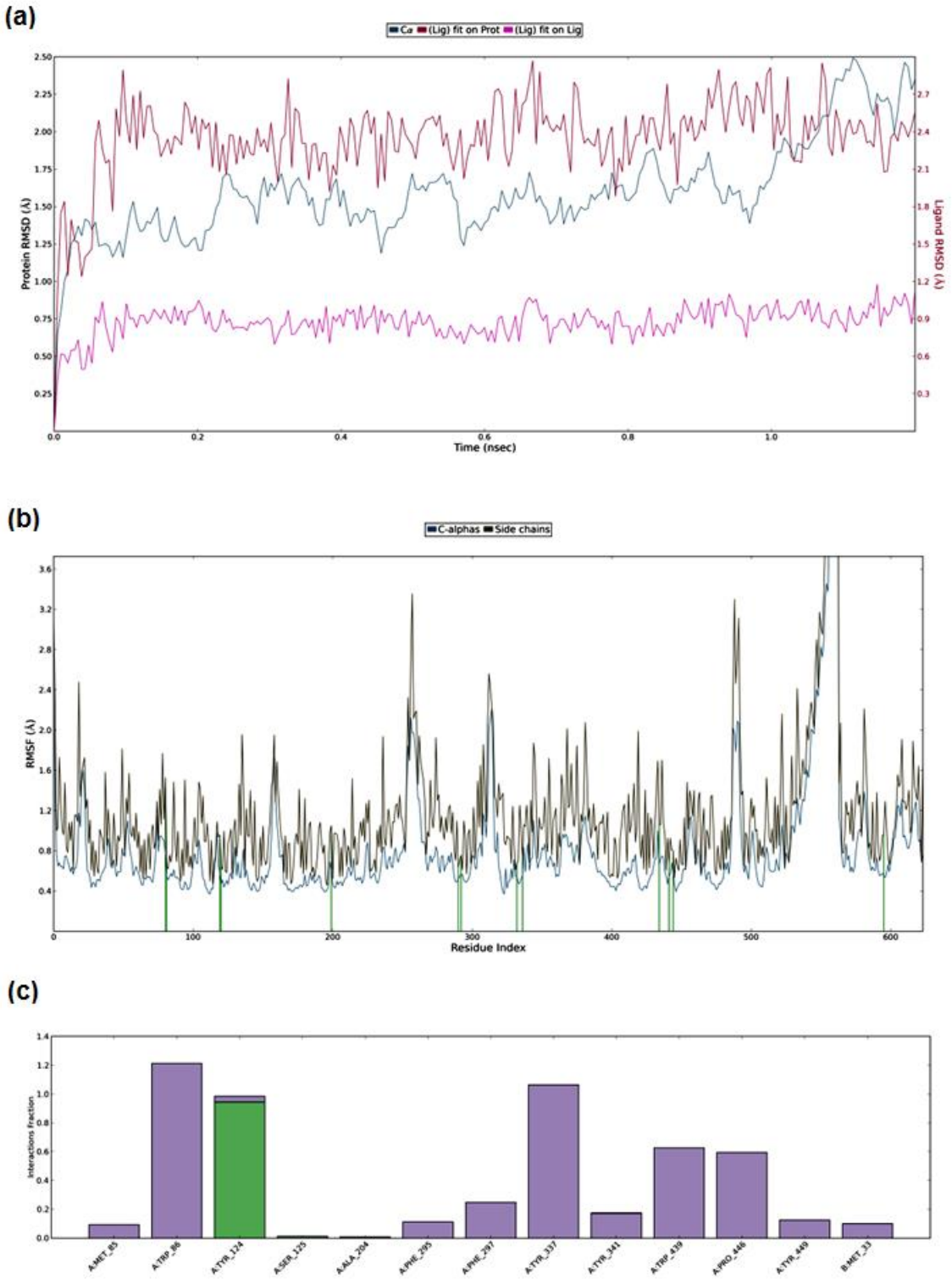

Figure S24. RMSDs (**a**), RMSFs (**b**), and Interaction diagrams (**c**) of *h*AChE in complex with tebufenozide. The green bars present hydrogen bonds, the purple bars show hydrophobic interactions, the pink bars show ionic interaction, the blue bars present water bridges.

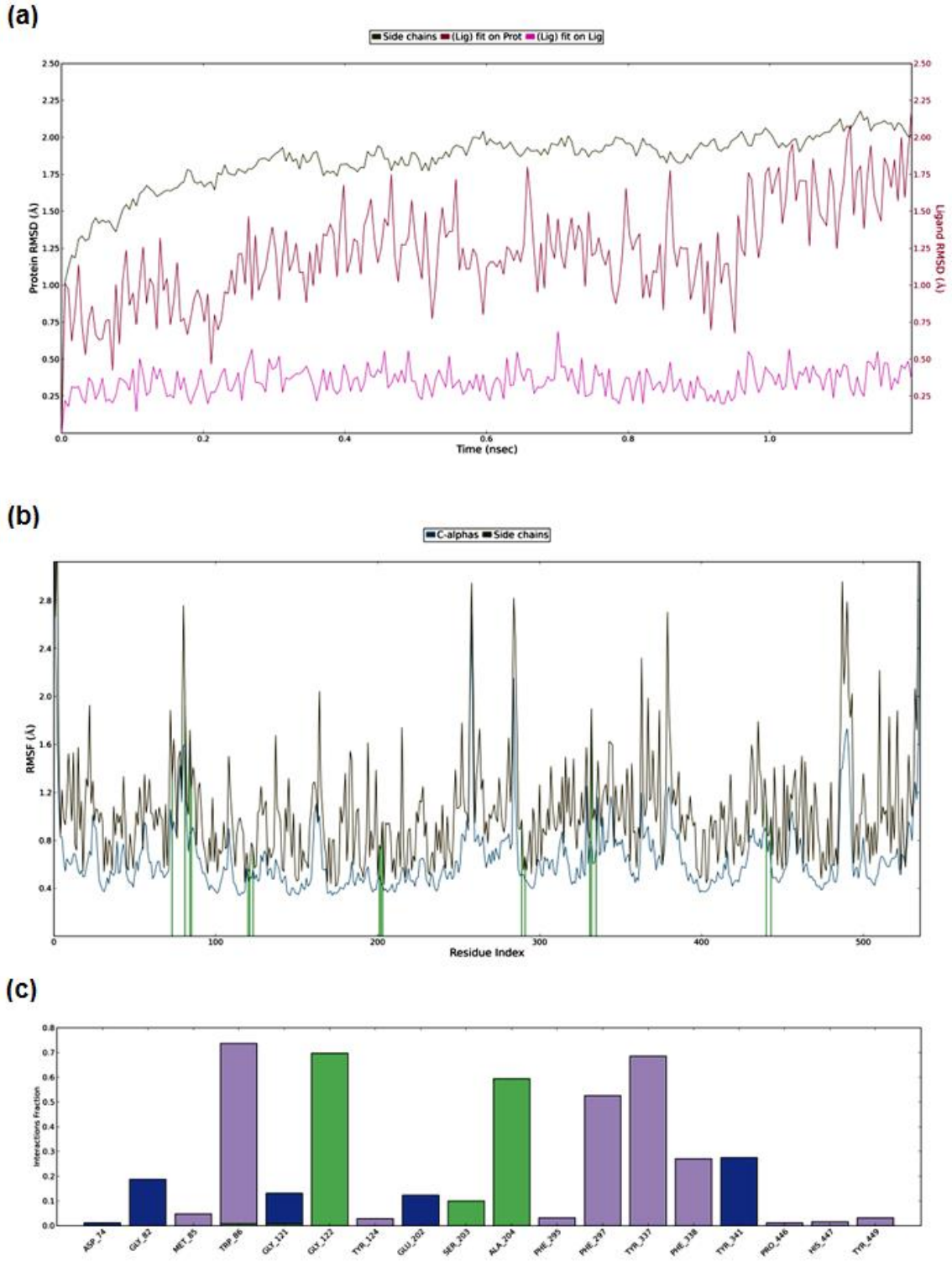

Figure S25. RMSDs (**a**), RMSFs (**b**), and Interaction diagrams (**c**) of *m*AChE in complex with imidacloprid. The green bars present hydrogen bonds, the purple bars show hydrophobic interactions, the pink bars show ionic interaction, the blue bars present water bridges.

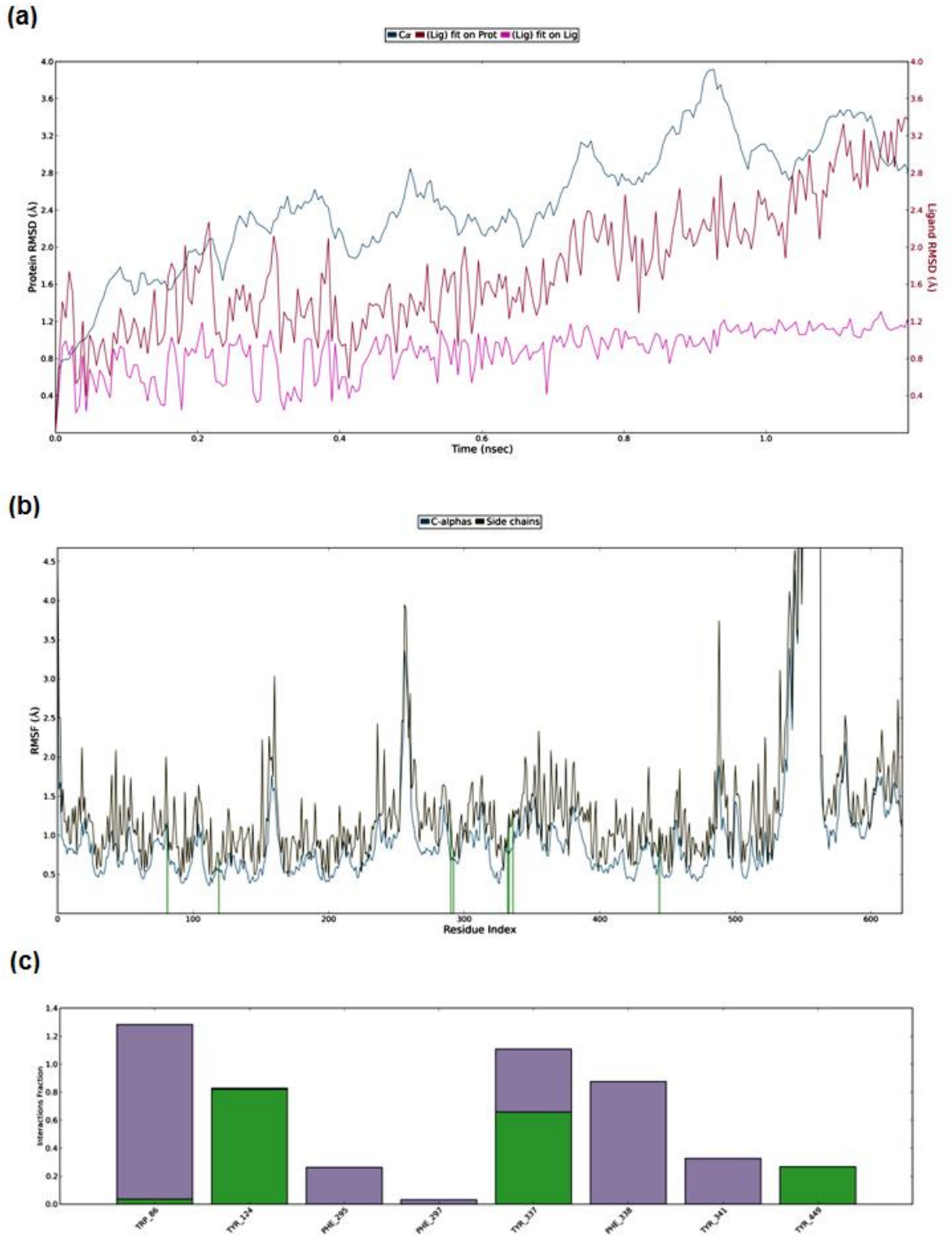

Figure S26. RMSDs (**a**), RMSFs (**b**), Interaction diagrams (**c**) of *h*AChE in complex with imidacloprid. The green bars present hydrogen bonds, the purple bars show hydrophobic interactions, the pink bars show ionic interaction, the blue bars present water bridges.

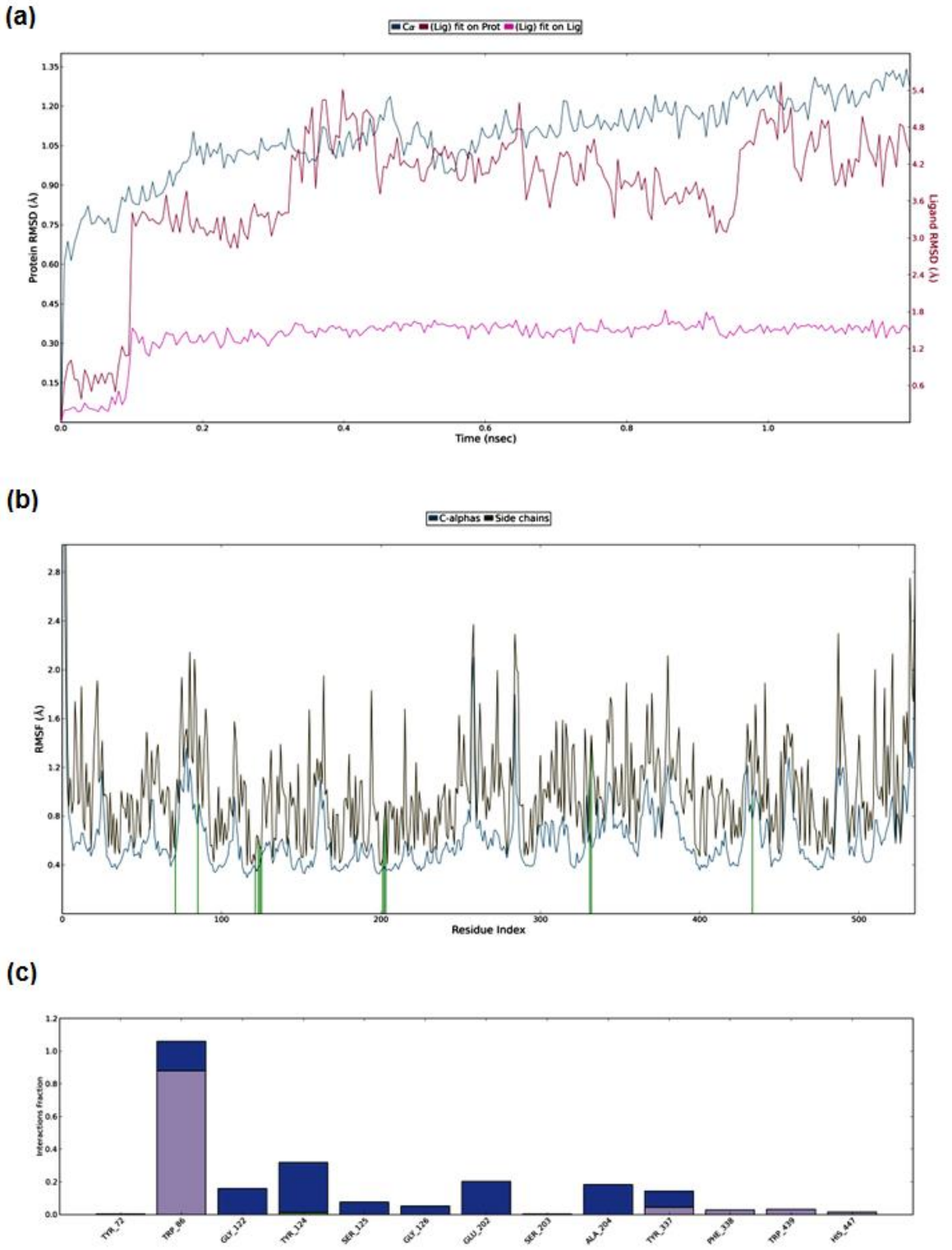

Figure S27. RMSDs (**a**), RMSFs (**b**), and Interaction diagrams (**c**) of *m*AChE in complex with acetamiprid. The green bars present hydrogen bonds, the purple bars show hydrophobic interactions, the pink bars show ionic interaction, the blue bars present water bridges.

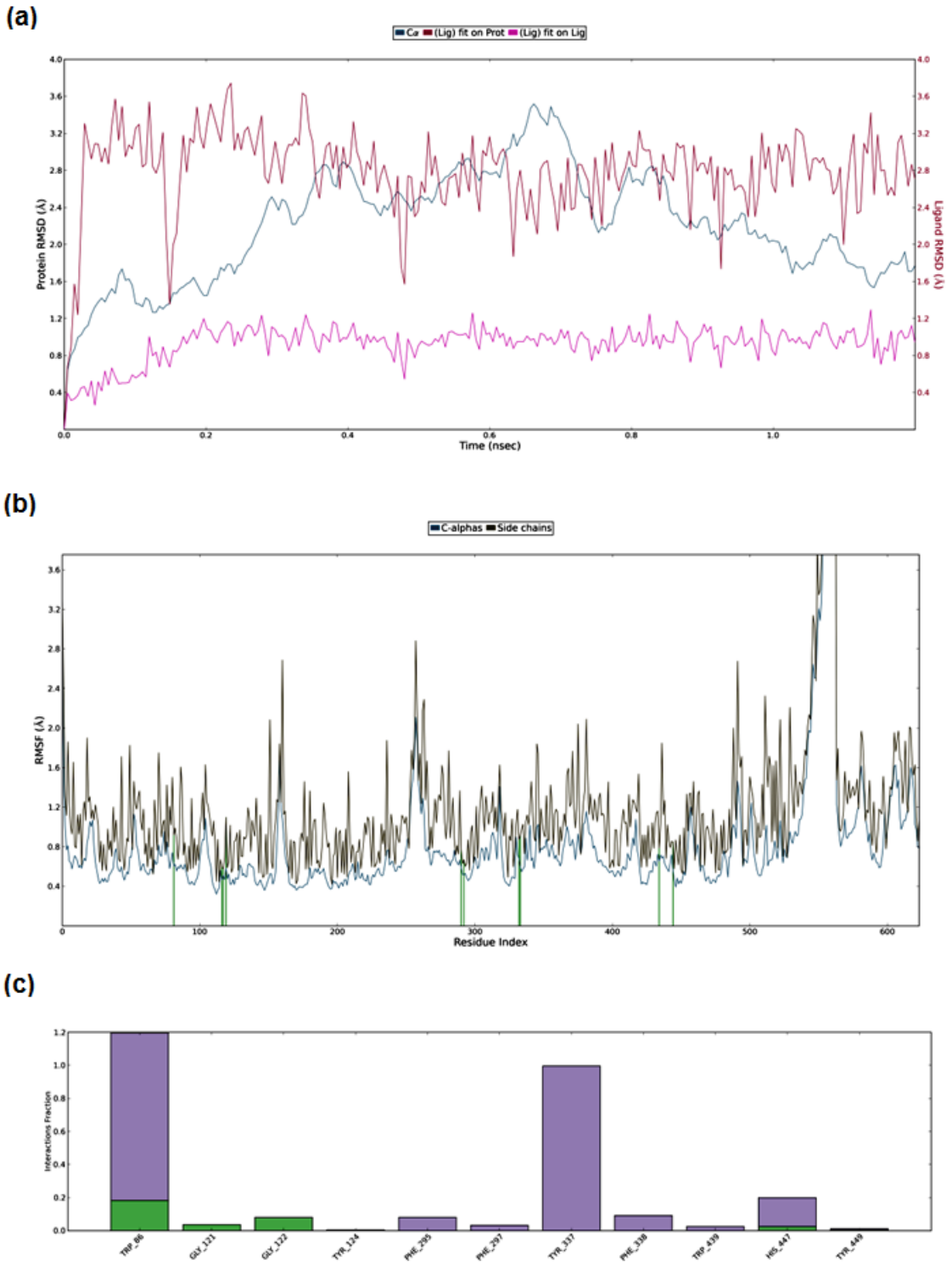

Figure S28. RMSDs (**a**), RMSFs (**b**), and Interaction diagrams (**c**) of *h*AChE in complex with acetamiprid. The green bars present hydrogen bonds, the purple bars show hydrophobic interactions, the pink bars show ionic interaction, the blue bars present water bridges.

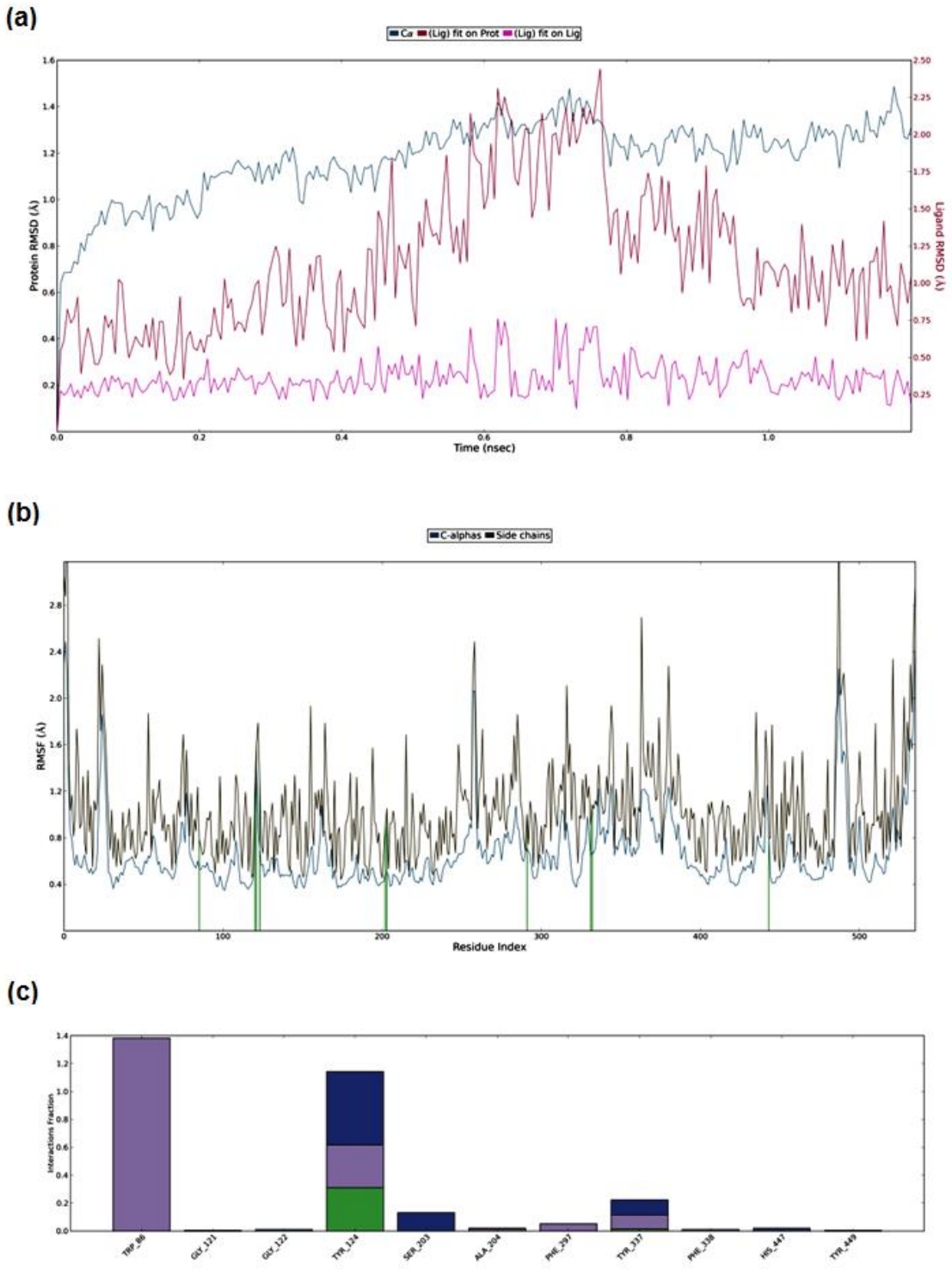

Figure S29. RMSDs (**a**), RMSFs (**b**), and Interaction diagrams (**c**) of *m*AChE in complex with diuron. The green bars present hydrogen bonds, the purple bars show hydrophobic interactions, the pink bars show ionic interaction, the blue bars present water bridges.

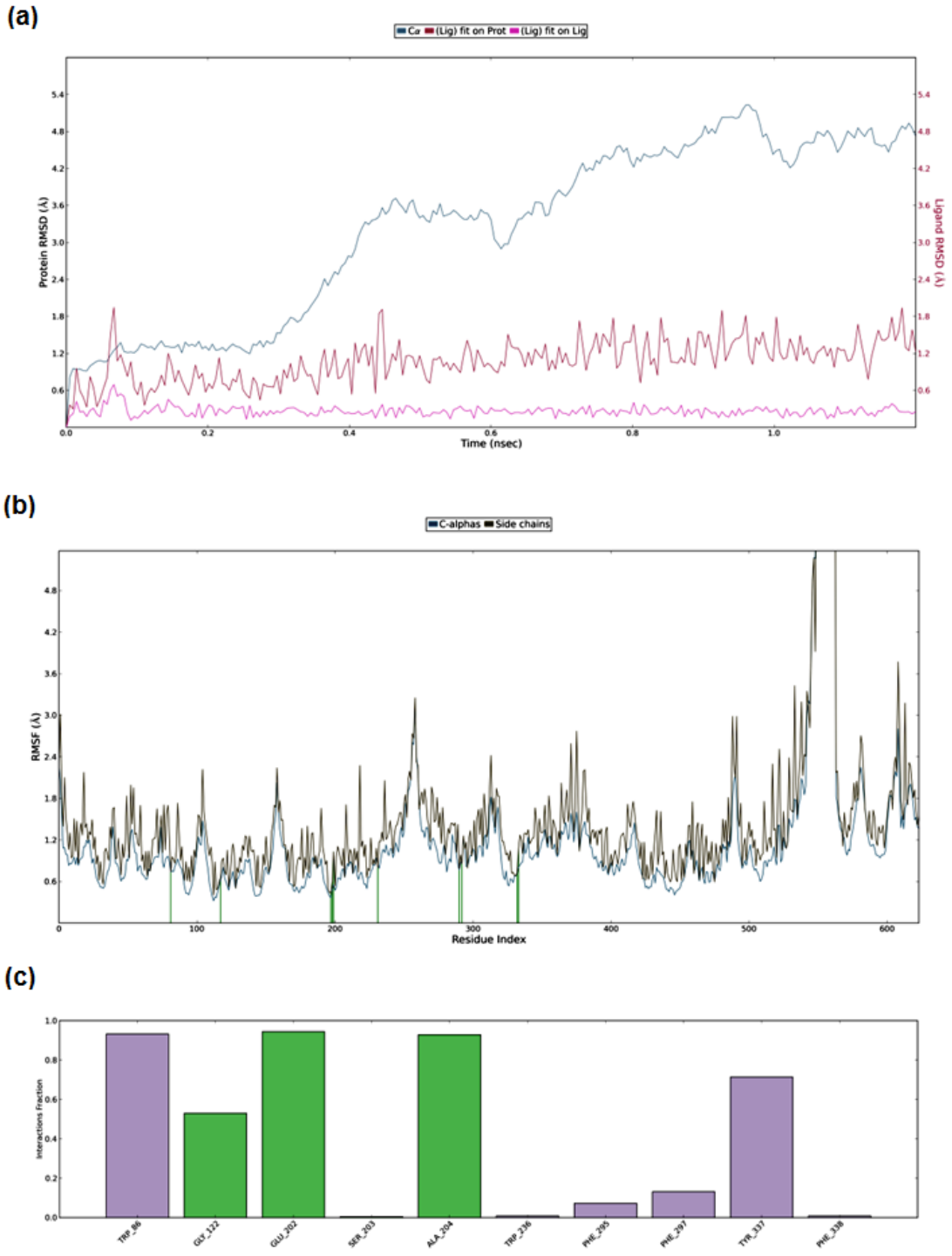

Figure S30. RMSDs (**a**), RMSFs (**b**), and Interaction diagrams (**c**) of *h*AChE in complex with diuron. The green bars present hydrogen bonds, the purple bars show hydrophobic interactions, the pink bars show ionic interaction, the blue bars present water bridges.

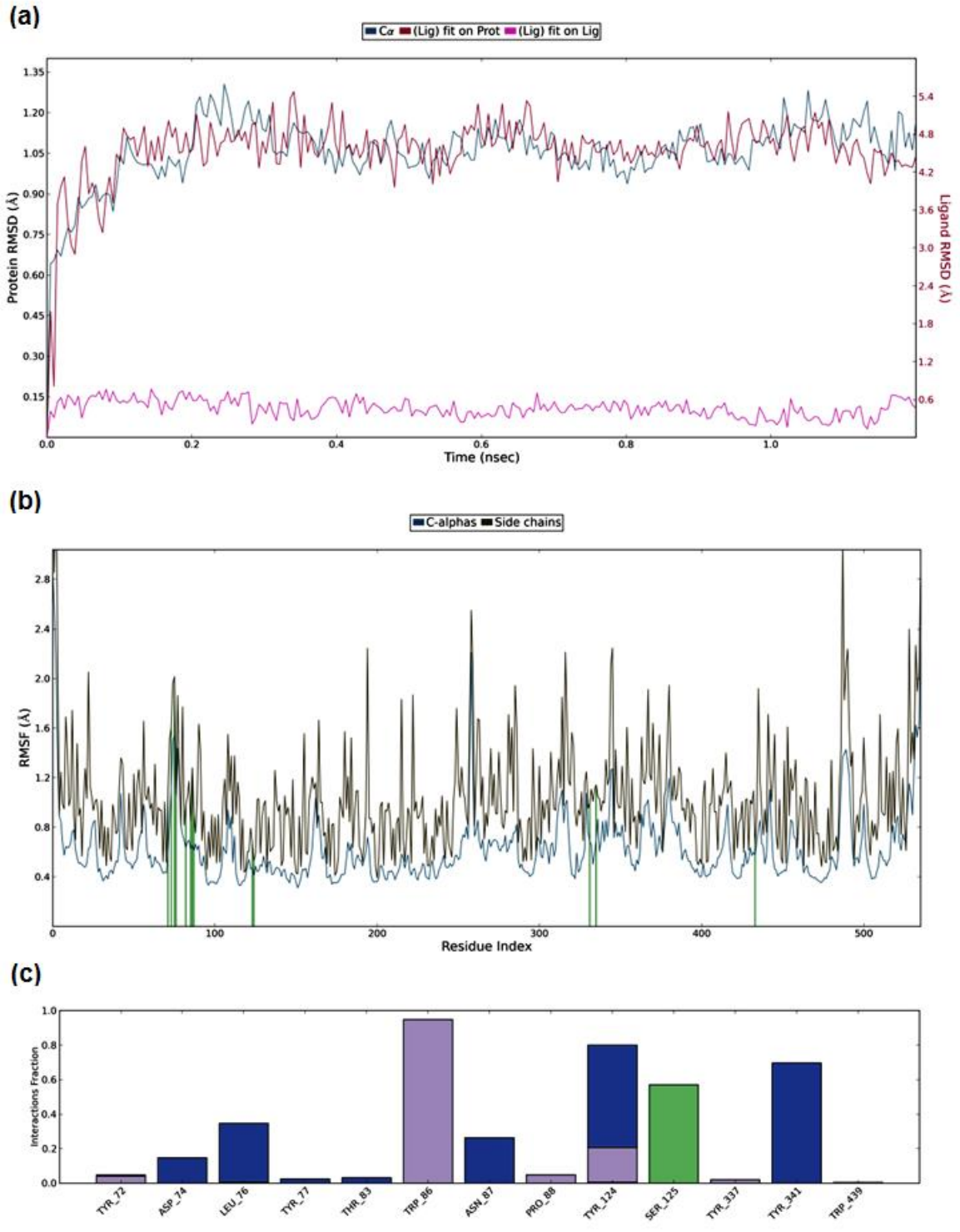

Figure S31. RMSDs (**a**), RMSFs (**b**), and Interaction diagrams (**c**) of *m*AChE in complex with monuron. The green bars present hydrogen bonds, the purple bars show hydrophobic interactions, the pink bars show ionic interaction, the blue bars present water bridges.

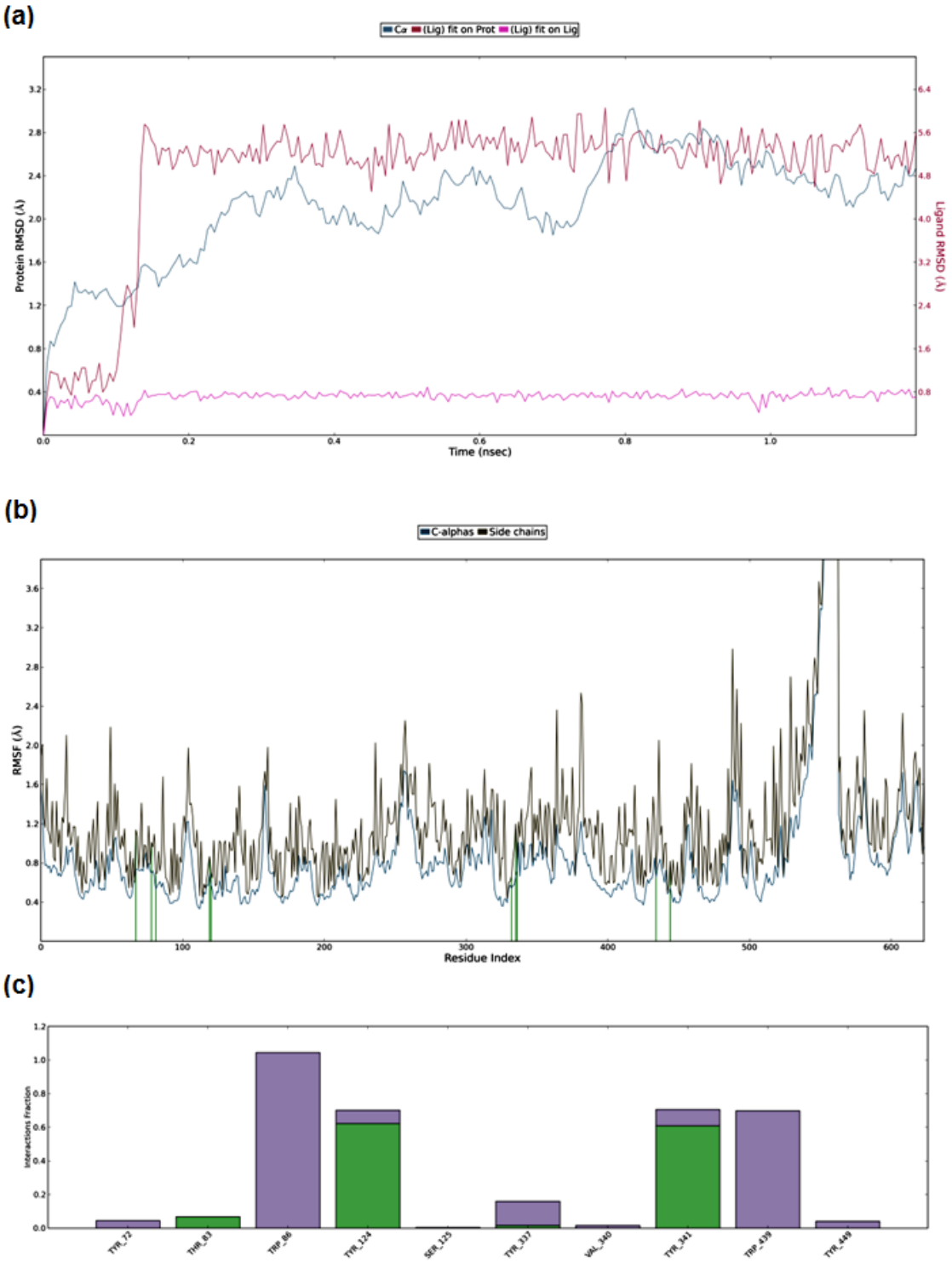

Figure S32. RMSDs (**a**), RMSFs (**b**), and Interaction diagrams (**c**) of *h*AChE in complex with monuron. The green bars present hydrogen bonds, the purple bars show hydrophobic interactions, the pink bars show ionic interaction, the blue bars present water bridges.

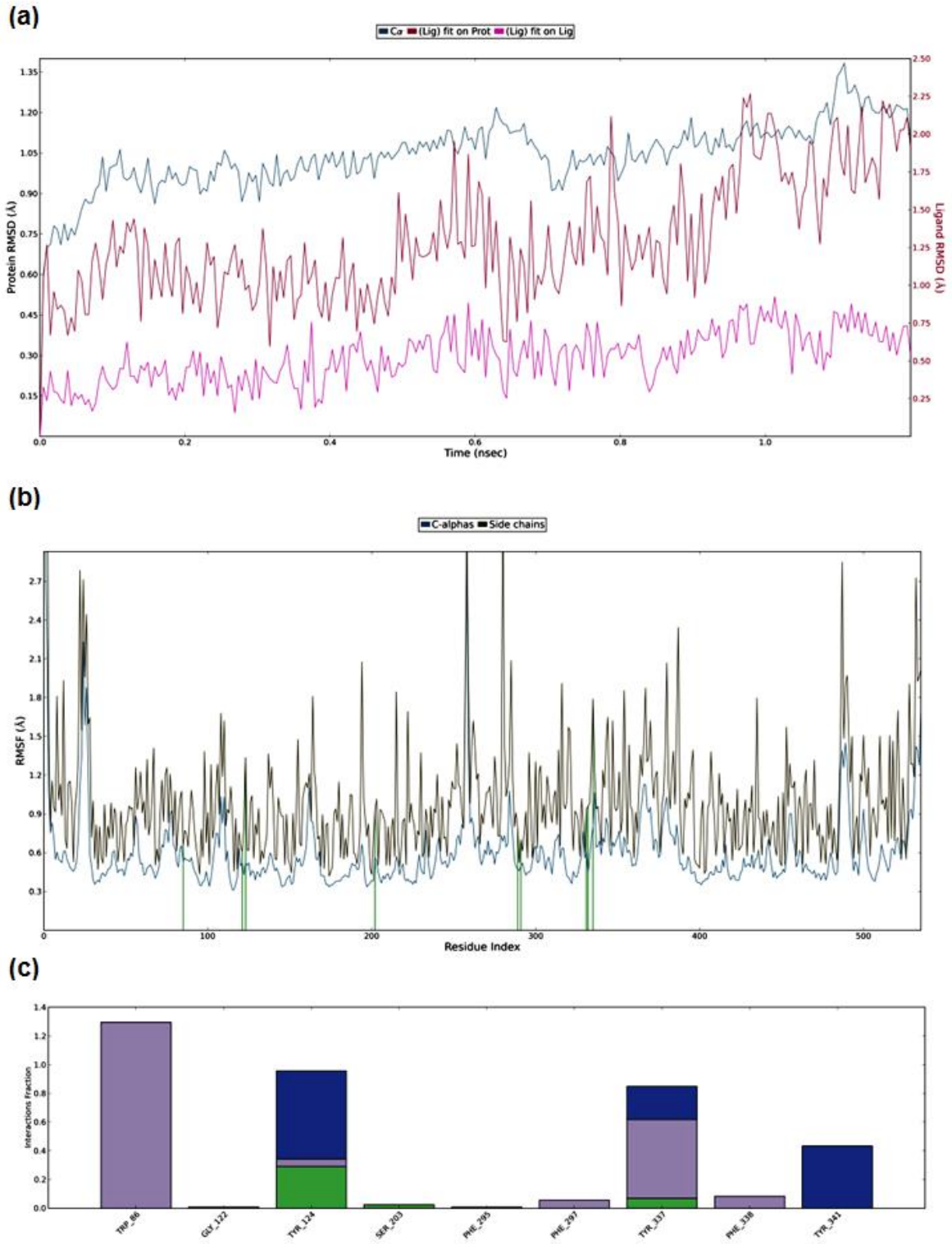

Figure S33. RMSDs (**a**), RMSFs (**b**), and Interaction diagrams (**c**) of *m*AChE in complex with linuron. The green bars present hydrogen bonds, the purple bars show hydrophobic interactions, the pink bars show ionic interaction, the blue bars present water bridges.

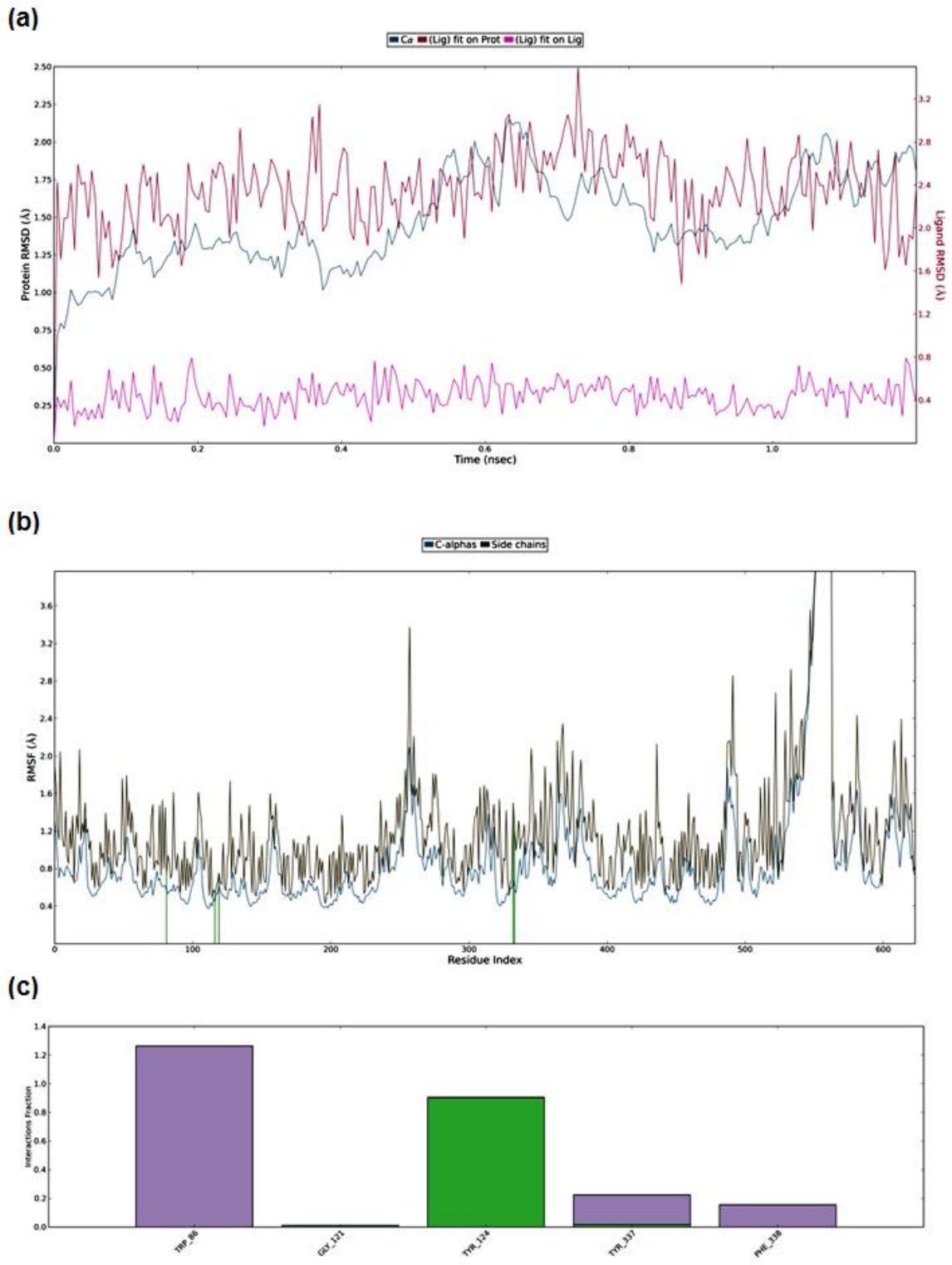

Figure S34. RMSDs (**a**), RMSFs (**b**), and Interaction diagrams (**c**) of *m*AChE in complex with linuron. The green bars present hydrogen bonds, the purple bars show hydrophobic interactions, the pink bars show ionic interaction, the blue bars present water bridges.

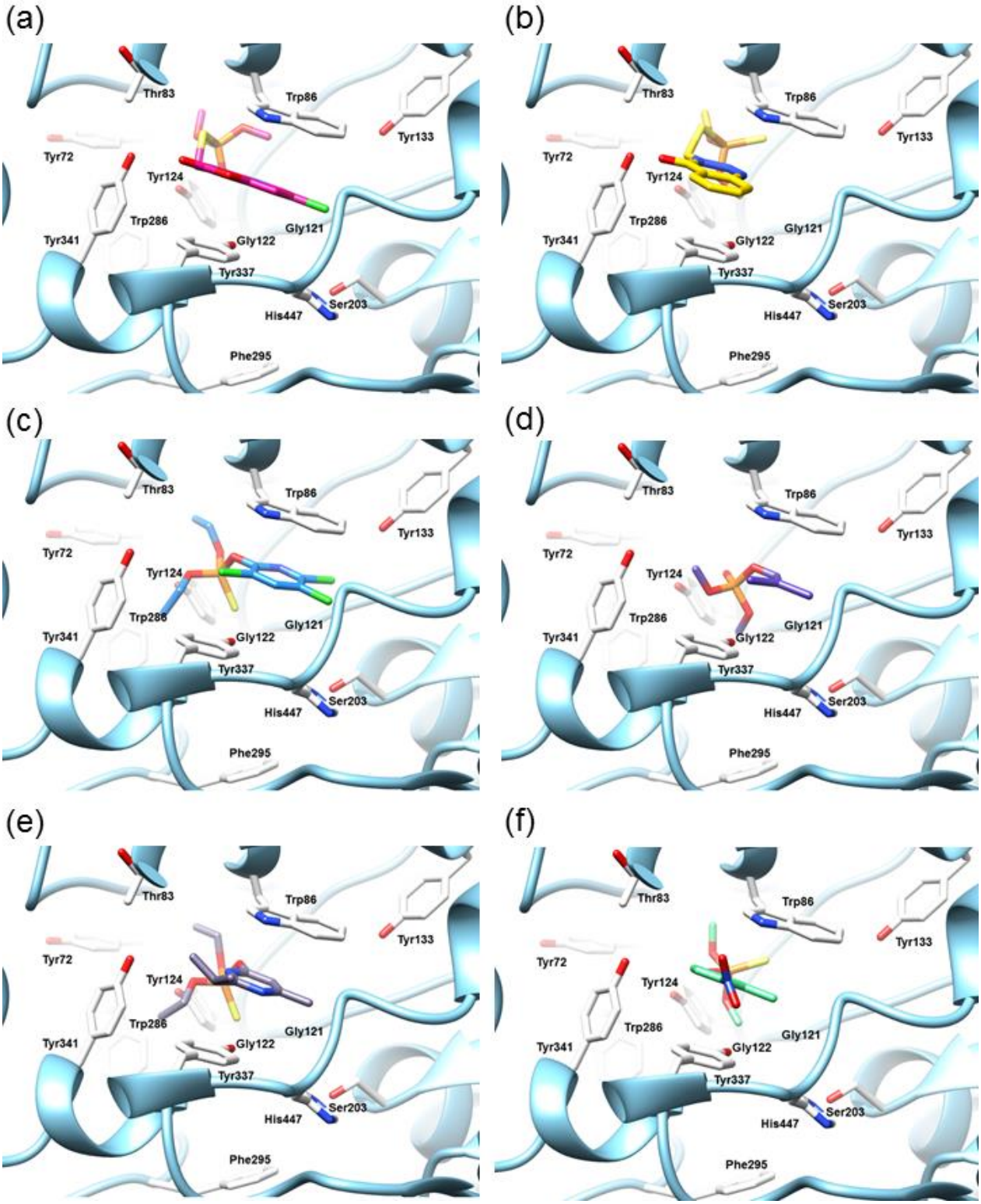

Figure S35. The SB alignment of azamethiphos (**a**), azinphos-methyl (**b**), chlorpyrifos (**c**), DDVP (**d**), diazinon (**e**), and fenitrothion (**f**) into the *m*AChE active site. The enzyme ribbons are presented in blue, active site amino acids are depicted in white. For the clarity purpose, hydrogen atoms are omitted from presentation.

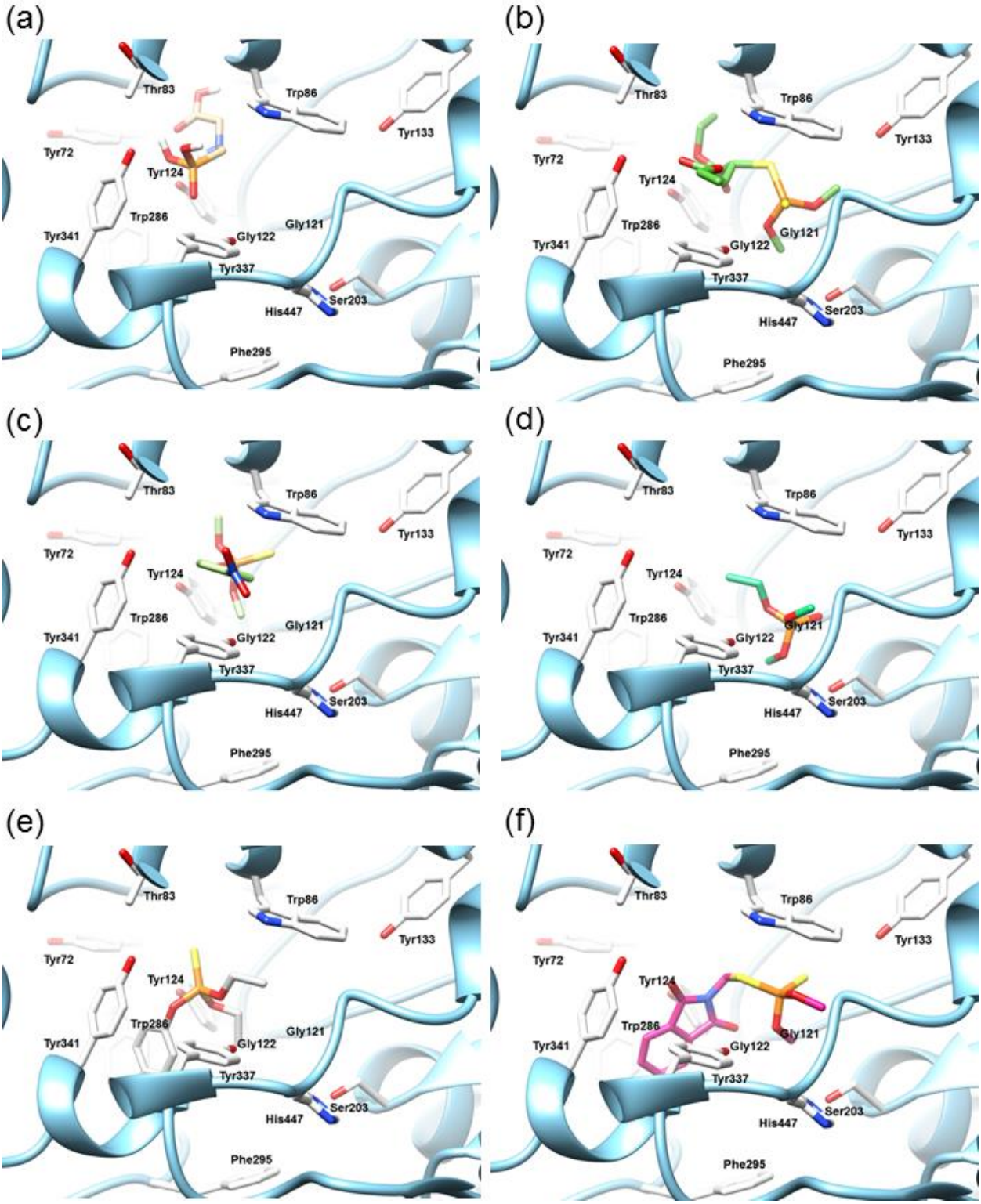

Figure S36. The SB alignment of glyphosate (**a**), malathion (**b**), methyl parathion (**c**), naled (dibrom) (**d**), parathion (**e**), and phosmet (**f**) into the *m*AChE active site. The enzyme ribbons are presented in blue, active site amino acids are depicted in white. For the clarity purpose, hydrogen atoms are omitted from presentation.

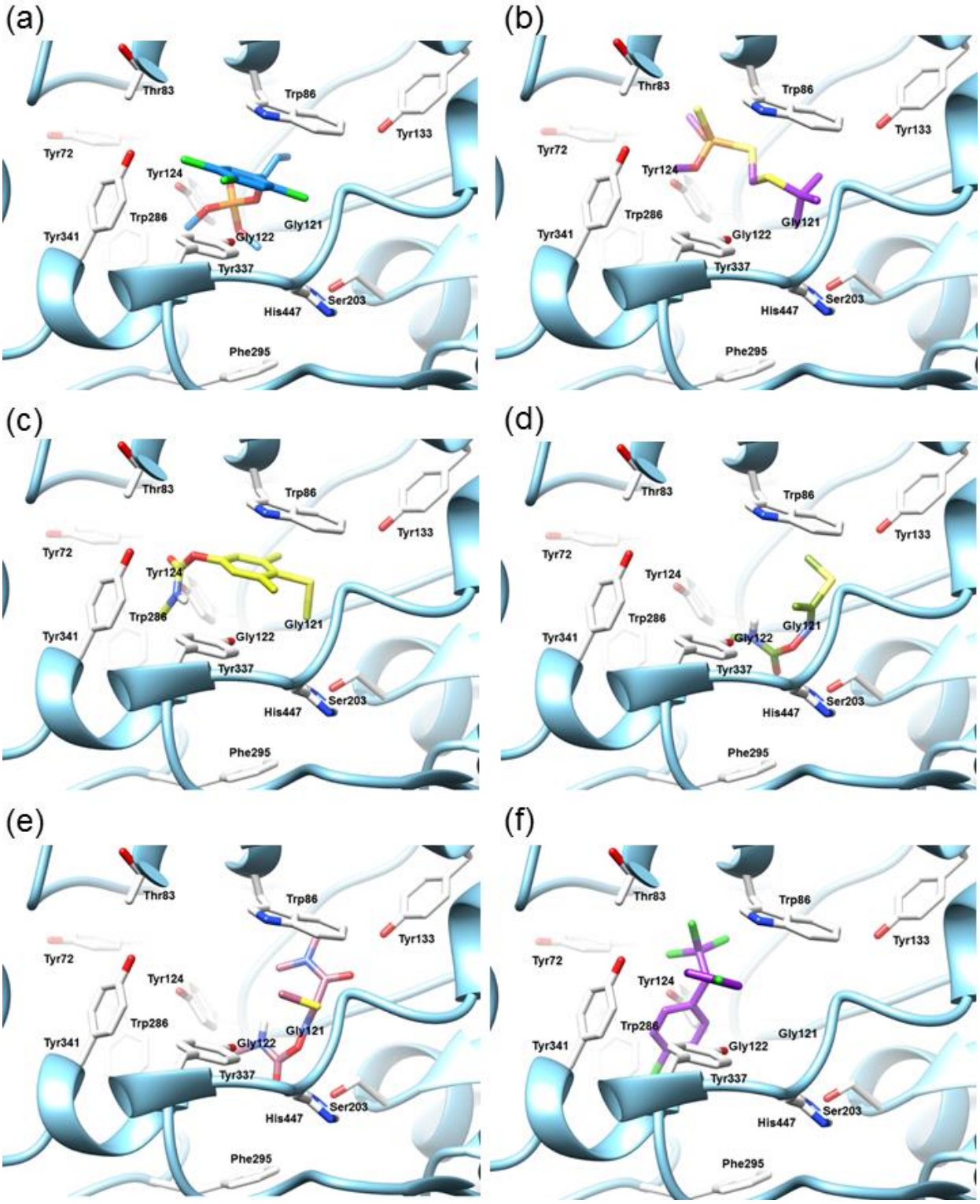

Figure S37. The SB alignment of TCVP (**a**), terbufos (**b**), methiocarb (**c**), methomyl (**d**), oxamyl (**e**), and DDT (**f**) into the *m*AChE active site. The enzyme ribbons are presented in blue, active site amino acids are depicted in white. For the clarity purpose, hydrogen atoms are omitted from presentation.

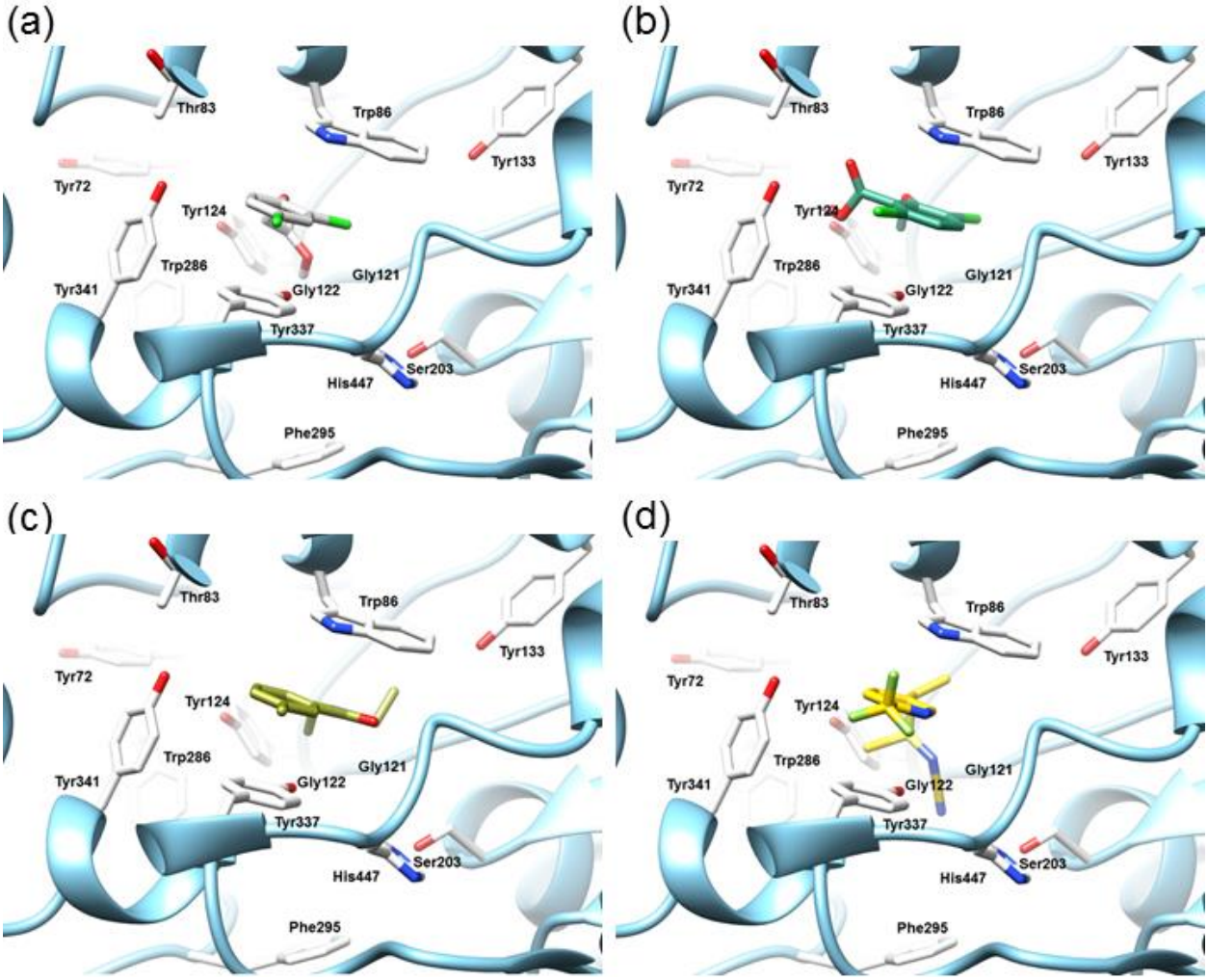

Figure S38. The SB alignment of 2,4-D (**a**), dicamba (**b**), DEET (**c**), and sulfoxaflor (**d**) into the *m*AChE active site. The enzyme ribbons are presented in blue, active site amino acids are depicted in white. For the clarity purpose, hydrogen atoms are omitted from presentation.

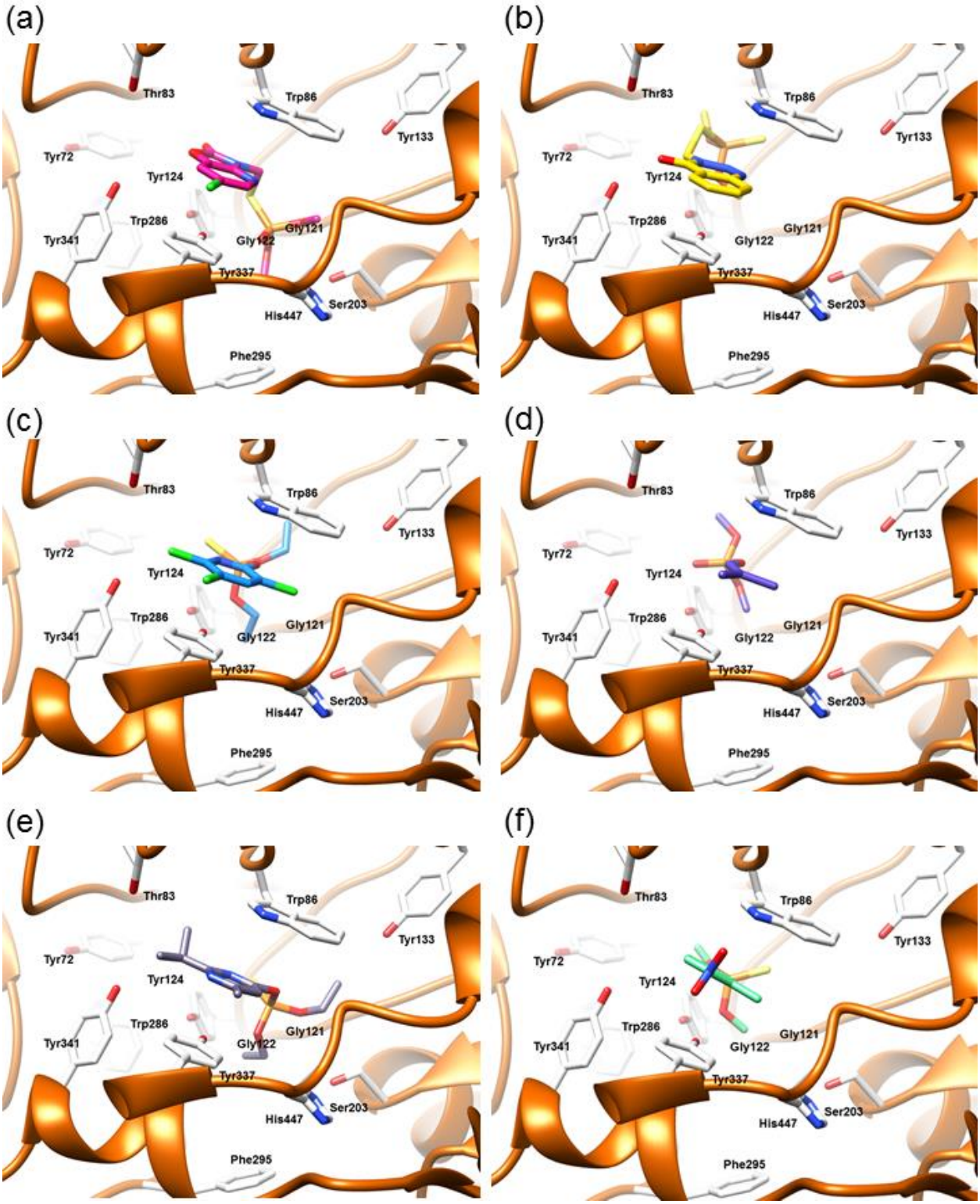

Figure S39. The SB alignment of azamethiphos (**a**), azinphos-methyl (**b**), chlorpyrifos (**c**), DDVP (**d**), diazinon (**e**), and fenitrothion (**f**), into the *h*AChE active site. The enzyme ribbons are presented in orange, active site amino acids are depicted in white. For the clarity purpose, hydrogen atoms are omitted from presentation.

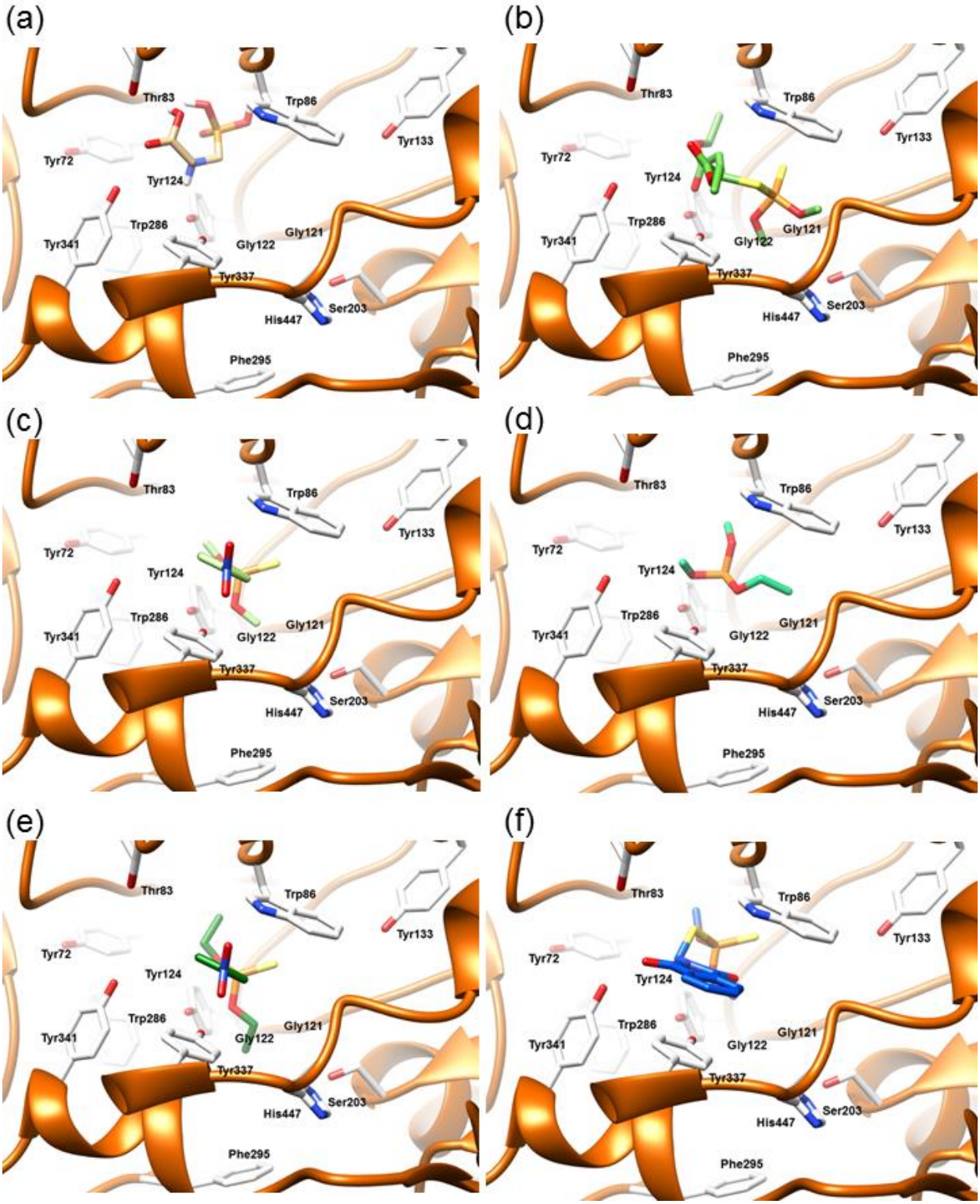

Figure S40. The SB alignment of glyphosate (**a**), malathion (**b**), methyl parathion (**c**), naled (dibrom) (**d**), parathion (**e**), and phosmet (**f**) into the *h*AChE active site. The enzyme ribbons are presented in orange, active site amino acids are depicted in white. For the clarity purpose, hydrogen atoms are omitted from presentation.

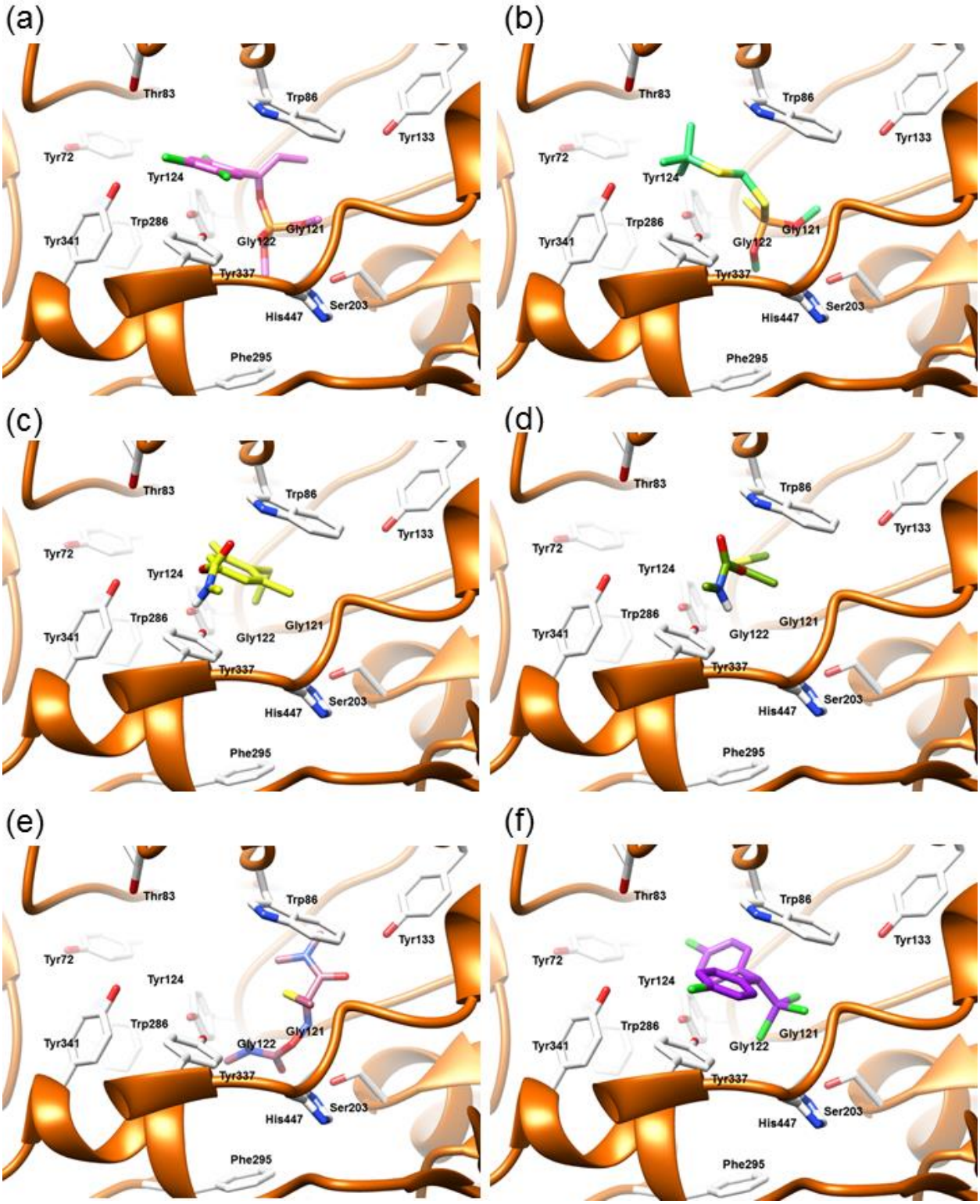

Figure S41. The SB alignment of TCVP (**a**), terbufos (**b**), methiocarb (**c**), methomyl (**d**), oxamyl (**e**), and DDT (**f**) into the *h*AChE active site. The enzyme ribbons are presented in blue, active site amino acids are depicted in white. For the clarity purpose, hydrogen atoms are omitted from presentation.

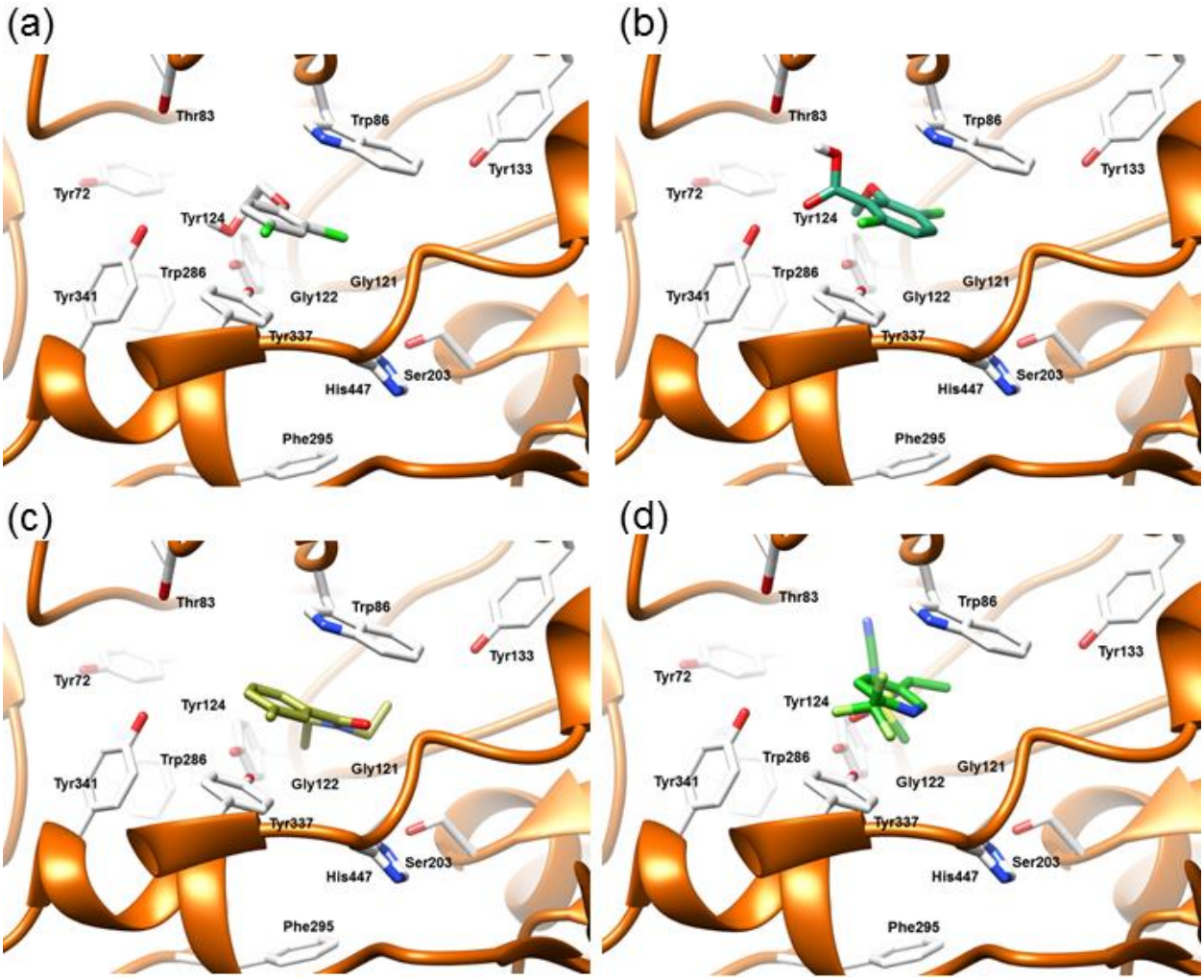

Figure S42. The SB alignment of 2,4-D (**a**), dicamba (**b**), DEET (**c**), and sulfoxaflor (**d**) into the *h*AChE active site. The enzyme ribbons are presented in orange, active site amino acids are depicted in white. For the clarity purpose, hydrogen atoms are omitted from presentation.

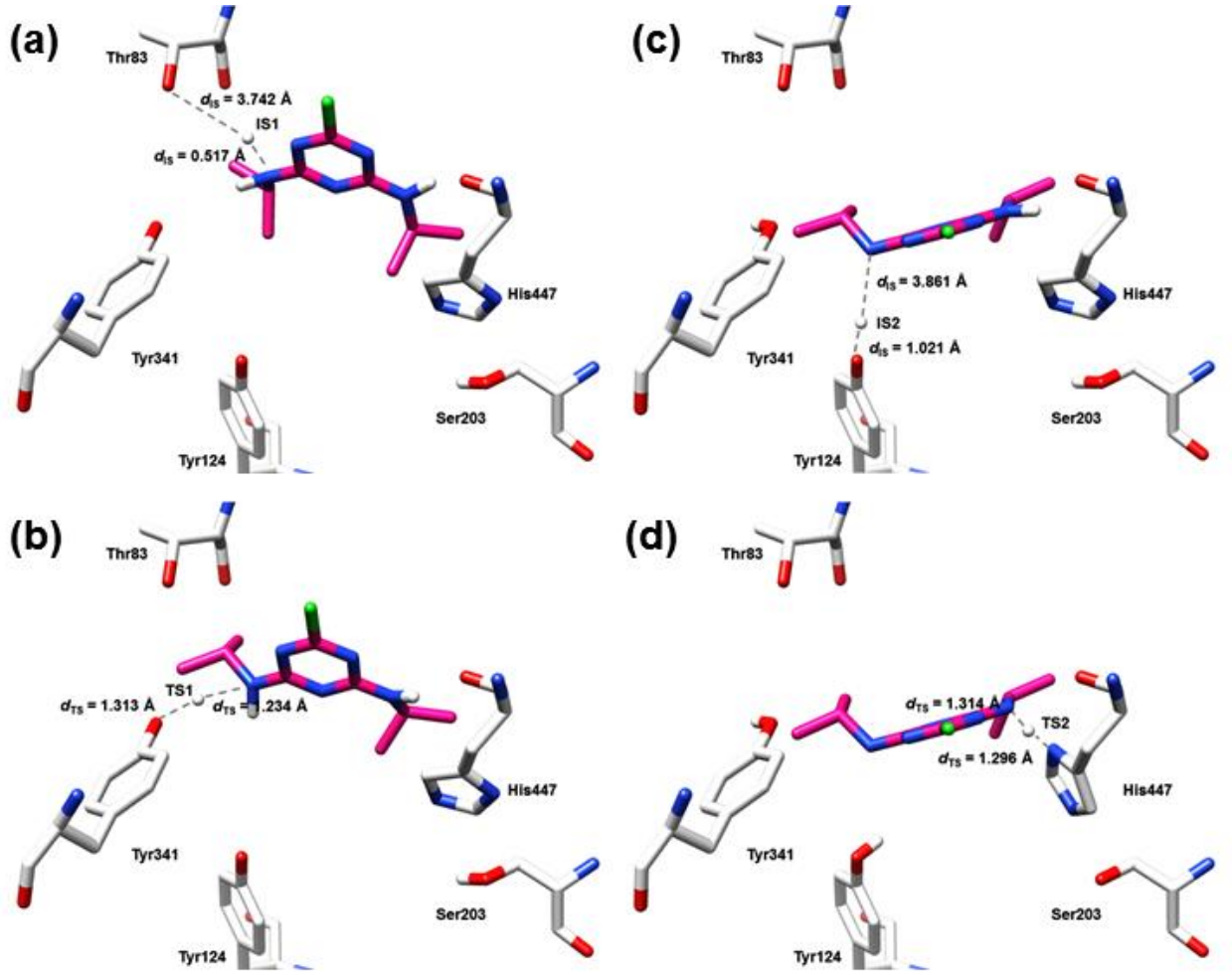

Figure S43. The quantum chemical mechanism of *Homo sapiens* acetylcholinesterase inhibition by propazine. The extracted geometry of IS1 (a); TS1 (b); IS2 (c); TS2 (d).

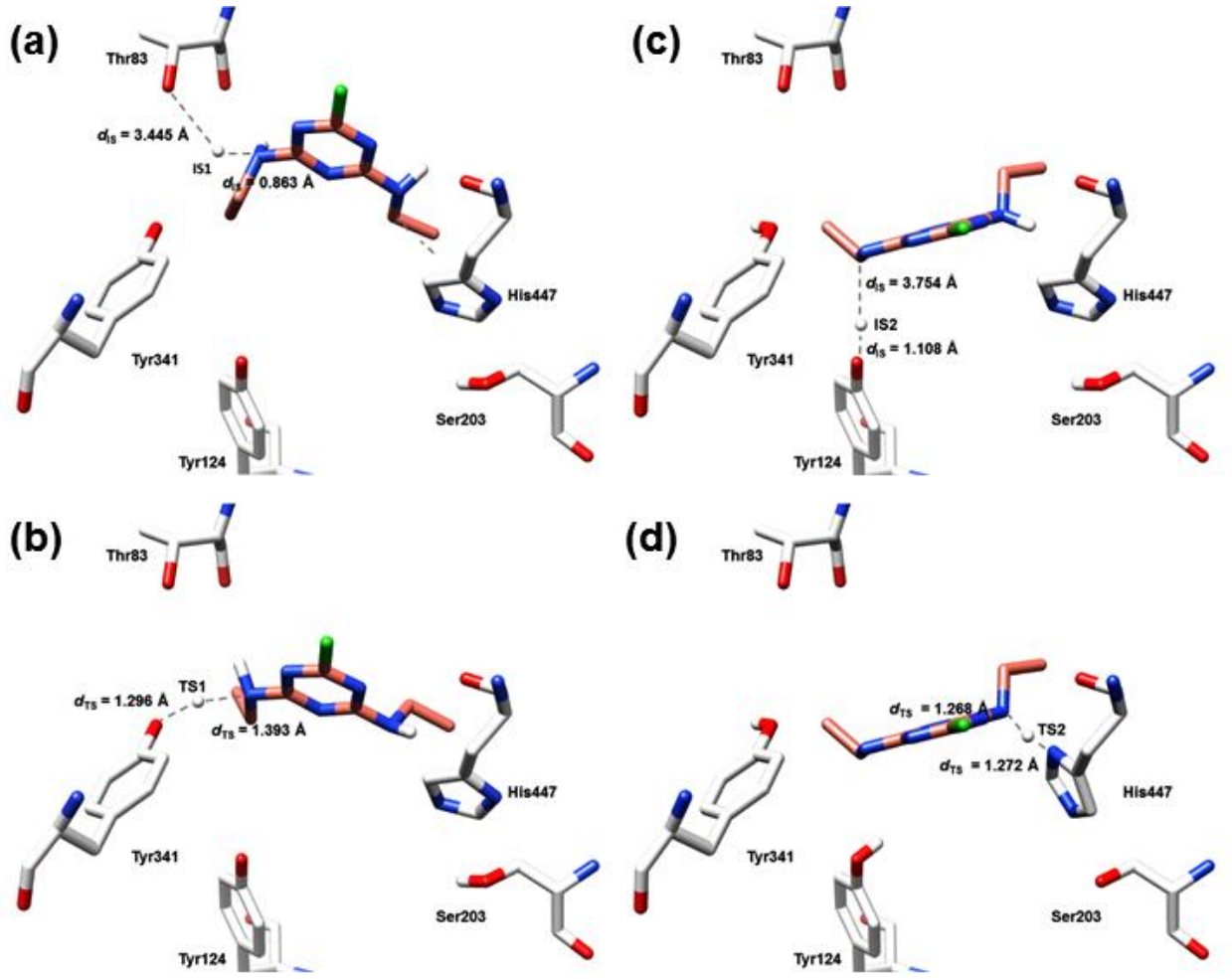

Figure S44. The quantum chemical mechanism of *Homo sapiens* acetylcholinesterase inhibition by simazine. The extracted geometry of IS1 (a); TS1 (b); IS2 (c); TS2 (d).

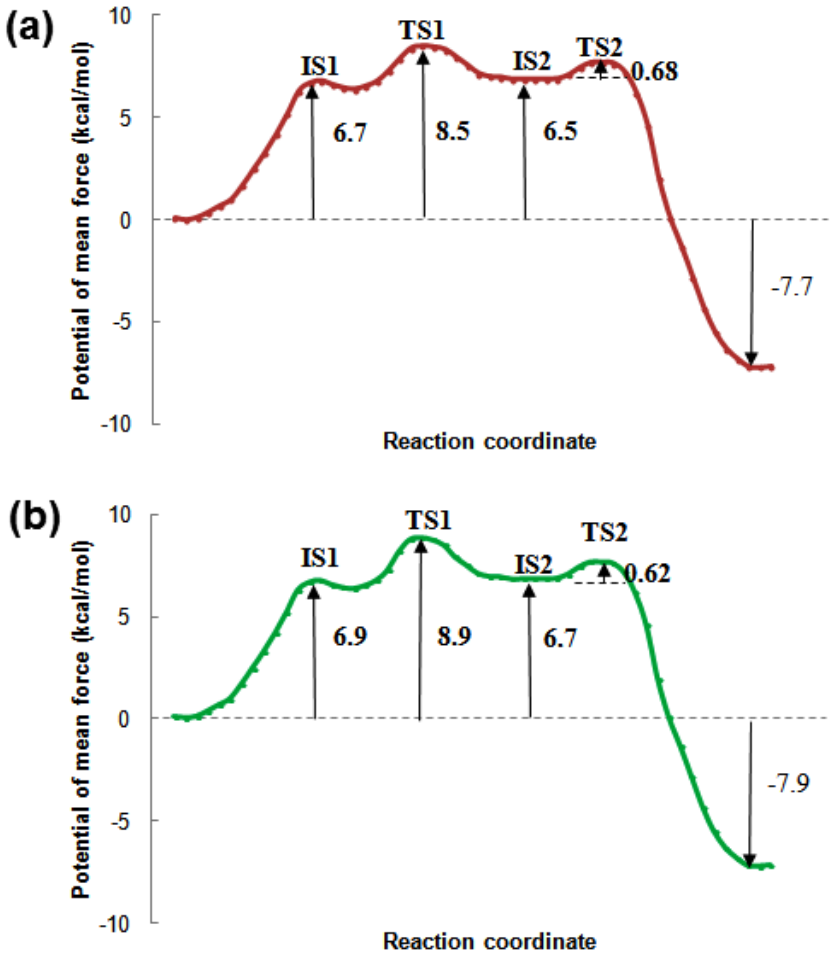

Figure S45. Free energy profile for *Homo sapiens* acetylcholinesterase inhibition by propazine (**a**) and simazine (**b**) by means of B3LYP (6-31G*) QM simulations.

Table S1. Training set pesticides chemical structures, conformational analysis, superposition of generated global minima using various force fields.

Pesticide	FF[a]	E_{glob_min}[b] (kJ/mol)	NGMS[c]	NF[d]	Pesticide alignment[e]	FFDAA[f] RMSD (Å)[g]
acetylcholine 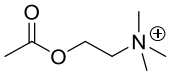	MM3	-924.67	41	3026	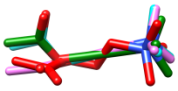	MM3/MMFF 1.086
	AMBER 94	NA[h]	NA	NA		MM3/MMFFs 1.703
	MMFF	-992.47	45	3066		MM3/OPLSAA 1.329
	MMFFs	-979.02	497	4897		MMFF/MMFFs 1.165
	OPLSAA	-773.90	888	2075		MMFF/OPLSAA 1.004
						MMFFs/OPLSAA 0.649
atrazine 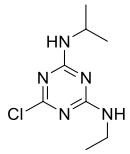	MM3	-1161.48	445	23	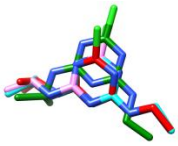	MM3/MMFF 0.892
	AMBER 94	NA	NA	NA		MM3/MMFFs 0.931
	MMFF	-1007.32	147	62		MM3/OPLSAA 2.523
	MMFFs	-992.63	509	20		MMFF/MMFFs 0.343
	OPLSAA	-783.57	364	19		MMFF/OPLSAA 2.487
						MMFFs/OPLSAA 2.514
propazine 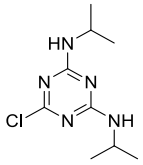	MM3	-1154.42	445	4370	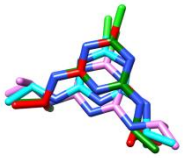	MM3/MMFF 6.346
	AMBER 94	NA	NA	NA		MM3/MMFFs 6.077
	MMFF	-992.47	34	3131		MM3/OPLSAA 5.727
	MMFFs	-979.02	577	4413		MMFF/MMFFs 2.092
	OPLSAA	-773.9	877	2086		MMFF/OPLSAA 2.842
						MMFFs/OPLSAA 1.990
simazine 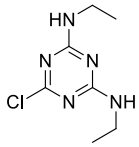	MM3	NA	NA	NA	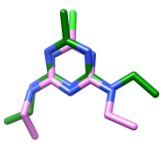	MM3/MMFF NA
	AMBER 94	NA	NA	NA		MM3/MMFFs NA
	MMFF	-1022.18	136	2782		MM3/OPLSAA NA
	MMFFs	NA	NA	NA		MMFF/MMFFs
	OPLSAA	-793.61	158	2306		

	NA
	MMFF/OPLSAA
	2.109
	MMFFs/OPLSAA
	NA

[a]Force field; [b]Energy of the global minimum; [c]Number of times that a single global minimum structure was found in 10000 processed structures; [d]Number of families *i.e.* different conformations found in 10000 processed structures; [e]Red - experimental conformation, Violet - MMFF conformation, Blue – MMFFs conformation, Green - OPLSAA conformation; [f]Force field dependent alignment accuracy; [g]RMSD measured between the heavy atoms of pesticides experimental and best performing force field conformations; [h]Not Available.

Table S2. Training set pesticides chemical structures, conformational analysis, superposition of generated global minima using various force fields.

Pesticide	FF[a]	E_{glob_min} [b] (kJ/mol)	NGMS[c]	NF[d]	Pesticide alignment[e]	FFDAA[f] RMSD (Å)[g]
carbofuran 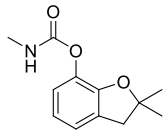	MM3	29.60	3617	2	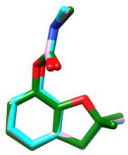	MM3/MMFF NA
	AMBER 94	NA[h]	NA	NA		MM3/MMFFs NA
	MMFF	20.30	3307	2		MM3/OPLSAA NA
	MMFFs	15.92	3384	2		MMFF/MMFFs NA
	OPLSAA	73.27	5621	75		MMFF/OPLSAA 2.109
						MMFFs/OPLSAA NA
monocrotophos 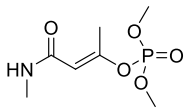	MM3	NA	NA	NA	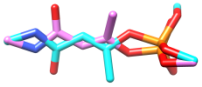	MM3/MMFF NA
	AMBER 94	NA	NA	NA		MM3/MMFFs NA
	MMFF	-307.36	241	62		MM3/OPLSAA NA
	MMFFs	-310.26	218	61		MMFF/MMFFs 3.419
	OPLSAA	NA	NA	NA		MMFF/OPLSAA NA
						MMFFs/OPLSAA NA
dimethoate 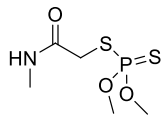	MM3	NA	NA	NA		MM3/MMFF NA
	AMBER 94	NA	NA	NA		MM3/MMFFs NA
	MMFF	-383.68	340	44		MM3/OPLSAA NA
	MMFFs	-386.71	215	40		MMFF/MMFFs 3.347
	OPLSAA	-228.66	998	15		MMFF/OPLSAA 1.724
						MMFFs/OPLSAA 3.328
carbaryl 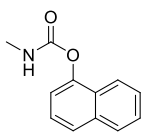	MM3	-0.88	10000	1	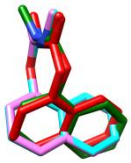	MM3/MMFF 2.019
	AMBER 94	NA	NA	NA		MM3/MMFFs 2.022
	MMFF	20.43	10000	1		MM3/OPLSAA 0.454
	MMFFs	15.66	10000	1		MMFF/MMFFs
	OPLSAA	59.34	9986	1		

						0.088 MMFF/OPLSAA 1.957 MMFFs/OPLSAA 2.514
tebufenozide 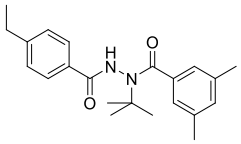	MM3 AMBER 94 MMFF MMFFs OPLSAA	NA NA 467.38 470.26 13.33	NA NA 1759 1799 1474	NA NA 4 4 8	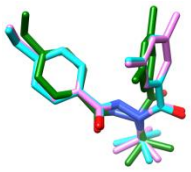	MM3/MMFF NA MM3/MMFFs NA MM3/OPLSAA NA MMFF/MMFFs 0.370 MMFF/OPLSAA 2.769 MMFFs/OPLSAA 2.686

[a]Force field; [b]Energy of the global minimum; [c]Number of times that a single global minimum structure was found in 10000 processed structures; [d]Number of families *i.e.* different conformations found in 10000 processed structures; [e]Red - experimental conformation, Violet - MMFF conformation, Blue – MMFFs conformation, Green - OPLSAA conformation; [f]Force field dependent alignment accuracy; [g]RMSD measured between the heavy atoms of pesticides experimental and best performing force field conformations; [h]Not Available.

Table S3. Training set pesticides chemical structures, conformational analysis, superposition of generated global minima using various force fields.

Pesticide	FF[a]	E_{glob_min}[b] (kJ/mol)	NGMS[c]	NF[d]	Pesticide alignment[e]	FFDAA[f] RMSD (Å)[g]
imidacloprid 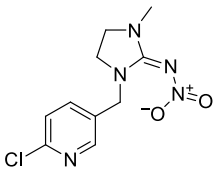	MM3	NA[h]	NA	NA	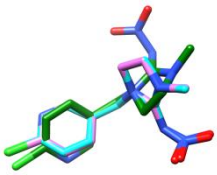	MM3/MMFF NA
	AMBER 94	NA	NA	NA		MM3/MMFFs NA
	MMFF	-168.00	1027	5		MM3/OPLSAA NA
	MMFFs	-165.41	3643	3		MMFF/MMFFs 0.122
	OPLSAA	90.86	365	23		MMFF/OPLSAA 3.282
						MMFFs/OPLSAA 3.277
acetamiprid 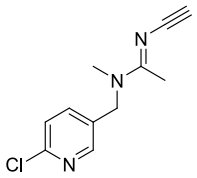	MM3	NA	NA	NA	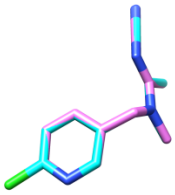	MM3/MMFF NA
	AMBER 94	NA	NA	NA		MM3/MMFFs NA
	MMFF	-31.45	1916	14		MM3/OPLSAA NA
	MMFFs	-31.29	1816	6		MMFF/MMFFs 0.041
	OPLSAA	NA	NA	NA		MMFF/OPLSAA NA
						MMFFs/OPLSAA NA
diuron 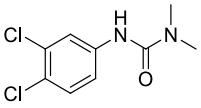	MM3	-37.27	3108	2	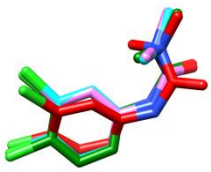	MM3/MMFF 1.886
	AMBER 94	NA	NA	NA		MM3/MMFFs 1.882
	MMFF	-142.96	2537	2		MM3/OPLSAA 1.899
	MMFFs	-140.51	2523	2		MMFF/MMFFs 0.121
	OPLSAA	-3.52	2908	2		MMFF/OPLSAA 0.399
						MMFFs/OPLSAA 0.330
monuron 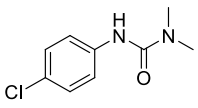	MM3	-76.13	10000	1	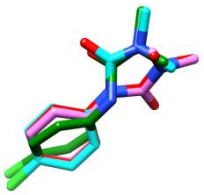	MM3/MMFF 0.533
	AMBER 94	NA	NA	NA		MM3/MMFFs 2.004
	MMFF	-197.63	10000	1		MM3/OPLSAA 2.629
	MMFFs	-199.43	10000	1		MMFF/MMFFs
	OPLSAA	-74.72	7691	2		

						2.049 MMFF/ OPLSAA 2.695 MMFFs/OPLSAA 2.032
linuron	MM3	NA	NA	NA		MM3/MMFF
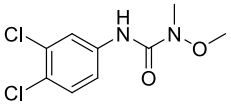	AMBER 94 MMFF MMFFs OPLSAA	NA -992.47 -979.02 -773.90	NA 45 497 888	NA 3066 4897 2075	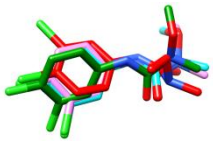	3.597 MM3/MMFFs 3.574 MM3/OPLSAA 2.951 MMFF/MMFFs 0.523 MMFF/OPLSAA 1.833 MMFFs/OPLSAA 1.889

[a]Force field; [b]Energy of the global minimum; [c]Number of times that a single global minimum structure was found in 10000 processed structures; [d]Number of families *i.e.* different conformations found in 10000 processed structures; [e]Red - experimental conformation, Violet - MMFF conformation, Blue – MMFFs conformation, Green - OPLSAA conformation; [f]Force field dependent alignment accuracy; [g]RMSD measured between the heavy atoms of pesticides experimental and best performing force field conformations; [h]Not Available.

Table S4. Test set pesticides chemical structures and obtained global minima using MMFF as the best performing force field.

Pesticide	E_{glob_min}[a] (kJ/mol)	Conformation	Pesticide	E_{glob_min}[a] (kJ/mol)	Conformation
azamethiphos	-561.48	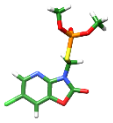	**phosmet**	-549.21	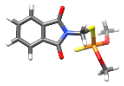
azinphos-methyl	-361.00	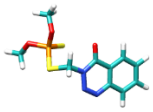	**TCVP**	-130.74	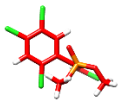
chlorpyrifos	-247.37	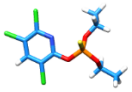	**terbufos**	-382.19	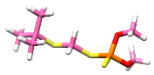
DDVP	-214.58	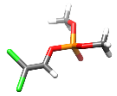	**methiocarb**	-75.96	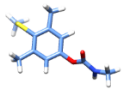
diazinon	-274.36	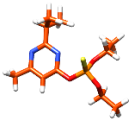	**methomyl**	-72.25	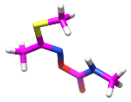
fenitrothion	-45.79	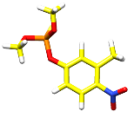	**oxamyl**	118.32	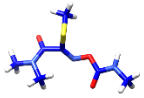
glyphosate	-221.48	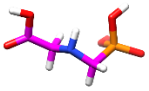	**DDT**	352.49	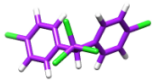
malathion	-498.14	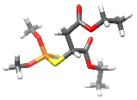	**2,4-D**	28.66	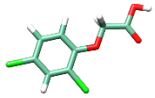
methyl parathion	-74.64	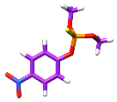	**dicamba**	63.27	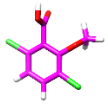
naled (dibrom)	-337.18	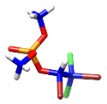	**DEET**	70.17	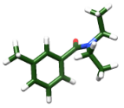
parathion	-90.35	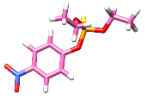	**sulfoxaflor**	178.42	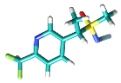

[a] $E_{global\_minimum}$

Table S5. Linear regression parameters for QSAR model 2 (acute toxicity against *Mus musculus*).

Compound	LD_{50} (mg/kg)	MW	E_{glob_min} MMFF (kJ/mol)	Exp. pLD_{50}	Fitted pLD_{50}
atrazine	0.85	215.69	-1007.3	5.40	4.28
propazin	3.18	229.71	-992.47	4.86	4.26
simazine	5	201.66	-1022.2	4.61	4.30
carbofuran	2	221.11	20.3	5.04	3.09
monocrotophos	14	223.16	-307.36	4.20	3.47
dimethoate	60	229.25	-383.68	3.58	3.56
carbaryl	100	201.22	20.43	3.30	3.09
tebufenozide	5000	352.48	467.38	1.85	2.58
imidacloprid	131	269.69	-168	3.31	3.31
acetamiprid	184	221.69	-31.45	3.08	3.15
diuron	500	233.09	-142.96	2.67	3.28
monuron	1700	198.65	-197.63	2.07	3.35
linuron	2400	249.09	-992.47	2.02	4.26

Table S6. External validation of QSAR model 2 (acute toxicity against *Mus musculus*).

Compound	LD_{50} (mg/kg)	MW	E_{glob_min} MMFF (kJ/mol)	Exp. pLD_{50}	Fitted pLD_{50}
azamethiphos	1040.00	324.68	-561.48	4.07	1.98
azinphos-methyl	7.00	317.32	-361.00	6.25	2.36
chlorpyrifos	2000.00	350.59	-247.37	3.79	2.58
DDVP	17.00	220.98	-214.58	5.86	2.64
diazinon	66.00	304.35	-274.36	5.27	2.53
fenitrothion	500.00	277.23	-45.79	4.39	2.96
glyphosate	5000.00	169.07	-221.48	3.39	2.63
malathion	290.00	330.36	-498.14	4.63	2.10
methyl parathion	18.00	263.21	-74.64	5.84	2.91
naled (dibrom)	160.00	380.78	-337.18	4.89	2.41
parathion	2.00	291.26	-90.35	6.79	2.88
phosmet	113.00	317.32	-549.21	5.04	2.01
TCVP	465.00	365.96	-130.74	4.42	2.80
terbufos	1.60	288.43	-382.19	6.89	2.32
methiocarb	350.00	225.31	-75.96	4.55	2.91
methomyl	12.00	162.21	-72.25	6.01	2.91
oxamyl	5.40	219.26	118.32	6.36	3.27
DDT	113.00	354.49	352.49	5.04	3.72
2,4-D	639.00	221.04	28.66	4.29	3.10
dicamba	757.00	221.04	63.27	4.21	3.17
DEET	1.95	191.27	70.17	6.80	3.18
sulfoxaflor	750.00	277.27	178.42	4.22	3.39

Table S7. Linear regression parameters for QSAR model 4 (acute toxicity against *Homo sapiens*).

Compound	LD_{50} (mg/kg)	MW	E_{glob_min} MMFF (kJ/mol)	Calculated pLD_{50}	Fitted pLD_{50}
atrazine	0.07	215.69	-1007.30	6.50	5.52
propazin	0.26	229.71	-992.47	5.95	5.21
simazine	0.41	201.66	-1022.20	5.70	4.74
carbofuran	0.16	221.11	20.30	6.14	5.13
monocrotophos	1.14	223.16	-307.36	5.29	4.34
dimethoate	4.86	229.25	-383.68	4.67	4.10
carbaryl	8.11	201.22	20.43	4.39	3.71
tebufenozide	405.40	352.48	467.38	2.94	1.98
imidacloprid	10.62	269.69	-168.00	4.40	3.95
acetamiprid	14.92	221.69	-31.45	4.17	3.63
diuron	40.54	233.09	-142.96	3.76	3.00
monuron	137.84	198.65	-197.63	3.16	2.84
linuron	194.59	249.09	-992.47	3.11	2.21

Table S8. External validation of QSAR model 4 (acute toxicity against *Homo sapiens*).

Compound	LD_{50} (mg/kg)	MW	E_{glob_min} MMFF (kJ/mol)	Calculated pLD_{50}	Fitted pLD_{50}
azamethiphos	1040.00	324.68	-561.48	2.49	4.10
azinphos-methyl	7.00	317.32	-361.00	4.66	4.62
chlorpyrifos	2000.00	350.59	-247.37	2.24	3.48
DDVP	17.00	220.98	-214.58	4.11	4.02
diazinon	66.00	304.35	-274.36	3.66	4.03
fenitrothion	500.00	277.23	-45.79	2.74	4.57
glyphosate	5000.00	169.07	-221.48	1.53	5.10
malathion	290.00	330.36	-498.14	3.06	4.29
methyl parathion	18.00	263.21	-74.64	4.17	4.79
naled (dibrom)	160.00	380.78	-337.18	3.38	3.81
parathion	2.00	291.26	-90.35	5.16	4.40
phosmet	113.00	317.32	-549.21	3.45	4.32
TCVP	465.00	365.96	-130.74	2.90	4.29
terbufos	1.60	288.43	-382.19	5.26	4.67
methiocarb	350.00	225.31	-75.96	2.81	4.56
methomyl	12.00	162.21	-72.25	4.13	5.19
oxamyl	5.40	219.26	118.32	4.61	4.24
DDT	113.00	354.49	352.49	3.50	5.22
2,4-D	639.00	221.04	28.66	2.54	4.84
dicamba	757.00	221.04	63.27	2.47	4.88
DEET	1.95	191.27	70.17	4.99	4.29
sulfoxaflor	750.00	277.27	178.42	2.57	3.93

Table S9. Structure-based alignment assessment for wild type *Mus musculus* AChE inhibitors.

Ligand	Ref.	AutoDock		Vina	DOCK6		AutoDock		Vina	DOCK6	
PDB		BD[a]	BC[b]		R[c]	F[d]	BD[a]	BC[b]		R[c]	F[d]
		Experimental Conformation Re-Docking					*Randomized Conformation Re-Docking*				
1J07	[SR1]	17.236	18.232	13.274	21.343	22.768	18.396	18.432	16.728	22.341	22.761
1N5M	[SR1]	3.942	4.231	4.241	5.941	6.928	3.726	3.246	5.921	6.314	7.043
1N5R	[SR1]	2.767	3.243	1.928	3.841	3.992	3.242	3.531	2.941	4.323	4.447
1Q83	[SR2]	2.072	2.576	1.248	2.761	2.997	2.437	3.231	1.764	3.347	3.471
1Q84	[SR2]	1.076	1.224	0.692	4.271	5.226	1.574	2.248	1.248	5.176	5.449
2C0P	[SR3]	7.321	8.246	5.494	9.274	10.111	8.321	9.326	6.724	12.471	13.226
2C0Q	[SR3]	8.436	9.072	6.726	11.246	13.276	8.773	9.323	2.892	14.178	14.326
2GYU	[SR4]	3.941	3.893	1.547	2.748	2.673	4.276	4.832	1.663	3.437	3.543
2GYV	[SR4]	2.996	2.934	1.894	2.896	2.937	2.993	2.837	1.893	3.324	3.333
2GYW	[SR4]	2.534	2.637	1.747	2.731	2.834	2.539	2.639	1.767	2.076	2.113
2H9Y	[SR5]	3.121	3.276	2.793	7.394	7.776	4.214	5.432	2.992	9.317	10.116
2HA0	[SR5]	1.974	2.127	2.432	3.293	4.727	2.126	3.213	2.748	5.471	5.557
2JEY	[SR6]	1.006	1.118	2.947	5.436	5.445	1.763	1.846	2.894	1.839	1.937
2JEZ	[SR6]	1.872	1.936	2.846	4.373	4.437	2.793	2.937	2.993	1.993	1.973
2JF0	[SR6]	2.034	2.122	2.373	3.391	4.937	2.184	2.617	2.446	1.643	1.643
2JGI	[SR7]	1.993	1.973	8.476	1.935	2.317	2.932	3.143	8.562	4.374	4.551
2WHP	[SR8]	2.967	2.939	1.747	1.993	2.074	3.327	3.446	1.754	1.236	1.279
2WHQ	[SR8]	2.224	2.517	1.647	2.851	2.935	3.247	3.536	1.673	1.973	1.984
2WHR	[SR8]	1.973	1.868	1.993	2.661	2.639	1.831	1.884	1.961	1.837	1.883
2WU3	[SR9]	2.831	2.993	2.713	2.743	2.839	3.936	3.974	2.831	2.532	2.631
2WU4	[SR9]	3.296	3.348	2.262	2.276	2.374	4.333	4.536	2.341	2.617	2.814
3ZLT	[SR10]	1.276	2.574	1.894	2.761	2.432	2.574	3.473	1.964	2.714	2.971
3ZLU	[SR10]	1.543	1.673	1.627	2.641	3.241	2.313	3.116	1.892	2.774	2.931
3ZLV	[SR10]	2.056	2.157	1.942	3.417	3.776	2.746	3.547	1.972	2.561	2.549
4A16	[SR11]	1.478	1.723	0.712	3.278	3.796	1.536	1.928	1.942	2.736	2.931
4A23	[SR12]	4.334	4.593	2.347	2.459	2.547	4.763	4.863	2.492	3.913	3.977
4ARA	[SR12]	4.328	4.446	1.336	2.583	2.593	4.331	4.371	1.368	2.031	2.213
4ARB	[SR12]	3.287	3.371	0.946	1.943	2.074	4.328	4.463	1.032	1.224	1.237
4B7Z	[SR13]	1.924	3.896	2.614	3.293	3.326	1.983	1.976	2.684	2.546	2.661
4B80	[SR13]	1.791	1.931	2.761	2.791	3.763	1.883	1.936	2.781	3.073	3.116
4B81	[SR13]	2.554	2.668	2.663	3.291	3.394	2.439	2.636	2.669	2.837	2.891
4B82	[SR13]	2.437	2.673	3.617	8.639	8.743	2.693	2.721	3.613	4.116	4.227
4B83	[SR13]	3.839	3.937	2.461	4.263	4.638	4.261	2.274	2.531	2.674	2.668
4B84	[SR13]	2.673	2.769	3.334	4.293	4.398	3.296	3.297	3.557	4.132	4.339
4B85	[SR13]	2.553	2.663	2.637	5.324	5.371	2.583	2.661	2.745	3.113	3.273
4BC0	[SR14]	2.931	2.537	1.763	1.283	1.334	2.971	3.046	1.893	2.743	2.663
4BC1	[SR14]	2.671	2.761	1.831	1.713	1.831	2.772	2.884	1.884	1.743	1.838
5DTJ	[SR15]	4.231	4.447	2.398	6.341	6.477	8.392	10.326	2.576	2.838	3.091
5EHN	[SR16]	3.928	3.936	6.893	5.432	5.543	4.326	4.436	7.452	6.831	6.373
5EHQ	[SR16]	4.331	4.749	5.437	5.448	5.793	3.298	3.393	4.631	5.346	5.519
5EHZ	[SR16]	4.237	4.563	4.831	6.831	6.939	4.237	4.117	4.448	3.931	4.126
5EIA	[SR16]	6.891	6.661	11.839	5.237	5.831	6.921	6.974	12.903	9.313	9.884
5EIE	[SR16]	7.327	6.971	8.396	8.329	8.437	7.432	8.063	8.996	7.439	7.661

5EIH	[SR16]	1.561	1.663	1.941	8.883	8.736	1.763	1.833	1.893	2.354	2.931
5HCU	[SR15]	1.229	1.291	1.836	7.329	7.638	1.339	1.354	1.884	2.551	2.689
DA		44.55%	40%	55.55	25.55%	20%	34.44%	26.67%	57.78%	28.89%	30%
		Experimental Conformation Cross-Docking					*Randomized Conformation Cross-Docking*				
1J07	[SR1]	22.732	24.328	16.872	24.371	25.293	24.372	25.761	22.841	24.873	25.297
1N5M	[SR1]	5.231	5.432	7.241	7.341	8.226	6.393	8.426	9.326	7.891	8.137
1N5R	[SR1]	3.213	3.738	3.296	4.374	4.448	4.761	4.923	5.841	5.441	5.761
1Q83	[SR2]	3.076	3.214	2.741	4.371	4.439	3.573	3.926	4.321	5.484	5.716
1Q84	[SR2]	2.327	2.438	1.639	3.917	3.938	3.117	3.234	2.276	4.138	3.348
2C0P	[SR3]	10.346	10.713	7.284	12.648	12.732	11.741	11.926	10.232	14.397	14.556
2C0Q	[SR3]	10.437	10.891	2.736	12.435	12.681	10.437	10.576	12.984	13.874	13.943
2GYU	[SR4]	4.663	4.379	1.743	2.792	3.014	4.679	4.699	1.937	2.804	2.814
2GYV	[SR4]	2.991	3.039	1.935	2.934	2.973	3.042	3.037	2.047	2.942	2.763
2GYW	[SR4]	2.629	2.693	1.874	7.471	7.536	2.671	2.675	1.963	7.463	7.437
2H9Y	[SR5]	4.216	4.378	2.894	6.372	6.449	5.372	5.848	3.342	7.316	7.398
2HA0	[SR5]	3.296	3.434	2.220	1.343	1.761	4.327	4.541	3.926	4.378	4.478
2JEY	[SR6]	1.939	2.032	2.996	6.391	7.328	1.993	2.146	3.044	6.471	6.484
2JEZ	[SR6]	1.937	2.044	2.910	7.341	7.391	1.984	1.989	2.963	7.461	7.473
2JF0	[SR6]	2.543	2.633	2.537	4.393	4.551	2.591	2.607	2.668	4.591	4.666
2JGI	[SR7]	2.726	2.774	9.373	2.937	3.026	2.831	2.841	10.374	3.116	3.273
2WHP	[SR8]	3.039	3.046	1.836	2.591	2.671	2.116	3.598	1.936	2.741	2.794
2WHQ	[SR8]	2.791	3.037	1.732	4.397	4.538	2.843	3.868	1.747	4.617	4.882
2WHR	[SR8]	2.024	2.071	2.039	2.791	2.937	2.056	2.118	1.993	2.941	2.876
2WU3	[SR9]	2.939	3.038	2.883	2.883	2.931	3.049	3.076	2.437	2.995	2.935
2WU4	[SR9]	4.326	4.768	2.393	2.973	2.946	4.767	4.794	2.449	3.017	3.176
3ZLT	[SR10]	3.394	3.641	2.210	1.393	1.446	4.376	4.222	2.250	2.439	2.556
3ZLU	[SR10]	2.719	2.841	2.140	2.439	2.576	3.761	3.814	2.728	2.431	2.316
3ZLV	[SR10]	2.764	2.937	2.222	4.325	4.439	3.731	3.941	3.612	2.139	2.261
4A16	[SR11]	4.326	4.174	1.821	5.517	5.669	4.438	5.556	2.798	2.249	3.116
4A23	[SR12]	4.773	4.934	2.541	3.493	3.561	4.839	4.884	2.674	3.547	3.673
4ARA	[SR12]	4.543	4.631	1.559	4.293	4.316	4.661	4.679	1.791	4.397	4.318
4ARB	[SR12]	3.637	3.839	1.393	2.553	2.717	3.748	3.791	1.493	2.641	2.661
4B7Z	[SR13]	2.092	2.114	3.839	4.393	4.439	2.114	2.174	3.936	4.388	4.397
4B80	[SR13]	1.883	1.739	2.946	3.093	3.129	1.984	1.891	3.116	3.273	3.318
4B81	[SR13]	2.593	2.542	2.883	3.559	3.776	2.604	2.663	3.731	3.619	3.719
4B82	[SR13]	2.938	3.336	4.113	12.931	13.073	2.946	2.944	4.273	12.997	12.874
4B83	[SR13]	4.393	4.739	3.096	7.395	7.776	4.484	4.516	3.283	7.436	7.839
4B84	[SR13]	2.771	2.895	3.529	6.313	6.416	2.937	2.939	3.661	6.417	6.473
4B85	[SR13]	2.636	2.731	3.839	6.419	6.519	2.748	2.816	3.739	6.444	6.393
4BC0	[SR14]	3.041	3.077	1.984	2.193	2.293	3.247	3.346	1.996	2.273	2.439
4BC1	[SR14]	2.793	2.939	1.739	2.553	2.594	2.811	2.814	1.831	2.617	2.881
5DTJ	[SR15]	7.241	7.392	2.935	8.931	8.937	8.321	8.336	3.012	9.241	9.117
5EHN	[SR16]	4.436	4.776	7.394	6.931	7.438	4.371	4.384	8.349	6.971	6.593
5EHQ	[SR16]	4.363	4.362	6.883	6.771	7.014	4.444	4.472	6.931	6.761	6.831
5EHZ	[SR16]	4.373	4.351	6.831	6.931	7.226	4.831	4.829	6.831	6.943	6.933
5EIA	[SR16]	7.091	7.116	12.393	6.317	6.339	7.216	7.141	12.449	6.471	6.173
5EIE	[SR16]	7.438	7.691	9.837	10.439	10.739	7.519	7.516	10.241	10.558	10.441
5EIH	[SR16]	1.737	1.841	2.447	10.536	10.631	1.971	1.988	3.293	10.739	10.432

5HCU	[SR15]	1.439	1.553	1.934	10.249	10.555	1.553	1.512	1.974	10.312	10.516
DA		25.55%	22.22%	25.55%	16.67%	13.33%	24.44%	22.22%	32.22%	13.33%	12.22%

[a]Best docked conformation; [b]Best clustered conformation; [c]Rigid docking; [d]F - flexible docking.

Table S10. Structure-based alignment assessment for wild type *Homo sapiens* AChE inhibitors.

Ligand	Ref.	AutoDock		Vina	DOCK6		AutoDock		Vina	DOCK6	
		BDa	BCb		Rc	Fd	BDa	BCb		Rc	Fd
		Experimental Conformation Re-Docking					*Randomized Conformation Re-Docking*				
2X8B	[SR17]	5.437	4.974	7.437	1.893	1.764	5.551	5.831	6.393	1.836	1.848
4BDT	[SR18]	2.937	2.973	1.697	2.713	2.741	3.491	3.617	1.784	2.973	2.741
4EY5	[94]	4.376	4.117	1.761	2.892	2.393	4.372	4.391	1.931	2.931	3.073
4EY6	[94]	2.561	2.984	1.936	3.946	3.834	3.072	3.092	2.032	4.032	4.417
4EY7	[94]	3.976	3.761	1.774	2.176	2.768	4.894	4.932	1.559	2.813	2.935
4M0E	[SR19]	1.773	2.671	1.076	2.076	2.224	1.996	2.081	1.339	1.983	1.996
4M0F	[SR19]	2.261	2.558	2.761	1.743	1.839	2.837	2.841	2.547	1.784	1.776
5FOQ	[SR20]	2.936	3.041	2.076	3.437	3.338	3.492	3.504	2.841	3.439	3.513
DA		37.5%	18.75%	75.00%	50.00%	50.00%	18.75%	12.50%	68.75%	56.25%	56.25%
		Experimental Conformation Cross-Docking					*Randomized Conformation Cross-Docking*				
2X8B	[SR17]	6.838	7.324	4.393	1.949	1.838	5.652	5.559	6.327	2.436	2.389
4BDT	[SR18]	2.392	2.224	1.761	2.976	3.721	3.496	3.517	2.937	3.218	3.261
4EY5	[94]	4.886	4.596	1.948	3.042	2.984	4.733	4.638	2.996	3.491	3.476
4EY6	[94]	2.731	2.837	2.271	1.768	2.072	3.017	2.983	2.746	1.883	1.906
4EY7	[94]	3.931	3.915	1.936	1.931	1.836	4.931	4.873	1.582	1.974	1.983
4M0E	[SR19]	1.924	2.079	1.948	2.714	2.932	2.041	2.116	1.564	2.892	2.974
4M0F	[SR19]	2.736	2.839	2.263	2.046	2.591	2.888	2.913	2.673	2.117	2.217
5FOQ	[SR20]	3.498	3.736	2.437	3.966	4.574	3.884	3.941	2.932	3.765	3.964
DA		31.25%	25%	68.75%	56.26%	50%	12.5%	18.75%	56.25%	43.75%	43.75%

[a]Best docked conformation; [b]Best clustered conformation; [c]Rigid docking; [d]F - flexible docking.

Table S11. Binding free energies and individual energy terms of *Mus Musculus* (upper part) and *Homo sapiens* (lower part) AChE in complex with acetylcholine and various targeted pesticides inhibitors.

Complex	ΔE_{ele}[a] (kcal/mol)	ΔE_{vdw}[b] (kcal/mol)	ΔG_{solv}[c] (kcal/mol)	$T\Delta S$[a] (kcal/mol)	ΔG_{bind}[e] (kcal/mol)
atrazine-*m*AChE[f]	-41.48±0.62	-51.24±0.91	4.74±0.45	-8.74±0.38	-79.24±0.18
propazine-*m*AChE	-52.43±0.47	-50.82±0.35	5.22±0.15	-26.00±0.52	-72.03±0.26
simazine-*m*AChE	-53.26±0.41	-50.24±0.63	5.26±0.73	-28.70±0.51	-69.54±0.32
carbofuran-*m*AChE	-52.84±0.88	-55.28±0.61	4.37±0.28	-33.32±0.57	-70.43±0.44
monocrotophos-*m*AChE	-58.43±0.32	-39.26±0.58	8.24±0.38	-33.99±0.39	-55.46±0.75
dimethoate-*m*AChE	-61.24±0.73	-31.36±0.33	9.27±0.27	-30.77±0.22	-52.56±0.43
carbaryl-*m*AChE	-51.32±0.38	-49.26±0.68	5.41±0.86	-46.19±0.92	-48.98±0.44
tebufenozide-*m*AChE	-41.39±0.41	-39.28±0.19	4.28±0.36	-50.63±0.73	-25.76±0.88
imidacloprid-*m*AChE	-38.26±0.78	-51.43±0.28	6.28±0.92	-27.45±0.92	-55.96±0.47
acetampirid-*m*AChE	-26.37±0.99	-58.24±0.53	6.32±0.24	-24.93±0.67	-53.36±0.65
diuron-*m*AChE	-31.46±0.26	-49.28±0.89	6.03±0.55	-27.87±0.93	-46.84±0.95
monuron-*m*AChE	-35.24±0.51	-43.28±0.49	6.33±0.37	-29.66±0.63	-42.53±0.94
linuron-*m*AChE	-41.23±0.41	-41.26±0.29	6.05±0.36	-37.50±0.72	-38.94±0.16
acetylcholine-*m*AChE	-43.23±0.31	-46.98±0.63	5.28±0.48	-53.48±0.73	-31.45±0.74
atrazine-*h*AChE[g]	-53.31±0.62	-41.76±0.91	5.74±0.35	-8.92±0.47	-80.41±0.34
propazine-*h*AChE	-58.36±0.47	-47.72±0.35	5.15±0.15	-29.00±0.41	-71.93±0.53
simazine-*h*AChE	-57.62±0.74	-51.34±0.41	5.92±0.51	-34.21±0.83	-68.83±0.61
carbofuran-*h*AChE	-56.63±0.88	-54.82±0.61	4.95±0.31	-34.56±0.42	-71.94±0.31
monocrotophos-*h*AChE	-64.25±0.32	-31.84±0.73	7.89±0.51	-33.38±0.51	-54.82±0.96
dimethoate-*h*AChE	-58.43±0.51	-32.72±0.51	8.56±0.46	-28.94±0.68	-53.65±0.93
carbaryl-*h*AChE	-53.61±0.63	-48.26±0.22	5.82±0.73	-47.73±0.39	-48.32±0.63
tebufenozide-*h*AChE	-40.21±0.37	-42.78±0.22	4.79±0.41	-52.38±0.52	-25.82±0.83
imidacloprid-*h*AChE	-47.31±0.83	-50.26±0.45	7.11±0.92	-31.42±0.99	-59.04±0.73
acetampirid-*h*AChE	-24.52±0.83	-58.73±0.26	6.57±0.41	-22.70±0.42	-53.98±0.68
diuron-*h*AChE	-29.37±0.72	-50.74±0.51	6.17±0.42	-27.72±0.93	-46.22±0.92
monuron-*h*AChE	-36.73±0.41	-44.17±0.28	6.54±0.81	-31.24±0.73	-43.12±0.77
linuron-*h*AChE	-41.78±0.41	-42.03±0.61	6.52±0.61	-37.57±0.74	-39.72±0.53
acetylcholine-*h*AChE	-42.42±0.62	-48.35±0.22	5.41±0.83	-52.69±0.82	-32.67±0.31

[a]Electrostatic energy difference; [b]van der Waals energy difference; [c]Solvation free energy; [d]The entropy change; [e]Predicted binding free energy; [f]*Mus musculus* AChE; [g]*Homo sapiens* AChE.

Table S12. Linear regression parameters for QSAR model 5 (acute toxicity against *Mus musculus*).

Compound	LD_{50} (mg/kg)	MW	$\Delta G_{binding}$ (kcal/mol)	Exp. pLD_{50}	Fitted pLD_{50}
atrazine	0.85	215.69	-9.50	5.40	5.05
propazin	3.18	229.71	-9.20	4.86	4.81
simazine	5	201.66	-8.70	4.61	4.42
carbofuran	2	221.11	-8.70	5.04	4.42
monocrotophos	14	223.16	-8.40	4.20	4.18
dimethoate	60	229.25	-8.20	3.58	4.02
carbaryl	100	201.22	-6.10	3.30	2.37
tebufenozide	5000	352.48	-7.50	1.85	3.47
imidacloprid	131	269.69	-7.80	3.31	3.71
acetamiprid	184	221.69	-8.10	3.08	-2.44
diuron	500	233.09	-6.50	2.67	2.68
monuron	1700	198.65	-6.20	2.07	2.45
linuron	2400	249.09	-5.30	2.02	1.74

Table S13. External validation of QSAR model 5 (acute toxicity against *Mus musculus*).

Compound	LD_{50} (mg/kg)	MW	$\Delta G_{binding}$ (kcal/mol)	Exp. pLD_{50}	Fitted pLD_{50}
azamethiphos	1040.00	324.68	-8.10	4.07	3.95
azinphos-methyl	7.00	317.32	-7.80	6.25	3.71
chlorpyrifos	2000.00	350.59	-7.60	3.79	3.55
DDVP	17.00	220.98	-5.30	5.86	1.74
diazinon	66.00	304.35	-8.00	5.27	3.87
fenitrothion	500.00	277.23	-7.70	4.39	3.63
glyphosate	5000.00	169.07	-4.90	3.39	1.42
malathion	290.00	330.36	-6.80	4.63	2.92
methyl parathion	18.00	263.21	-7.20	5.84	3.24
naled (dibrom)	160.00	380.78	-5.70	4.89	2.05
parathion	2.00	291.26	-7.00	6.79	3.08
phosmet	113.00	317.32	-7.80	5.04	3.71
TCVP	465.00	365.96	-8.30	4.42	4.10
terbufos	1.60	288.43	-5.20	6.89	1.66
methiocarb	350.00	225.31	-7.00	4.55	3.08
methomyl	12.00	162.21	-5.30	6.01	1.74
oxamyl	5.40	219.26	-6.40	6.36	2.61
DDT	113.00	354.49	-9.10	5.04	4.74
2,4-D	639.00	221.04	-7.00	4.29	3.08
dicamba	757.00	221.04	-6.90	4.21	3.00
DEET	1.95	191.27	-7.80	6.80	3.71
sulfoxaflor	750.00	277.27	-8.30	4.22	4.10

Table S14. Linear regression parameters for QSAR model 5 (acute toxicity against *Homo sapiens*).

Compound	LD_{50} (mg/kg)	MW	$\Delta G_{binding}$ (kcal/mol)	Calculated pLD_{50}	Fitted pLD_{50}
atrazine	0.07	215.69	-10.10	6.50	5.52
propazin	0.26	229.71	-9.70	5.95	5.21
simazine	0.41	201.66	-9.10	5.70	4.74
carbofuran	0.16	221.11	-9.60	6.14	5.13
monocrotophos	1.14	223.16	-8.60	5.29	4.34
dimethoate	4.86	229.25	-8.30	4.67	4.10
carbaryl	8.11	201.22	-7.80	4.39	3.71
tebufenozide	405.40	352.48	-5.60	2.94	1.98
imidacloprid	10.62	269.69	-8.10	4.40	3.95
acetamiprid	14.92	221.69	-7.70	4.17	3.63
diuron	40.54	233.09	-6.90	3.76	3.00
monuron	137.84	198.65	-6.70	3.16	2.84
linuron	194.59	249.09	-5.90	3.11	2.21

Table S15. External validation of QSAR model 5 (acute toxicity against *Homo sapiens*).

Compound	LD_{50} (mg/kg)	MW	$\Delta G_{binding}$ (kcal/mol)	Calculated pLD_{50}	Fitted pLD_{50}
azamethiphos	1040.00	324.68	-8.20	2.49	4.03
azinphos-methyl	7.00	317.32	-8.00	4.66	3.87
chlorpyrifos	2000.00	350.59	-8.10	2.24	3.95
DDVP	17.00	220.98	-5.40	4.11	1.82
diazinon	66.00	304.35	-7.80	3.66	3.71
fenitrothion	500.00	277.23	-7.90	2.74	3.79
glyphosate	5000.00	169.07	-4.90	1.53	1.42
malathion	290.00	330.36	-6.30	3.06	2.53
methyl parathion	18.00	263.21	-7.50	4.17	3.47
naled (dibrom)	160.00	380.78	-5.70	3.38	2.05
parathion	2.00	291.26	-7.90	5.16	3.79
phosmet	113.00	317.32	-8.20	3.45	4.03
TCVP	465.00	365.96	-8.00	2.90	3.87
terbufos	1.60	288.43	-4.90	5.26	1.42
methiocarb	350.00	225.31	-7.80	2.81	3.71
methomyl	12.00	162.21	-5.40	4.13	1.82
oxamyl	5.40	219.26	-6.30	4.61	2.53
DDT	113.00	354.49	-9.20	3.50	4.81
2,4-D	639.00	221.04	-7.50	2.54	3.47
dicamba	757.00	221.04	-7.30	2.47	3.32
DEET	1.95	191.27	-7.90	4.99	3.79
sulfoxaflor	750.00	277.27	-8.70	2.57	4.42

Supplementary material references (SRs)

SR1. Bourne, Y.; Taylor, P.; Radić, Z.; Marchot, P. Structural insights into ligand interactions at the acetylcholinesterase Peripheral Anionic Site. *EMBO J* **2003**, *22*, 1–12. DOI: 10.1093/emboj/cdg005

SR2. Bourne, Y.; Kolb, H.C.; Radić, Z.; Sharpless, K.B.; Taylor, P.; Marchot, P. Freeze-frame inhibitor captures acetylcholinesterase in a unique conformation. *Proc Natl Acad Sci USA* **2004**, *101*, 1449–1454. DOI: 10.1073/pnas.0308206100

SR3. Ekstrom, F.; Akfur, C.; Tunemalm, A.-K.; Lundberg, S. Structural changes of phenylalanine 338 and histidine 447 revealed by the crystal structures of tabun-inhibited murine acetylcholinesterase. *Biochemistry* **2006**, *45*, 74–81. DOI: 10.1021/bi051286t

SR4. Ekstrom, F.; Pang, Y.P.; Boman, M.; Artursson, E.; Akfur, C.; Borjegren, S. Crystal structures of acetylcholinesterase in complex with HI-6, ortho-7 and obidoxime: Structural basis for differences in the ability to reactivate tabun conjugates. *Biochem Pharmacol* **2006**, *72*, 597–607. DOI: 10.1016/j.bcp.2006.05.027

SR5. Bourne, Y.; Radić, Z.; SulzenbAChEr, G.; Kim, E.; Taylor, P.; Marchot, P. Substrate and product trafficking through the active center gorge of acetylcholinesterase analyzed by crystallography and equilibrium binding. *J Biol Chem* **2006**, *281*, 29256–29267. DOI: 10.1074/jbc.M603018200

SR6. Ekstrom, F.J.; Astot, C.; Pang, Y.P. Novel nerve-agent antidote design based on crystallographic and mass spectrometric analyses of tabun-conjugated acetylcholinesterase in complex with antidotes. *Clin Pharmacol Ther* **2007**, *82*, 282–293. DOI: 10.1038/sj.clpt.6100151

SR7. Hornberg, A.; Tunemalm, A.K.; Ekstrom, F. Crystal structures of acetylcholinesterase in complex with organophosphorus compounds suggest that the acyl pocket modulates the aging reaction by precluding the formation of the trigonal bipyramidal transition state. *Biochemistry* **2007**, *46*, 4815–4825. DOI: 10.1021/bi0621361

SR8. Ekstrom, F.; Hornberg, A.; Artursson, E.; Hammarstrom, L.G.; Schneider, G.; Pang, Y.P. Structure of HI-6•sarin-acetylcholinesterase determined by x-ray crystallography and molecular dynamics simulation: Reactivator mechanism and design. *Plos One* **2009**, *4*, e5957 1–19. DOI: 10.1371/journal.pone.0005957

SR9. Hornberg, A.; Artursson, E.; Warme, R.; Pang, Y-P.; Ekstrom, F. Crystal structures of oxime-bound fenamiphos-acetylcholinesterases: Reactivation involving flipping of the His447 ring to form a reactive Glu334-His447-oxime triad. *Biochem Pharmacol* **2010**, *79*, 507–515. DOI: 10.1016/j.bcp.2009.08.027

SR10. Artursson, E.; Andersson, P.O.; Akfur, C.; Linusson, A.; Borjegren, S.; Ekstrom, F. Catalytic-site conformational equilibrium in nerve-agent adducts of acetylcholinesterase: Possible implications for the HI-6 antidote substrate specificity. *Biochem Pharmacol* **2013**, *85*, 1389–1397. DOI: 10.1016/j.bcp.2013.01.016

SR11. Ronco, C.; Carletti, E.; Colletier, J-P.; Weik, M.; Nachon, F.; Jean, L.; Renard, P-Y. Huprine derivatives as sub-nanomolar human acetylcholinesterase inhibitors: From rational design to validation by x-ray crystallography. *ChemMedChem* **2012**, *7*, 400–405. DOI: 10.1002/cmdc.201100438

SR12. Berg, L.; Andersson, C.D.; Artursson, E.; Hornberg, A.; Tunemalm, A-K.; Linusson, A.; Ekstrom, F. Targeting acetylcholinesterase: Identification of chemical leads by high throughput screening,

structure determination and molecular modelling. *Plos One* **2011**, *6*, e26039 1–12. DOI: 10.1371/journal.pone.0026039

SR13. Andersson, C.D.; Forsgren, N.; Akfur, C.; Allgardsson, A.; Berg, L.; Engdahl, C.; Qian, W.; Ekstrom, F.; Linusson, A. Divergent structure-activity relationships of structurally similar acetylcholinesterase inhibitors. *J Med Chem* **2013**, *56*, 7615–7624. DOI: 10.1021/jm400990p

SR14. Carletti, E.; Colletier, J-P.; Schopfer, L.M.; Santoni, G.; Masson, P.; Lockridge, O.; Nachon, F.; Weik, M. Inhibition pathways of the potent organophosphate CBDP with cholinesterases revealed by x-ray crystallographic snapshots and mass spectrometry. *Chem Res Toxicol* **2013**, *26*, 280–289. DOI: 10.1021/tx3004505

SR15. Katz, F.S.; Pecic, S.; Tran, T.H.; Trakht, I.; Schneider, L.; Zhu, Z.; Ton-That, L.; Luzac, M.; Zlatanic, V.; Damera, S.; Macdonald, J.; Landry, D.W.; Tong, L.; Stojanovic, M.N. Discovery of new classes of compounds that reactivate acetylcholinesterase inhibited by organophosphates. *ChemBioChem* **2015**, *16*, 2205–2215. DOI: 10.1002/cbic.201500348

SR16. Bourne, Y.; Sharpless, K.B.; Taylor, P.; Marchot, P. Steric and dynamic parameters influencing *in situ* cycloadditions to form triazole inhibitors with crystalline acetylcholinesterase. *J Am Chem Soc* **2016**, *138*, 1611–1621. DOI: 10.1021/jacs.5b11384

SR17. Carletti, E.; Colletier, J-P.; Dupeux, F.; Trovaslet, M.; Masson, P.; Nachon, F. Structural evidence that human acetylcholinesterase inhibited by tabun ages through o-dealkylation. *J Med Chem* **2010**, *53*, 4002–4008. DOI: 10.1021/jm901853b

SR18. Nachon, F.; Carletti, E.; Ronco, C.; Trovaslet, M.; Nicolet, Y.; Jean, L.; Renard, P.Y. Crystal structures of human cholinesterases in complex with huprine w and tacrine: Elements of specificity for anti-Alzheimer's drugs targeting acetyl- and butyryl-cholinesterase. *Biochem J* **2013**, *453*, 393–399. DOI: 10.1042/BJ20130013

SR19. Cheung, J.; Gary, E.N.; Shiomi, K.; Rosenberry, T.L. Structures of human acetylcholinesterase bound to dihydrotanshinone i and territrem b show peripheral site flexibility. *ACS Med Chem Lett* **2013**, *4*, 1091–1096. DOI: 10.1021/ml400304w

SR20. Berg, L.; Mishra, B.K.; Andersson, C.D.; Ekstrom, F.; Linusson, A. The nature of activated non-classical hydrogen bonds: A case study on acetylcholinesterase-ligand complexes. *Chemistry* **2016**, *22*, 2672–2681. DOI: 10.1002/chem.201503973